Dielectric Characterization of Biological Tissues for Medical Applications

Instituto de Telecomunicaciones y Aplicaciones Multimedia
Universitat Politècnica de València

A thesis for the degree of
PhD in Technologies for Health and Wellbeing
Valencia, September 2019

Author:
Alejandro Fornés Leal

Supervisors:
Prof. Narcís Cardona Marcet
Dr. Concepción García Pardo

Abstract

Nowadays, a careful knowledge of the electromagnetic properties of biological tissues is required for developing a great number of applications. The development of wireless medical devices, the design of in-body and on-body antennas, specific absorption rate evaluations, cancer treatment techniques such as hyperthermia and detection techniques like medical imaging are some examples of applications that rely on these data.

Since cancer causes modifications on the biological structure of cells that can lead in turn to changes in the electromagnetic properties of the tissues, it is possible to develop novel detection applications taking advantage of it. One potential target is colorectal cancer (CRC), as suspicious tissues can be accessed quite easily through colonoscopy procedures. This kind of cancer is one of the most spread kinds, being responsible of about 1 out of 10 new cancer cases and deaths. There are several risk factors currently related to the apprising of this cancer, although in essence the higher the age of the population, the higher the incidence of CRC.

Screening programs are key for detecting and diagnosing cancer: if found at early stages, the probability of survival increases greatly, and the cost of the treatment can be reduced as well. One of the major objectives of this dissertation is proposing applications for detecting CRC that aid in the colonoscopy procedures by making use of the differences in electromagnetic properties. Aside from enhancement in the diagnosis of CRC, improving the colonoscopy procedure can lead to collateral benefits like a lowering of the burden of anatomical pathology unit.

With the aim at demonstrating the feasibility and the potential future development of these applications, in the framework of this thesis the dielectric properties of healthy, cancerous and pathological human colon tissues are measured and compared in order to find electromagnetic differences. Measurements are carried out by means of an open-ended coaxial system. Its principle of operation has been revisited with the aim at maximizing the accuracy of the method, and the calibration procedure has been optimized serving the same purpose.

ABSTRACT

Two main sources of colon tissue have been analyzed: samples from colonoscopy biopsies and samples from surgery resections. Besides healthy tissue, the following colon tissues have been characterized: Adenocarcinomas (CRC), adenomas without dysplasia, adenomas with low-grade dysplasia, adenomas with high-grade dysplasia, hyperplastic polyps and hamartomatous polyps. Given the variability that can appear among subjects, the electromagnetic properties of suspicious tissues from a particular patient have to be always compared with those of his healthy ones, not evaluated independently.

The second major objective of this thesis involves the development of a new database of electromagnetic properties of biological tissues obtained at *in vivo* conditions. Nowadays, the available collections are limited either in the number of tissues or the measured frequencies, and hence researchers have to make use of more complete databases but that were performed *ex vivo*. The drawback of using these collections is that results can be compromised by factors such as lack of blood perfusion and tissue dehydration. Developing this new database can facilitate the design of applications that needs of a careful knowledge of these properties.

Resumen

Conocer las propiedades electromagnéticas de los tejidos biológicos con la mayor exactitud posible tiene una gran importancia en el diseño de un elevado número de aplicaciones biomédicas. El diseño de dispositivos médicos inalámbricos, antenas superficiales e intracorporales, evaluación de tasas de absorción electromagnética, técnicas de tratamiento y detección de cáncer como la hipertermia e imágenes médicas son ejemplos de aplicaciones que requieren esta información para su desarrollo.

Debido a que el cáncer provoca modificaciones estructurales en las células que a su vez generan cambios en las propiedades electromagnéticas, es posible desarrollar aplicaciones de detección de cáncer que se basen en este hecho. Un objetivo potencial es el cáncer de colon (CRC), debido a que los tejidos de colon sospechosos son accesibles de forma más o menos sencilla durante procedimientos endoscópicos. Este tipo de cáncer es uno de los más extendidos, siendo responsable de aproximadamente el 10% de casos y muertes totales. Existe un gran número de factores de riesgo que pueden explicar la aparición de la enfermedad, aunque esencialmente la probabilidad se incrementa significativamente con el aumento de la edad de la población.

Los programas de cribado sobre la población son críticos: si el cáncer se detecta en etapas tempranas, la probabilidad de sobrevivir se incrementa en gran medida, y además se reducen los costes asociados. Uno de los objetivos principales de esta tesis es proponer aplicaciones que ayuden en la detección de CRC durante la colonoscopia haciendo uso de las diferencias en las propiedades electromagnéticas. Aparte de mejoras en el diagnóstico, complementar la colonoscopia puede conllevar otros beneficios colaterales como una reducción en la carga de anatomía patológica.

Para demostrar la viabilidad y el potencial desarrollo futuro de estas aplicaciones, en esta tesis se miden y se trata de encontrar diferencias entre las propiedades electromagnéticas de tejidos sanos, cancerosos y patológicos de colon humano. Las medidas han sido llevadas a cabo mediante la técnica del coaxial terminado en abierto. Con el propósito de incrementar la precisión del

método, se ha evaluado el principio de funcionamiento y se ha mejorado el proceso de calibración. Dos fuentes de tejido de colon han sido analizadas en esta tesis: tejidos procedentes de colonoscopias (biopsias) y tejidos obtenidos a partir de procedimientos quirúrgicos. Aparte de tejido sano, se estudian las siguientes patologías: Adenocarcinomas (CRC), adenomas sin displasia, adenomas con bajo grado de displasia, adenomas con alto grado de displasia, hiperplasias y hamartomas. Debido a la alta variabilidad entre distintos sujetos, las propiedades electromagnéticas de los tejidos sospechosos de un paciente en concreto deben ser siempre comparadas con las propiedades de sus tejidos sanos, no evaluadas de forma independiente.

El segundo gran objetivo de esta tesis es el desarrollo de una nueva base de datos de las propiedades electromagnéticas de tejidos biológicos medidas *in vivo*. Ahora mismo, las colecciones disponibles están limitadas en número de tejidos o frecuencias caracterizadas, obligando a los investigadores a escoger bases de datos más completas pero realizadas *ex vivo*. No obstante, usar este tipo de colecciones tienen fuentes de incertidumbre adicionales dado que las medidas están condicionadas por la deshidratación de los tejidos y la pérdida de flujo sanguíneo. El desarrollo de esta nueva base de datos puede facilitar el diseño de aplicaciones que requieran conocer las propiedades electromagnéticas con alto grado de precisión.

Resum

Conéixer les propietats electromagnètiques dels teixits biològics amb la major exactitud possible té una gran importància en el disseny d'un gran nombre d'aplicacions biomèdiques. El disseny de dispositius metges sense fil, antenes superficials i intracorporals, l'avaluació de taxes d'absorció electromagnètica, tècniques de tractament i detecció de càncer com ara la hipertèrmia i imatges mèdiques són exemples d'aplicacions que requerixen esta informació.

Com el càncer provoca modificacions estructurals en les cèl·lules que generen canvis en les propietats electromagnètiques, és possible desenrotllar aplicacions de detecció de càncer que es basen en este fet. Un objectiu potencial és el càncer de còlon (CRC), pel fet que els teixits de còlon sospitosos són accessibles de forma més o menys senzilla durant procediments endoscòpics. Este tipus de càncer és un dels més estesos, sent responsable d'aproximadament el 10% de casos i morts totals. N'hi ha un gran nombre de factors de risc que poden explicar l'aparició de la malaltia, encara que en resum la probabilitat s'incrementa significativament amb l'augment de l'edat de la població.

Els programes de cribratge sobre la població són crítics. Si el càncer es detecta en etapes primerenques, la probabilitat de sobreviure s'incrementa en gran manera, i a més es reduïxen els costos associats. Un dels objectius principals d'esta tesi és proposar aplicacions que ajuden en la detecció de CRC durant la colonoscòpia fent ús de les diferències en les propietats electromagnètiques. A banda de millores en el diagnòstic, complementar la colonoscòpia pot comportar altres beneficis col·laterals com una reducció en la càrrega d'anatomia patològica.

Per a demostrar la fiabilitat i el potencial desenrotllament d'aquestes aplicacions, en aquesta tesi es mesuren i es tracta de trobar diferències entre les propietats electromagnètiques de teixits sans, cancerosos i patològics de còlon humà. Les mesures han sigut realitzades mitjançant la tècnica del coaxial acabat en obert. Amb el propòsit d'incrementar la precisió del mètode, s'ha evaluat el seu principi de funcionament i s'ha millorat el process de calibratge. Dos fonts de teixit de colon s'han analitzat en aquesta tesi: teixits procedents de

colonoscòpies (biòpsies) i teixits obtinguts a partir de procediments quirúrgics. Apart de teixit sà, s'estudien els següents teixits: Adenocarcinomes (CRC), adenomes sense displàsia, adenomes amb baix grau de displàsia, adenomes amb alt grau de displàsia, hiperplàsies y hamartomes. Degut a l'alta viariabilitat entre diferents subjectes, les propietats electromagnètiques dels teixits sospitosos d'un pacient en particular han de ser comparades amb les propietats dels seus teixits sans, no evaluats independentment.

El segon gran objectiu d'esta tesi és el desenrotllament d'una nova base de dades de les propietats electromagnètiques de teixits biològics mesurades *in vivo*. Ara mateix, les col·leccions disponibles estan limitades en nombre de teixits o freqüències caracteritzades, obligant els investigadors a triar bases de dades més completes però realitzades *ex vivo*. No obstant això, este tipus de col·leccions te fonts d'incertesa addicionals atés que les mesures estan condicionades per la deshidratació dels teixits i la pèrdua de flux sanguini. El desenrotllament d'esta nova base de dades pot facilitar el disseny d'aplicacions que requerisquen conéixer les propietats electromagnètiques amb alt grau de precisió.

Acknowledgements

I would like to express my gratitude to those people who made this thesis possible. First of all, I would like to thank my supervisors for their guidance and support along these years and for giving me the opportunity to be part of the Mobile Communications Group (MCG) of the iTEAM. Thanks to Prof. Narcís Cardona, who from the very beginning made an effort to ensure that I had all the necessary means at my disposal to progress with my research. And thanks to Dr. Concepción García Pardo, who helped me to develop all the necessary skills to become a good researcher and to understand and overcome all the issues that emerged during the fulfillment of my thesis.

This thesis could not have been carried out without the effort, time, assistance and knowledge of an amazing group of people that I would like to mention. In the first place, I would like to thank to the Medical Doctors Vicente Pons and Matteo Frasson for dedicating part of their valuable time to my research and for facilitating the execution of my thesis in a medical environment. Special thanks to Andrea Nevárez, and also to the rest of the medical staff of the endoscopy unit of Hospital La Fe (Lidia, Marco, Marta, etc.), for aiding me during all these years. Thanks as well to Prof. Ana Vallés for her valuable assistance not only in the framework of my research, but also in the research lines of my department colleagues.

I really want to thank my colleagues of the MCG, with whom I have spent some amazing years that have made me grow both personally and professionally. Special mention to the two persons with whom I have worked side by side: Carlos Andreu and Sergio. With his amazing human quality, Andreu was able to turn our group of colleagues (the formerly so-called *Lords of iTEAM*) into almost a family. And I am not ashamed to acknowledge that, without Sergio, I would not have been able to achieve even half of the results of my thesis: he is always willing to help anybody in an almost altruist way. Thanks as well to the rest of the *lords*: Barjau, Edu, Gerardo, Manuel and Pepelú; to my other colleagues and friends of the MCG: Alicia, Álvaro, Andrea Parra, Andrea Ramos, Barquero, Danaisy, Dani, David García, David Martín, Elis-

abeth, Herranz, Irene, Josetxo, Josué, Marc, Martina, Samuel, Sandra, Santi, Saúl Inca, Sofía and Tere; and to all those colleagues that were part of the MCG some years ago: Cabrejas, Cristian, David Vargas, Jefferson, Jordi Joan, Juanan, Kevin, Nika, Saúl Fuster, Shitomi-san and Sonia. My apologies if I have forgotten anyone.

Por último, no quiero dejar pasar la oportunidad de acordarme también de mi hermano, de todos mis amigos de Denia, del padel, y de los grupos de Valencia, con quienes he pasado (y seguiremos pasando) unos grandes momentos. Y por supuesto, esta tesis va dedicada a mis padres por educarme, por darme la oportunidad de venir a Valencia a estudiar y por apoyarme siempre de forma incondicional en las elecciones que he ido tomando a lo largo de los años. Gracias a todos.

Table of contents

List of Figures

List of Tables

Acronyms

ASGE American Society of Gastrointestinal Endoscopy

BAN Body Area Networks

CAD Computer-Aided Design

CBIT Centre for Biomaterials and Tissue Engineering

CRC Colorectal cancer

CTC Computed Tomographic Colonography

DCBE Double Contrast Barium Enema

DMSO Dimethyl Sulfoxide

DNA Deoxyribonucleic Acid

FICE Flexible Imaging Color Enhancement

FIT Fecal Immunochemical Test

FN False Negative

FP False Positive

gFOBT Gualac-based Fecal Occult Blood Test

GPV Global Predictive Value

GVA Generalitat Valenciana

HC High definition Colonoscopy

HGD High-Grade Dysplasia

LIST OF ABBREVIATIONS

IARC International Association of Cancer Registries

IPD Incident Power Density

ISM Industrial, Scientific and Medical

ISO International Organization for Standardization

ITEAM Institute for Telecommunications and Multimedia Applications

LGD Low-Grade Dysplasia

MUT Material Under Test

NBI Narrow Band Imaging

NIST National Institute of Standards and Technology

NPV Negative Predictive Value

PDF Probability Density Function

PPV Positive Predictive Value

PTFE Polytetrafluoroethylene

SAR Specific Absorption Rate

SCPI Standard Commands for Programmable Instruments

SDM Standard Deviation of the Mean

SHF Super High Frequency

TN True Negative

TP True Positive

TRIMProb Tissue Resonance InterferoMeter Probe

UHF Ultra High Frequency

UPV Universitat Politècnica de València

VNA Vector Network Analyzer

WBAN Wireless Body Area Networks

WHO World Health Organization

WMD Wireless Medical Devices

Chapter 1

Introduction

1.1 Background

The research of the electromagnetic properties of biological tissues has grown steadily since the early years of the past century [1]. This interest has provided great contributions to the biophysical and physiological sciences [2], and it led to a rapid growth of many kinds of biomedical applications as well as different electromagnetic characterization techniques.

The interaction of the electromagnetic waves with a biological tissue is described by means of three electromagnetic properties: permittivity, conductivity and permeability. These properties, sometimes referred to as *dielectric properties*, are determined by different factors such as their molecular composition, cellular structure, the mobility and concentration of ions, and temperature, among others [3]. Because of these varying factors, these properties differ not only among tissues, but also among subjects and particular conditions. Understanding how the electromagnetic fields are affected in presence of biological tissues is critical for many wireless applications, especially if they are intended to work around or beyond Ultra High Frequency (UHF) frequencies (this is, above 300 MHz)

For instance, these properties have to be considered thoroughly in the design steps in order to develop Wireless Medical Devices (WMD) and propagation systems of a similar nature [4, 5]. They can be used for computing the path losses that the wireless signals may suffer at their frequencies of operation, as well as to know their propagation speed and delays. The performance of the antennas of these kinds of systems are heavily affected if they are in contact or very close to a human body in terms of radiation patterns and matching

[6], and hence these properties have to be carefully considered when designing them.

Specific Absorption Rate (SAR) and Incident Power Density (IPD) evaluations also make use of these properties [7], as the electromagnetic absorption is directly related to them. These dosimetry indicators have to be assessed for any wireless system that is aimed to be deployed, especially for systems that work beyond UHF and Super High Frequency (SHF). Due to the increasing concern in the society about the effect of electromagnetic fields on the human health, wireless systems must work within the exposure thresholds indicated by the regulatory agencies [8–10].

The aforementioned applications can be designed and tested with the aid of electromagnetic phantoms. On the one hand, there are software phantoms, which are CAD, voxel or geometry models used in software simulations [11]. They imitate the shape and the dielectric properties of the biological tissues to evaluate their electromagnetic interaction over the system or device that is being designed. On the other hand, there are physical phantoms, which have the same objective but once the device is manufactured or the system deployed. The latter phantoms can be either liquids, solids or gels, and mimic the electromagnetic properties of specific human tissues for certain frequency bands. It should be reminded that electromagnetic phantoms are simplified versions of real conditions, and hence the outcomes obtained with them should be interpreted with caution.

Cancer treatment techniques based on microwaves such as hyperthermia rely on the knowledge of these properties not only in healthy but also in malignant states [12, 13]. Lastly, dielectric properties can be used as well for developing applications that aid in the detection or diagnosis of medical pathologies, like in microwave imaging [14]. Diseases that change the biological structure of biological tissues, like cancer, can cause variations in their amount of water that are translated into changes of their properties.

1.2 Cancer in the modern society

In the recent decades, cancer has become a major concern for many countries. According to the estimations provided in International Association of Cancer Registries (IARC) for 2018 [15], a total of 18.1 million new cases were diagnosed and it caused the death of 9.6 million people around the world. In the Fig. 1.1, the incidence of cancer for each country is presented. One can observe that the higher the development of a country, the higher the incidence of cancer. Larger incidence rates are partially due to the ageing of the population, although there are many varying risk factors to explain the incidence of each cancer

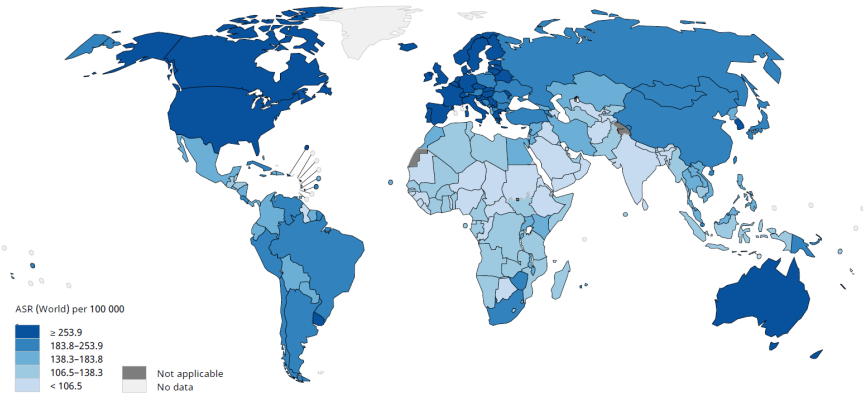

Figure 1.1: Incidence of cancer for each country [15].

type in different regions or countries. Cancer is, in fact, the leading cause of premature death at developed countries and one of the major reasons at countries under development, as stated in [16] (defining premature death as any decease occurred before 70 years of age). Moreover, 13 million people are expected to die because of this disease in 2030, which indicates a potential increment of the death rate of around a 35%. It should be highlighted that the data gathered of less developed regions are not as accurate, since many people are not covered by high-quality registries. For instance, in Africa only about 1% of the population is covered by these kind of registries, as explained in [16]. This implies that many cancer deaths have not been identified and accounted as such.

As the global incidence of cancer increases, so it does the worldwide economic impact of this disease, for both the individuals and the society. The direct costs of qualified specialists, treatments, drugs etc. is very high, being a heavy burden for the economies and the affected families. In addition, other costs have to be considered. On the one hand, there are indirect costs due to the decrease of productivity of the patients during treatment, or even the lost of it in case of retirement or death [17]. On the other hand, there are psychosocial costs, which are referred to the loss of quality of life and are related to pain, suffering or grief, among others [17].

Policies of cancer prevention and early diagnosis are being implemented in many countries in order to reduce the cancer burden. Awareness prevention campaigns are the most beneficial approaches to reduce both the morbidity and the mortality from cancer. Campaigns for avoiding tobacco consumption, reducing alcohol consumption, hepatitis B vaccination, promotion of physical

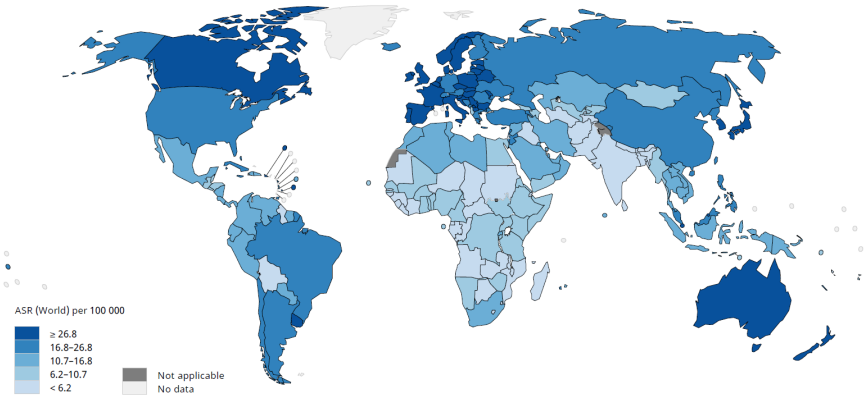

Figure 1.2: Incidence of CRC for each country [15].

activities and healthier diets are some strategies that can reduce the incidence of many kinds of cancer [15]. In [18], authors claim that around the 35% of cancer deaths can be avoided by modifying risk factors such as overweight and obesity, low fruit and vegetable intake, physical inactivity, smoking and alcohol consumption, unsafe sex, urban air pollution, smoking or be in presence of tobacco smoke and contaminated injections in healthcare settings. Besides, population screening programs are of huge importance to detect and diagnose cancer. If a cancer is found at early stages, the survival probability is generally higher and treatments can be more affordable, lowering the economic burden of families and states. Since many highly-developed countries invest in both prevention campaigns and screening programs, the cancer survival rate is higher in this countries than in less developed ones.

1.2.1 Colorectal cancer

Colorectal cancer (CRC) is the development of cancer in either the colonic wall or rectum. According to the estimations presented in [15], around 1.8 million new cases have occurred in 2018, being also responsible of approximately 881 000 deaths. Therefore, this cancer accounts about 1 out of 10 new cancer cases and deaths, being the third in terms of incidence and the second in terms of mortality. As most cancers, its incidence is directly related to the life expectancy of a country: the highest incident rates are found in Europe, Australia and New Zeland, Northern America and Eastern Asia, as shown in the Fig. 1.2. On the contrary, the incidence is lower in Africa and Southern Asia. The incidence rates of rectal cancer have a similar regional distribution.

Many risk factors have been related to this kind of cancer, as reviewed in [19]. With regard to nutritional factors, an increased consumption of vegetables and fruits can reduce the risk of suffering CRC [20, 21], because of their richness of fibre, antioxidants, folic acid and vitamins [22, 23]. Some studies have found out a correlation between a high-fibre diet and a reduction of risk of suffering CRC as well [24, 25]. Consuming high quantities of read meat (i.e., more than 160 grams of processed meat every day) and a long cook time of meats can contribute to an increment of CRC [26–29]. Besides, an association between alcohol consumption and CRC incidence has been also reported [30]. Ingesting more than 30 grams of ethanol per day or consuming alcohol more than twice a day can increase significantly the risk of CRC [31].

Regarding medical history, some reports have shown that subjects with diabetes mellitus have higher risk of suffering CRC [32, 33]. Patients with long-term inflammatory bowel disease [34, 35], or that have undergone a cholecystectomy [36, 37], or a pelvic radiotherapy [38, 39], also have a higher risk of suffering CRC. Other factors can be related to the incidence of CRC as well. Both obesity and a reduced physical activity can increase the risk of CRC [40, 41]. In [42], it was shown that the risk is higher for idle workers compared to those that have at least some physical activity. Tobacco consumption is a risk factor as well [43], existing studies that quantify the increase of risk up to 30% [44, 45]. Regarding family history, in the 20% of cases a relative had previously suffered a CRC [46].

Screening programs can be carried out only in case that their effectiveness have been demonstrated and their cost, including the treatments of the diagnosed patients, is affordable. Moreover, screening tests should be available in convenient places and not be painful and overly time-consuming in order to prevent a low participation of the population. The criteria followed by the World Health Organization (WHO) for assessing the benefits, risks and cost of a cancer screening are detailed in [47].

Because of its large incidence rate, as well as a long asymptomatic phase and treatability of precancerous lesions, CRC is an ideal target for screening. An early detection increases greatly the survival probability and decreases the cost of the treatments, since early neoplastic lesions require simpler surgical resections and cares in comparison with advanced stages of the disease. Among the different screening methods, the colonoscopy procedure is used as the main method in many countries. Besides, in case that non-invasive tests return abnormal or suspicious results, a colonoscopy has to be performed anyway. Therefore, due to its spread implementation, improving the colonoscopy procedure even slightly can have a great impact in the diagnosis of patients.

1.3 Electromagnetic differences between normal and cancerous tissues

Almost a century ago, a group of researchers stated that malignant tumours have higher capacity than benign tumours or normal tissues [48]. After their claim, other researchers started to contribute to the study of the interactions between biological matter and electromagnetic waves. A few studies were performed since then, but it was not until the 1980s when the number of works grew significantly. In general, these studies report the permittivity and/or the conductivity of some biological tissues.

While most of them were carried out with the aim at obtaining the electromagnetic properties of normal tissues, a minority was focused on obtaining the properties of cancerous tissues as well. But still, there is a non-negligible volume of studies in which the dielectric properties of both healthy and malignant tissues have been assessed. Many of them have found out significant differences between the properties of healthy and malignant tissues. Joines and his colleagues discover that the absorption of cancerous tissues is higher than in their analogous healthy ones [49, 50]. In [51], several normal and malignant *ex vivo* human tissue samples were measured in the 50 - 900 MHz frequency band, showing that the dielectric properties of malignant tissues had generally larger values than those of healthy ones. In [52], similar differences were obtained up to 5 GHz. The xenograft model was used, in which human tumours were cultivated in mice, grown, extracted and measured just after resection. As measurements were performed in "almost *in vivo* conditions", the obtained properties of malignant tissues are slightly higher than the data gathered from other sources. In [53], authors investigated the differences between normal, malignant and cirrhotic human liver from 0.5 to 20 GHz, concluding as well that statistically significant differences exist between the dielectric properties of *ex vivo* normal and malignant liver tissue. Besides, breast cancer has been one of the most investigated [54, 55]. This is due to the fact that the major electromagnetic differences between malignant and healthy cells have been obtained for this tissue, making it easier the development of cancer detection applications.

Clarbruno Verdruccio discovered that malignant and healthy tissues differ in their interaction with electromagnetic waves since proteins acquire more surface charges in malignant tumours, and the attraction of these charges for water molecules results in the presence of more "bound water" [56]. Moreover, dramatic changes in the metabolism, intercellular communication, and adhesion properties of cancer cells result in the modification of the number and nature of membrane proteins. Thanks to these findings, a prototype of

a device containing a non-linear tunable oscillator has been developed and used with encouraging results in the diagnosis of prostate [56–60], breast [61], thyroid [62], gastric [63], rectal [64] and bladder cancer [65]. The operating principle of this non-invasive device, known as Tissue Resonance InterferoMeter Probe (TRIMProb) and presently manufactured by Tema Sinergie (Faenza, Italy), is expounded in [56, 66]. The device is externally placed near the part of the patient's body that is under analysis and, according to the authors, it can detect a decrement of the received signal at the fundamental frequency if it finds cancerous tissue due to the tissue's damping effects.

TRIMProb is not the only device that make use of the interaction between cancerous cells and electromagnetic waves for cancer detection. Other devices have been developed to detect cancerous tissues, most of them focused on breast tissue. A review of the recent advances in microwave imaging for detecting breast cancer is provided in [67]. However, it is rather surprising that there is barely any cancer application based on measuring directly the electromagnetic properties of healthy and malignant tissues. To the best of our knowledge, only a device known as MarginProbe® has been deployed in this way, and again thought to be used for breast cancer [68].

As exposed at the previous section, for CRC detection and diagnosis, the colonoscopy is used not only as a main screening procedure but also in case that non-invasive tests return abnormal or suspicious results. In this dissertation, the development of applications for CRC detection based on measuring directly the electromagnetic properties of suspicious tissues is assessed, with the aim of complementing the colonoscopy rather than as an alternative to it. One important reason of selecting colon as a target of this work lies in the fact that its tissues can be accessed rather easily during endoscopy inspections.

1.4 Objectives and scope

In this dissertation, we investigate the most suitable method to obtain the dielectric properties of biological tissues and then we use it for two main objectives. On the one hand, we aim at **developing a collection of the electromagnetic properties of biological tissues at *in vivo* conditions**, focusing on the tissues of the thoracic and the abdominal regions. The main novelty of this collection lies in the great number of measured *in vivo* tissues, all of them characterized for the same wide frequency band (from 0.5 to 26.5 GHz), on the same animal species and under the same conditions. On the other hand, we aim at adapting this system **to propose applications to detect colorectal cancer that can be used within colonoscopy procedures**. We will take advantage of the fact that the differences in the biological structure of

cancerous cells with respect to non-cancerous tissue are translated as well in differences in the dielectric properties.

Dielectric characterization technique

- **To deploy and improve the accuracy of an open-ended coaxial system.** The performance of a commercial system is investigated at first. Afterwards, a new calibration procedure is proposed and assessed with the aim at reducing the uncertainty of the selected characterization system.

Measurement of biological samples

- **To measure the electromagnetic properties of biological tissues at *in vivo* conditions.** Most of the dielectric characterization studies have limitations either in the measurement conditions, the working frequency bandwidth or the number of characterized tissues. Therefore, we aim at making use of our deployed system in order to give a further insight regarding this matter.

- **To measure the electromagnetic properties of normal and pathological colon tissues, including cancer as well.** The objective is to find differences within the dielectric properties of colon healthy and pathological tissues that can be the basis of potential colorectal cancer detection applications. To this end, human colon samples are first collected from colonoscopy and surgery procedures and then characterized in *ex vivo* conditions.

CRC detection applications

- **To propose potential applications for colorectal cancer detection**. Based on the open-ended coaxial method, the objective is to propose different approaches for developing colon cancer detection applications.

- **To evaluate the performance of the preliminary cancer detection applications**. The proposed systems will be analyzed in terms accuracy of diagnosis (sensitivity, specificity and predictive values) and technical requirements for further implementation.

1.5 Thesis overview

This thesis is divided in six chapters and one additional appendix. The reader should refer to Section 1.6 for a complete reference of the publications originated from the work carried out in the thesis. The organization and content of each chapter of this thesis is summarized below.

Chapter 2 describes the measurement system deployed and improved for this thesis. First of all, we present the electromagnetic properties that will be measured in the subsequent chapters. The available methods for measuring these properties are summarized and the motivation for selecting the open-ended coaxial technique is provided. Then, a set of potential calibration procedures are evaluated, and finally the total uncertainty of the system achieved with the proposed calibration procedure is quantified. Publication [C3], listed in Section 1.6, is derived from this chapter.

Chapter 3 presents a collection of *in vivo* dielectric properties of the biological tissues. This is the largest *in vivo* database published so far, and measurements are focused on the tissues of the abdominal and the thoracic regions. An analysis of the data is performed, focusing on the uncertainty of the results, and a comparison with other relevant publications of the field is provided as well. Publications [J1], [C1], and [C2], listed in Section 1.6, are derived from this chapter.

In **Chapter 4**, the electromagnetic properties of the different types of colon tissues collected in this thesis are detailed. Two different sources of human colon tissue have been collected: samples obtained from colonoscopy procedures and samples gathered from surgery interventions. The protocol for gathering, manipulating and measuring the samples is provided, and the results are presented and discussed in both cases. The differences between healthy and non-healthy colon tissues are quantified. Publication [J2], listed in Section 1.6, is derived from this chapter.

Chapter 5 is focused on presenting potential applications for colon cancer detection based on both the open-ended coaxial system and the results reported in the previous chapter. Two different approaches have been studied: an *ex vivo* approach, which aims at measuring suspicious samples right after their removal with the colonoscopy, and an *in vivo* one, which can be embedded within a colonoscope and performs the diagnosis *in situ*. A preliminary analysis of the latter approach is provided. Publication [C6], listed in Section 1.6, is derived from this chapter.

This thesis concludes with the **Chapter 6**, where the general conclusions are summarized. Future research lines derived from this work are also listed at the end of this chapter. In addition, an extra appendix is reported at the end of the document.

1.6 Contributions

1.6.1 Publications and activities stemming to this thesis

International journals

[J1] **Alejandro Fornés Leal**, Narcís Cardona, Matteo Frasson, Sergio Castelló Palacios, Andrea Nevárez, Vicente Pons Beltrán, Concepción García Pardo, "Dielectric Characterization of *In Vivo* Abdominal and Thoracic Tissues in the 0.5–26.5 GHz Frequency Band for Wireless Body Area Networks," *IEEE Access*, vol. 7, pp. 31854-64, March 2019.

[J2] **Alejandro Fornés Leal**, Concepción García Pardo, Matteo Frasson, Vicente Pons Beltrán, Narcís Cardona, "Dielectric characterization of healthy and malignant colon tissues in the 0.5–18 GHz frequency band," *Physics in Medicine and Biology*, vol. 61, no. 20, pp. 7334-46, Oct. 2016.

[J3] Concepción García Pardo, Carlos Andreu Estellés, **Alejandro Fornés Leal**, Sergio Castelló Palacios, Sofía Pérez Simbor, Martina Barbi, Ana Vallés Lluch, Narcís Cardona, "Ultrawideband Technology for Medical In-Body Sensor Networks: An Overview of the Human Body as a Propagation Medium, Phantoms, and Approaches for Propagation Analysis," *IEEE Antennas and Propagation Magazine*, vol. 6, no. 3, pp. 19-33, June 2018.

[J4] Sergio Castelló Palacios, **Alejandro Fornés Leal**, Concepción García Pardo, Narcís Cardona, Ana Vallés Lluch, "Tailor-Made Tissue Phantoms Based on Acetonitrile Solutions for Microwave Applications up to 18 GHz," *IEEE Transactions on Microwave Theory and Techniques*, vol. 64, no. 11, pp. 3987-94, Nov. 2016

International conferences

[C1] **Alejandro Fornés Leal**, Concepción García Pardo, Sofía Pérez Simbor, Narcís Cardona, "Impact of the Variability of the EM Properties of Biological Tissues on UWB Channel Modelling for Implanted Devices," *IEEE 13th European Conference on Antennas and Propagation (EUCAP)*, pp. 1-5, Krakow, Poland, April 2019.

[C2] **Alejandro Fornés Leal**, Concepción García Pardo, Matteo Frasson, Sergio Castelló Palacios, Andrea Nevárez, Vicente Pons Beltrán, Narcís Cardona, "Variability of the Dielectric Properties Due to Tissue Heterogeneity and Its Influence on the Development of EM Phantoms," *IEEE*

29th Annual International Symposium on Personal, Indoor, and Mobile Radio Communications (PIMRC), pp. 365-9, Bologna, Italy, Sept. 2018.

[C3] **Alejandro Fornés Leal**, Concepción García Pardo, Sergio Castelló Palacios, Ana Vallés Lluch, Narcís Cardona, "Accurate Broadband Measurement of Electromagnetic Tissue Phantoms Using Open-Ended Coaxial Systems," *IEEE 11th International Symposium on Medical Information and Communication Technology (ISMICT)*, pp. 32-6, Lisbon, Portugal, Feb. 2017.

[C4] Sergio Castelló Palacios, Concepción García Pardo, **Alejandro Fornés Leal**, Narcís Cardona, Ana Vallés Lluch, "Full-spectrum phantoms for cm-wave and medical wireless communications," *IEEE 12th European Conference on Antennas and Propagation (EUCAP)*, pp. 1-3, London, England, April 2018.

[C5] Sergio Castelló Palacios, Concepción García Pardo, **Alejandro Fornés Leal**, Narcís Cardona, María Alloza-Pascual, Ana Vallés Lluch, "Initial Results of Semisolid Phantoms Based on Synthetic Hydrogels for the cmWave Band," *IEEE 29th Annual International Symposium on Personal, Indoor, and Mobile Radio Communications (PIMRC)*, pp. 1128-9, Bologna, Italy, Sept. 2018.

[C6] Sergio Castelló Palacios, Concepción García Pardo, **Alejandro Fornés Leal**, Narcís Cardona, Ana Vallés Lluch, "Wideband phantoms of different body tissues for heterogeneous models in body area networks," *39th Annual International Conference of the IEEE Engineering in Medicine and Biology Society (EMBC)*, pp. 3032-5, Seogwipo, South Korea, July 2017.

[C7] Sergio Castelló, Concepción García Pardo, **Alejandro Fornés Leal**, Narcís Cardona, Ana Vallés Lluch, "Formulas for Easy-To-Prepare Tailored Phantoms at 2.4 GHz ISM Band," *IEEE 11th International Symposium on Medical Information and Communication Technology (ISMICT)*, pp. 27-31, Lisbon, Portugal, Feb. 2017.

Patents

[P1] Narcís Cardona, Ana Vallés Lluch, Concepción García Pardo, Sergio Castelló, **Alejandro Fornés Leal**, "Modelo sintético de tejidos biológicos para la evaluación de la transmisión inalámbrica de ondas electromagnéticas," *Patent Number: ES2575731A1, PCT/ES2016/070*, June 2016.

COST technical documents

[TD1] **Alejandro Fornés Leal**, Concepción García Pardo, Sergio Castelló Palacios, Ana Vallés Lluch, Narcís Cardona, "Accurate Broadband Measurement of Electromagnetic Tissue Phantoms Using Open-Ended Coaxial Systems," *3rd MC and Technical Meeting, European COST IC15104 action*, Lisbon, Portugal, Feb. 2017.

[TD2] **Alejandro Fornés Leal**, Concepción García Pardo, Matteo Frasson, Sergio Castelló Palacios, Andrea Nevárez, Vicente Pons Beltrán, Narcís Cardona, "Variability of the Dielectric Properties Due to Tissue Heterogeneity and Its Influence on the Development of EM Phantoms," *8th MC and Technical Meeting, European COST IC15104 action*, Podgorica, Montenegro, Oct. 2018.

Supervision of bachelor thesis

[SP1] Andrea Parra Escrig, "Análisis del uso de sondas electromagnéticas para la detección precoz de lesiones colorrectales malignas," *Universitat Politècnica de València*, July 2018, Supervisors: Valery Naranjo Ornedo, Narcís Cardona, **Alejandro Fornés Leal**.

Research projects

[RP1] Electromagnetic Probe for Early Tumour Detection(UPV-FE-2017-B04).

- Funding institution: Universitat Politècnica de València, Spain.
- Start date: 01/05/2018
- Duration: 18 months

[RP2] Coalición Europea para la Detección del Cáncer basado en Técnicas Electromagnéticas (EUIN2017-88272).

- Funding institution: Agencia Estatal de Investigación.
- Start date: 01/01/2017
- Duration: 24 months

1.6.2 Other publications related to the thesis

International journals

[J5] Sergio Castelló Palacios, Concepción García Pardo, María Alloza Pascual, **Alejandro Fornés Leal**, Narcís Cardona Marcet, Ana Vallés Lluch:

"Gel Phantoms for Body Microwave Propagation in the 2 - 26.5 GHz Frequency Band", *IEEE Transactions on Antennas and Propagation*, May 2019, published in early access.

[J6] Carlos Andreu Estellés, Sergio Castelló Palacios, **Alejandro Fornés Leal**, Concepción García Pardo, Ana Vallés Lluch, Narcís Cardona, "Spatial In-Body Channel Characterization Using an Accurate UWB Phantom," *IEEE Transactions on Microwave Theory and Techniques*, vol. 64, no. 11, pp. 3995-4002, Nov. 2016.

[J7] Gerardo Martínez Pinzón, Narcís Cardona, Concepción García Pardo, **Alejandro Fornés Leal**, Jefferson A. Ribadeneira, "Spectrum Sharing for LTE-A and DTT: Field Trials of an Indoor LTE-A Femtocell in DVB-T2 Service Area," *IEEE Transactions on Broadcasting*, vol. 62, no. 3, pp. 552-61, Sept. 2016.

International conferences

[C8] Carlos Andreu Estellés, Concepción García Pardo, **Alejandro Fornés Leal**, Marta Cabedo Fabrés; Narcís Cardona, "UWB In-Body Channel Performance by Using a Direct Antenna Designing Procedure," *11th European Conference on Antennas and Propagation (EUCAP)*, pp. 278-82, Paris, France, March 2017.

[C9] Concepción García Pardo, **Alejandro Fornés Leal**, Narcís Cardona, Raúl Chávez Santiago, Jacob Bergsland, Ilangko Balasingham, Sverre Brovoll, Oyvind Aardal, Svein-Erik Hamran, Rafael Palomar, "Experimental ultra wideband path loss models for implant communications," *IEEE 27th Annual International Symposium on Personal, Indoor, and Mobile Radio Communications (PIMRC)*, pp. 1-6, Valencia, Spain, Sept. 2016.

National journals

[NJ1] Concepción García Pardo, Carlos Andreu Estellés, **Alejandro Fornés Leal**, Sergio Castelló Palacios; Sofía Pérez Simbor, Martina Barbi, Antonio Vila Jiménez, Marta Cabedo Fabrés, Vicente Pons Beltrán, Matteo Frasson, Ana Vallés Lluch, Narcís Cardona Marcet, "Wireless Communications for Medical In-Body Devices: Challenges for In-body Propagation," *Waves*, year 9, pp. 5-16, Sept. 2017.

National conferences

[NC1] Concepción García Pardo, Carlos Andreu Estellés, Sofía Pérez Simbor, Sergio Castelló Palacios, **Alejandro Fornés Leal**, Martina Barbi, Ana Vallés Lluch, Narcís Cardona, "UWB Propagation for Medical In-body Devices," *XXXIII Simposium Nacional de la Unión Científica Internacional de Radio (URSI)*, Granada, Spain, Sept. 2018.

Chapter 2

Measurement system

This chapter aims at presenting the open-ended coaxial method used in this thesis for measuring the electromagnetic properties of biological samples. The improvements performed on the calibration procedure of this method are described, and the accuracy achieved by using this procedure is provided. The principle of operation exposed in this chapter is used in the measurements presented in Chapter 3 and Chapter 4. Besides, the measurements presented in Chapter 5 have been obtained considering small modifications on this principle of operation, modifications that will be detailed further on that chapter.

2.1 Dielectric properties of biological tissues

As explained in the previous chapter, the interaction between biological materials and electromagnetic waves can be characterized by means of their dielectric properties: permittivity, conductivity and permeability. The permeability (μ_0) describes the magnetization of a material in response to an applied magnetic field. At microwave frequencies, the biological tissues have permeabilities that are close to that of free space, being independent of frequency [69]. On the other hand, both permittivity and conductivity are properties that are highly frequency dependent.

The permittivity ϵ [F/m] of a material describes its tendency to polarize when an electromagnetic field is applied to it, which is related to its capacity to store energy. The permittivity of the biological tissues is highly related to their water content: the larger the water content of a tissue, the greater its permittivity. The permittivity is generally normalized to that of the vacuum, as one can observe in the following equation:

$$\epsilon_r(f) = \epsilon(f)/\epsilon_0 = \epsilon'_r(f) - j\epsilon''_r(f) \tag{2.1}$$

where ϵ_r is the relative permittivity, f [Hz] is the frequency, ϵ_0 [F/m] is the permittivity of the vacuum, ϵ'_r is the real part of the relative permittivity, known as dielectric constant, and ϵ''_r is its imaginary part, known also as loss factor. For the sake of simplicity, we will refer to relative permittivity simply as permittivity in the remainder of this dissertation.

The conductivity σ [S/m] is a property that describes the ease at which an electric charge can pass through a material. It comprises the electrical losses due to ionic conductivity and those due to dielectric polarization. The conductivity can be related to the loss factor as:

$$\sigma(f) = \sigma_d(f) + \sigma_i(f) = 2\pi f \epsilon_0 \epsilon''_r(f) \tag{2.2}$$

where σ_d [S/m] is the conductivity due to dielectric polarization and σ_i [S/m] is the ionic conductivity.

The permittivity of biological tissues presents some dispersion regions where the value of permittivity varies strongly with frequency [70]. At these regions, the dielectric constant, which always decrease with frequency, shows a steeper slope. The four major regions are α, β, δ and γ, affecting in different frequency bands [71]. With the aim at making permittivity data accessible, reports usually fit their measurements into a Cole-Cole equation. The Cole-Cole equation is given by:

$$\epsilon_r(f) = \epsilon_\infty + \sum_{m=1}^{M} \frac{\Delta\epsilon_m}{1 + (j\omega\tau_m)^{(1-\alpha_m)}} + \frac{\sigma_s}{j\omega\epsilon_0} \tag{2.3}$$

where M is the number of poles of the Cole-Cole equation (each of them representing a particular dispersion region), ω [rad/s] is the angular frequency and $\Delta\epsilon_m$, τ_m [s], α_m and σ_s [S/m] are the fitting coefficients of the equation.

2.2 Dielectric characterization techniques

Nowadays, many techniques for obtaining the electromagnetic properties of materials are available. The selection of a suitable technique for a particular material depends on various factors like its shape, thickness, physical state and the frequencies in which we want to characterize it. In general, a Vector Network Analyzer (VNA) is used to get the physical measurements that will be translated into the dielectric properties of a material. A VNA measures the scattering parameters of a device or network: it sends a signal with a specific power from one of its ports and computes how much energy comes back to

that port and arrives to the rest, for each frequency of interest. For instance, taking as a reference a system of two ports (e.g., filters, amplifiers...) in which the signal is transmitted by the first port and received in the second one, the parameter corresponding to the signal reflected to the first one is known as reflection coefficient or S_{11}, and the transmitted to the second port is known as transmission coefficient or S_{21}. The most representative characterization techniques are:

Free space method

This method allow measuring a Material Under Test (MUT) at high temperatures and hostile environments. It consists of two antennas connected to a VNA, typically facing each other, with the MUT placed between them. A previous calibration of the elements as well as measurements with reference materials are necessary prior to characterize any material. Once this calibration is completed, the permittivity of a material can be extracted from an S_{21} measurement.

- **MUT types**: They may require some preparation, since they must be large, flat, homogeneous solids with parallel faces.
- **Working frequencies**: From 6 GHz up to 500 GHz. The bandwidth depends on the antennas used.
- **Advantages**: Wide bandwidth, allows characterizing at high frequencies, it can be used in high temperature environments and it can measure also the permeability of materials.
- **Disadvantages**: The accuracy can be reduced by the appearance of reflections between the antennas and the MUT, and by diffraction effects at the edge of the MUT.

Transmission line method

This method consists of a transmission line (i.e., a coaxial line or a waveguide) connected to a VNA. The MUT is placed in a prepared section of the transmission line. A previous calibration of the elements as well as measurements with reference materials are necessary prior to characterize any material. Once this calibration is completed, the permittivity of a material can be extracted from S_{11} and S_{21} measurements.

- **MUT types**: They require a previous preparation, since they should fit the section as tightly as possible. They should be homogeneous, with flat and perpendicular faces.

- **Working frequencies**: From 50 MHz up to 75 GHz approximately. The bandwidth depends on the transmission line used.
- **Advantages**: Accurate for measuring lossy materials. It allows permeability measurements as well.
- **Disadvantages**: Accuracy may be limited by the presence of air gaps. It is lower for low loss materials.

Resonant methods

There are many resonant techniques available: Fabry-Perot resonators, split cylinder resonators, resonant cavities etc. These methods measure the quality factor (Q) and the resonant frequency of the cavity using again a VNA. The electromagnetic properties of a MUT can be obtained from the change of these factors with respect to the empty case, without the need of a previous calibration.

- **MUT types**: They may require some preparation to be inserted in the cavity. Samples have to be small, and some cavities work with thin, flat sheets.
- **Working frequencies**: Depending on the specific method considered, they allow measurements below 1 GHz and up to more than 100 GHz.
- **Advantages**: Great accuracy, does not need a previous calibration and it is indicated for low loss materials.
- **Disadvantages**: Typically limited to a single frequency or low bandwidth measurements. It requires a VNA with high frequency resolution.

Parallel plates

This is the only listed technique which does not make use of a VNA. In this case, the system consists of an impedance analyzer connected to two electrodes that form a capacitor, with the MUT placed between those electrodes. The permittivity can be extracted from a measurement of capacity.

- **MUT types**: They must be flat, thin sheets, and thus they require of a careful previous preparation.
- **Working frequencies**: From 20 Hz up to 1 GHz, depending on the impedance analyzer used.

- **Advantages**: Very accurate method useful to characterizing electronic substrates.
- **Disadvantages**: The maximum operating frequency is limited, and the measured MUTs require of a careful preparation.

Open-ended coaxial method

This technique consists of a rigid coaxial cable, with a flat cut end, connected to a VNA through the necessary cables and connectors. A previous calibration of the elements as well as measurements with reference materials are necessary prior to characterize any material. Once this calibration is completed, the permittivity of a MUT can be extracted from an S_{11} measurement.

- **MUT types**: They must be non-magnetic and homogeneous liquids or semi solids.
- **Working frequencies**: From 50 MHz up to 67 GHz, depending on the probe. It allows measuring very wide bandwidths.
- **Advantages**: Does not require of a previous sample preparation and its accuracy is better for lossy materials.
- **Disadvantages**: Its accuracy is limited, and the calibration procedure can compromise the measurements.

2.3 Open-ended coaxial system

Among the different characterization techniques, we chose the open-ended coaxial method to perform the measurements required to carry out the present thesis due to multiple reasons. As we aimed at measuring biological tissues, we needed a system capable of characterizing semi-solid small samples, samples that should be manipulated as low as possible to avoid dehydration. Its low measurement time also reduces potential tissue dehydration. Moreover, this technique allows characterizing tissues in wide measurement bandwidths, giving thus much more electromagnetic information that a method with a lower acquisition bandwidth.

The system used in this thesis is shown in the Fig. 2.1. It consists mainly of a VNA (Keysight's Fieldfox N9918A), an open-ended coaxial probe (Keysight's N1501A slim form probe), and a computer to acquire, process and store the measurements. In addition, calibration standards, hardware to connect the VNA with the probe and the computer (adapters, flexible coaxial cable and

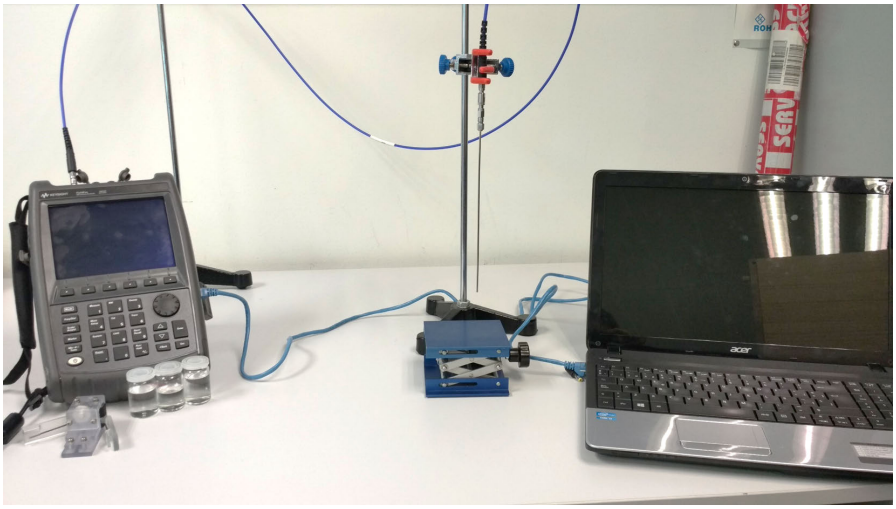

Figure 2.1: Open-ended coaxial system used in this thesis.

Ethernet cable) and mechanical elements to place the biological samples in contact with the sensor (laboratory stand, sample elevator and glass sheets) are required.

In this section, we aim at explaining different parts of the utilized system. First of all, the equations involved for obtaining the permittivity are developed. Then, the choice of the calibration standards is assessed and motivated. The total uncertainty of the measurement system is evaluated considering the selected standards. And finally, the main software application used during the execution of this thesis is presented.

2.3.1 Principle of operation

As aforementioned, the open-ended coaxial method aims at obtaining the dielectric properties of materials from measurements of electromagnetic reflections. This technique is based on the fact that the reflection that occurs in the sensor's tip varies depending on the dielectric properties of the material that is placed on it. In literature, different approaches have been used to relate a physical reflection measurement with its corresponding electromagnetic properties. Some authors make use of mathematical approaches by developing Taylor series [72], while other authors use the data obtained from electromagnetic simulation software [73] and lastly others apply equivalent circuit models [74].

Equivalent circuit model

Within the framework of this thesis, we have made use of the equivalent circuit model depicted in the Fig. 2.2 since it is accurate enough without involving an excessive complexity [75]. This model describes the normalized admittance y of the discontinuity at the measurement plane. Complex equations need to be avoided since results should be given and store in a few seconds, thinking in possible future applications in a medical environment (i.e., if many measurements have to be performed by a medical expert, the elapsed time among them should be as low as possible).

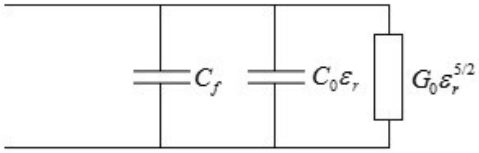

Figure 2.2: Equivalent circuit model of the open-ended coaxial probe's tip.

This model is composed of a free-space radiation conductance, $G_0\epsilon_r^{5/2}$, and two capacity terms, $C_0\epsilon_r$ and C_f, which denote the fringing fields outside the coaxial cable and in its dielectric. Thus, with this model the admittance of the probe can be related to the permittivity of the measured material by:

$$y(w, \epsilon_r) = G_0 Z_0 \epsilon_r^{5/2} + jwZ_0(\epsilon_r C_0 + C_f) \tag{2.4}$$

where w is the angular frequency and Z_0 is the characteristic impedance of the sensor. The relationship between the reflection coefficient Γ_m and the permittivity of the MUT can be obtained simply as:

$$\Gamma_m(w, \epsilon_r) = \frac{1 - y(w, \epsilon_r)}{1 + y(w, \epsilon_r)} = \frac{1 - G_0 Z_0 \epsilon_r^{5/2} - jwZ_0(\epsilon_r C_0 + C_f)}{1 + G_0 Z_0 \epsilon_r^{5/2} + jwZ_0(\epsilon_r C_0 + C_f)} \tag{2.5}$$

Error correction procedure

The reflection coefficient of the previous equation is ideal. This means that, if the reflection coefficient ρ_m captured by the VNA is used directly as Γ_m in 2.5, the returned permittivity would not be correct due to two reasons. On the one hand, the measurement plane is not located in the discontinuity, but in the VNA's port. On the other hand, the instrumentation (e.g., cables, connectors)

introduces errors because of its imperfections, which lead to a higher inaccuracy of the results. Hence, in order to minimize those errors and to translate the measurement plane to the sensor's tip, an error correction procedure must be applied. To this end, the elements located between the VNA's port and the sensor's tip are modelled as a two-port network, also known as "error network" [76, 77]. In this manner, an ρ_m measurement can be related to the reflection coefficient at the discontinuity as:

$$\Gamma_m = \frac{\rho_m - E_{11}}{\rho_m E_{22} + E_{12}E_{21} - E_{11}E_{22}} \tag{2.6}$$

where E_{11}, E_{12}, E_{21} and E_{22} are the scattering parameters of the error network. Developing the two previous equations, a simple relationship between the captured reflection coefficient ρ_m and the admittance y is obtained:

$$\rho_m = \frac{\frac{E_{11}+E_{12}E_{21}-E_{11}E_{22}}{1+E_{22}} + y\frac{E_{11}-E_{12}E_{21}+E_{11}E_{22}}{1+E_{22}}}{y + \frac{1-E_{22}}{1+E_{22}}} \tag{2.7}$$

Then, the Eq. 2.4 is combined jointly with the latter in order to relate the measured reflection with the corresponding permittivity. Then, the constants are grouped in four unknowns coefficients giving rise to Eq. 2.8. It should be mentioned that a bilinear transformation is applied to 2.4 before substituting it into 2.7 in order to facilitate this grouping of constants, as done also in [76, 78].

$$\rho_m = \frac{A_2 + A_3(\epsilon_r + G_n\epsilon_r^{5/2})}{A_1 + \epsilon_r + G_n\epsilon_r^{5/2}} \tag{2.8}$$

where A_1, A_2, A_3 and G_n are unknown coefficients that depend on the frequency, the characteristic impedance of the sensor, the equivalent circuit model and the parameters of the error network. These coefficients can be expressed as:

$$A_1 = \frac{1 - E_{22}}{(1 + E_{22})jwC_0Z_0} + \frac{C_f}{C_0} \tag{2.9}$$

$$A_2 = \frac{E_{11} + E_{12}E_{21} - E_{11}E_{22}}{(1 + E_{22})jwC_0Z_0} + \frac{C_f}{C_0}\frac{E_{11} - E_{12}E_{21} + E_{11}E_{22}}{(1 + E_{22})} \tag{2.10}$$

$$A_3 = \frac{E_{11} - E_{12}E_{21} + E_{11}E_{22}}{1 + E_{22}} \tag{2.11}$$

$$G_n = \frac{G_0}{jwC_0} \tag{2.12}$$

Many researchers that consider equivalent circuit models neglect the term G_n, especially when the sensor is not radiating into de MUT [76, 79]. Still, we consider it since the solution is more rigorous and it allows calibrating with an extra standard in the calibration procedure.

System calibration

The calibration procedure is quite simple. The Eq. 2.8 has four unknowns that have to be found out in order to relate the measured reflection coefficient with its corresponding permittivity. Therefore, the reflections of four calibration standards whose dielectric properties are well-known have to be measured in order to solve a system of four equations with four unknowns. Since the permittivity varies depending on the frequency, these coefficients have to be solved for each frequency of interest.

2.3.2 Choice of calibration standards

The calibration plays a crucial role since thanks to this process a reflection measurement can be related to a permittivity value, as aforementioned. In general, authors make use of air, short circuit and water as calibration standards because they are easily accessible and their dielectric properties are characterized in literature with great accuracy. Nevertheless, using this "typical calibration" has some drawbacks. Due to the large gap between the dielectric properties of air and those of water and short circuit, the intermediate dielectric region is not perfectly characterized [80]. This is an important factor as the properties of all tissues are found in this region, and therefore enhancing the accuracy of the system at this region would improve the results presented throughout the thesis. In addition, using just these references provides a limited accuracy for loss factor, especially above a few GHz [81].

Within the framework of this thesis, an extra liquid standard is added to the typical calibration for improving its accuracy. The candidate liquids have to meet two considerations: they should be cheap and easily accessible for laboratories, and their electromagnetic properties have to be known accurately (this is, previously characterized with a method with low uncertainty). In this section, the accuracy achieved by calibrating "typically" and with "enhanced" calibrations is assessed by measuring some test liquids whose electromagnetic properties are also well-known. They were selected trying to mimic the properties of different types of tissues (i.e., tissues with different degrees of water content). A total of three liquids (hereinafter referred as "tested samples") were measured using four different calibration setups. The calibration setups were:

- **Typical calibration** using open circuit and short circuit standards as well as distilled water.
- Three **enhanced calibrations**, which consist in the addition of one polar liquid to the typical calibration:
  - Typical standards and methanol.
  - Typical standards and ethanol.
  - Typical standards and isopropanol (2-propanol).

As tested samples we used the following liquids, whose permittivity values are reported in [82].

- Ethylene Glycol.
- Dimethyl Sulfoxide (DMSO).
- Butanol (1-butanol).

The dielectric properties of the aforementioned standards and tested samples are depicted in the Fig. 2.3. It should be highlighted that a measurement session consisted simply in measuring consecutively the reflection coefficients of the calibration standards and the tested samples, as all the processing for calibrating and for obtaining the permittivities was performed mathematically afterwards. Five different sessions were carried out in order to minimize the effect of random errors. Measurements were carried out from 0.5 just up to 8.5 GHz because at that point we did not have any VNA that worked at higher frequencies. The error achieved in the dielectric constant by each calibration for each tested sample is computed as shown in Eq. 2.13, in percentage terms by comparing the obtained results with the theoretical values.

$$\Delta\epsilon'_r = 100\left|\frac{\epsilon'_m - \epsilon'_{ref}}{\epsilon'_{ref}}\right| \tag{2.13}$$

where $\Delta\epsilon'_r$ is the error committed in dielectric constant, ϵ'_m is the measured dielectric constant and ϵ'_{ref} is the dielectric constant of the reference. The error committed in loss factor $\Delta\epsilon''_r$ are computed analogously.

The errors made at measuring ethylene glycol samples by the four calibration setups are represented in the Fig. 2.4. One can observe that the lowest error is achieved by the enhanced calibration that uses methanol as the additional calibration standards, in both the real part and the imaginary one. This can be explained by the fact that the permittivities of methanol and ethylene glycol are quite similar in parts of the permittivity, as one can observe in

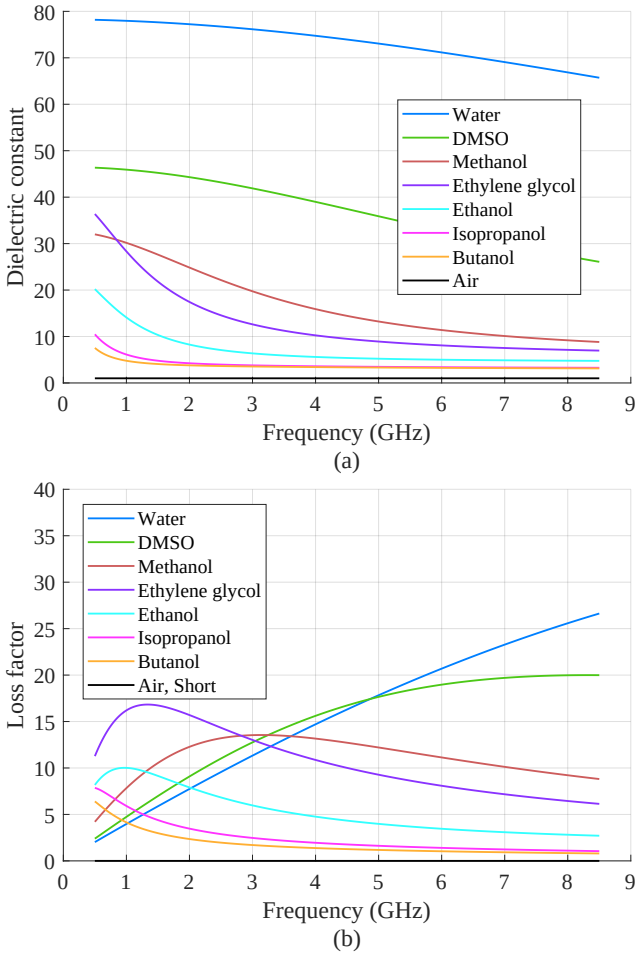

Figure 2.3: Dielectric properties of the calibration standards and the tested samples considered at a temperature of 25 °C: (a) dielectric constant, (b) loss factor.

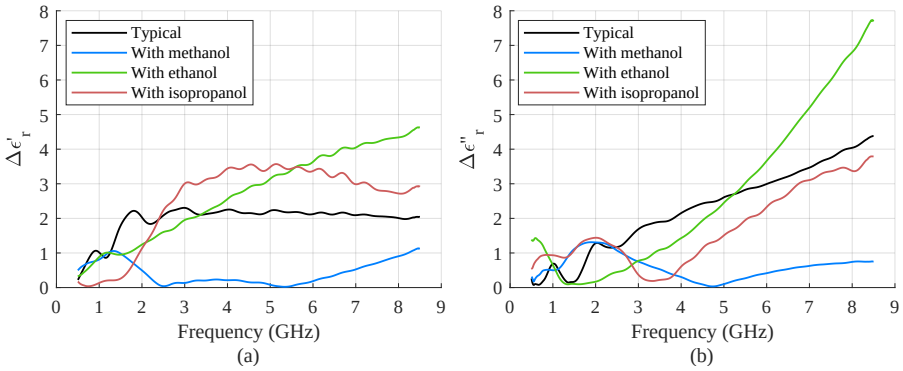

Figure 2.4: Percentage of the errors in the measurement of ethylene glycol with the typical (open, air and water) and the enhanced calibration setups: (a) dielectric constant, (b) loss factor.

the Fig. 2.3. On the contrary, the enhanced calibrations with isopropanol and ethanol are only slightly useful at lower frequencies in comparison to the typical calibration. In particular, the addition of ethanol improves the measurements below 5 GHz, while isopropanol enhances the measurement of the imaginary part, comparing both with the typical calibration.

On the other hand, the errors committed at measuring the permittivity of DMSO's samples are shown in the Fig. 2.5. The conclusions are similar to the previous case. The addition of methanol to the calibration process decreases the error with respect to the typical calibration while the adding the other two liquids only has improved the characterization of the loss factor. Calibrating with either isopropanol or ethanol is not very useful in this case since their respective dielectric constants are very distinct compared to DMSO's.

Lastly, the errors at measuring the permittivity of butanol by each calibration setup are presented in the Fig. 2.6. In this case, all the enhanced calibration proposed achieve higher accuracy than the typical one, being the calibration with ethanol the one that improves more the accuracy of the calibration. For this particular liquid, the addition of methanol has not improved the results with respect to the typical calibration as much as before. Although the errors are higher for this liquids, this is provoked by the low values of permittivity that butanol has, as it can be seen in the Fig. 2.3.

Observing the errors committed by the typical calibration, it can be noticed that it is higher for the loss factor in all cases and it has an increasing trend above 5 GHz, agreeing well with the data presented in [81]. The fact that both the air and the short circuit have the same very low loss factor ($e''_r = 0$, Fig.

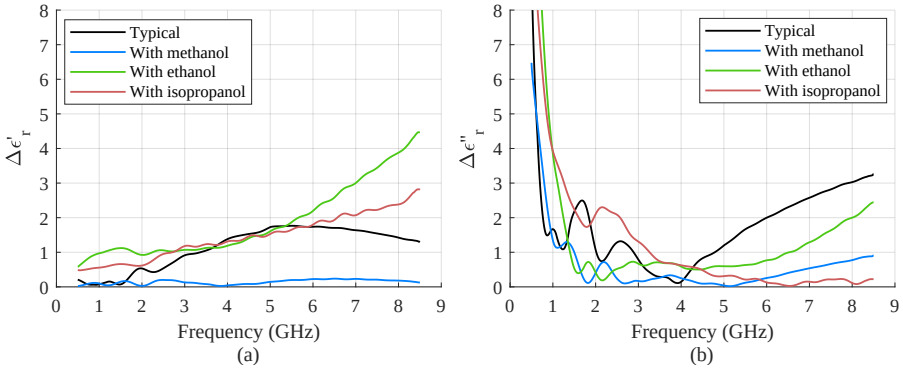

Figure 2.5: Percentage of the errors in the measurement of DMSO with the typical (open, air and water) and the enhanced calibration setups: (a) dielectric constant, (b) loss factor.

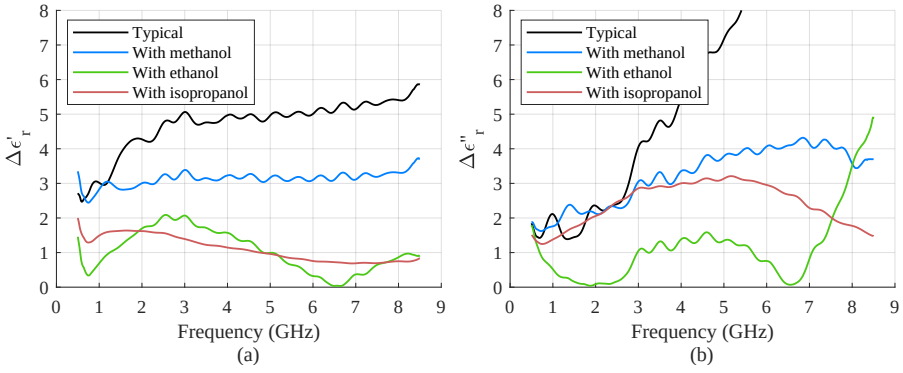

Figure 2.6: Percentage of the errors in the measurement of butanol with the typical (open, air and water) and the enhanced calibration setups: (a) dielectric constant, (b) loss factor.

2.3) makes that the typical calibration is not providing a very good mapping of the imaginary part.

Results are summarized in the Table 2.1, where the percentage errors are averaged for the measured bandwidth. They have proved that the addition of an extra standard to the typical calibration can improve the accuracy of the loss factor greatly, especially if it complements well the properties of the other standards. Since methanol has improved significantly the performance of the calibration for a wider range of permittivities, the **measurements presented in the current dissertation have been performed considering the methanol enhanced calibration, unless otherwise indicated.**

	Ethylene glycol		**DMSO**		**Butanol**	
	$\Delta\epsilon_r'$	$\Delta\epsilon_r''$	$\Delta\epsilon_r'$	$\Delta\epsilon_r''$	$\Delta\epsilon_r'$	$\Delta\epsilon_r''$
Typical calibration	1.98%	2.27%	1.15%	1.74%	4.71%	5.74%
With methanol	0.43%	0.60%	0.14%	0.62%	3.13%	3.24%
With ethanol	2.71%	2.66%	1.88%	1.45%	1.04%	1.13%
With isopropanol	2.52%	1.72%	1.45%	1.21%	1.10%	2.43%

Table 2.1: Averaged errors made by each calibration at measuring the tested liquids.

It should be mentioned that the description and analysis of the results have been performed qualitatively rather than quantitative, as the main objective was to show why we chose methanol by characterizing some test samples rather than the values themselves, which are not the key aspect of the section. In the same manner, the fact that this measurements were carried out only up to 8.5 GHz for the reason commented previously does not compromise the latter results of the thesis, since a more rigorous analysis of the accuracy of the selected calibration is carried out in the following section (this time, up to 26.5 GHz).

2.3.3 Assessment of system's uncertainty

Any measurement system return specific results with a lower or greater amount of uncertainty. In this section, the total uncertainty of the measurement system is evaluated, considering the methanol enhanced calibration described previously. For performing this assessment, the VNA has been configured considering the same parameters that will be used in most of the measurements presented in later chapters: **output power of -10 dBm, IF bandwidth of 1 kHz, and 1601 evenly-spaced frequency points within the 0.5 - 26.5 GHz frequency band**. We followed the assessment methodology described in [83] since they identified the different sources of uncertainty that this method

has and they agree with the guidelines presented by International Organization for Standardization (ISO) [84] and National Institute of Standards and Technology (NIST) [85]. There are four different sources of uncertainty:

- **Repeatability.** This source is related to the random errors that can appear within a measurement session. It was evaluated by measuring the permittivity of 3 homogeneous samples of a saline solution (0.1 M NaCl) in 5 different calibration sessions, obtaining afterwards the Standard Deviation of the Mean (SDM) of this pool of measurements.
- **Systematic errors due to the instrumentation and methodology.** These errors depend on the hardware used and greatly on the calibration procedure chosen. These are evaluated by averaging the permittivities gathered from the saline solutions, and computing the deviation of these mean with the values presented in [86]. The mean permittivity obtained from the saline solution is presented in the Fig. 2.7, jointly with the one used as reference.
- **Drift of the system with time.** This systematic error is caused by slight changes of the performance of the VNA with time and possible rise in warming of the hardware elements. This drifting was evaluated by computing the difference of the permittivity of three saline samples measured just after the calibration, and others performed 15 minutes later (also in 5 different calibration sessions).
- **Cable movement.** This source of errors is related to the movement of the coaxial cable that connects the probe to the VNA, and thus depend on the performance of the coaxial used. In our case, we chose Mini-circuits® FLC-1M-SMSM+, as it has with very low phase noise with bending. Again, errors were evaluated within 5 different calibration sessions in which measurements of the saline solution were carried out in static mode at the calibration position and then repeated after moving the coaxial cable.

The uncertainties were evaluated in laboratory conditions at a temperature of 20 °C. The VNA was turned on 3 hours before doing any of these measurements in order to avoid completely possible changes of its performance during its warming up. It is worth mentioning that the coaxial cable was moved depending on the nature of the measurements. For instance, *ex vivo* measurements could be performed in the calibration position, whereas *in vivo* ones required some movement. The uncertainty related to this source was assessed emulating the kind of bending that occurred during the *in vivo* trials that will be described in future chapters.

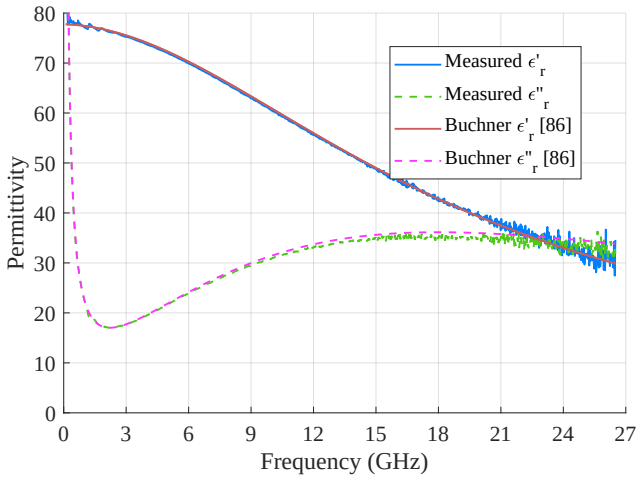

Figure 2.7: Average permittivity of 0.1 M NaCl solutions.

The combined uncertainty is computed as the square root of the sum of the squares of each source, considering as well the distribution of their errors in its calculation as explained in [83]. In the Table 2.2 are presented the values obtained for the different uncertainty sources, as well as the combined uncertainty with and without considering the source related to cable movement. They are presented in relative terms of the relevant parameter, and averaged for three spectrum regions. The uncertainty of the measurement system is higher for loss factor than for dielectric constant, and generally it increases with frequency as also occurs in [83]. This is explained by the fact that the measurement of the imaginary part of the permittivity is more sensitive to small errors in the reflection measurements than the real part.

It should be mentioned that measurements had some noticeable noise above approximately 20 GHz. This extra noise was caused by the VNA used, as connectors, cables and coaxial sensors could work perfectly within the frequencies considered and their performance could be checked with the VNA of another department. Since this noise did not affect to the "shape" of the dielectric properties with frequency (as it was Gaussian), we kept on measuring them throughout the execution of the thesis.

2.3.4 Measurement software

With the aim at facilitating the execution of the several measurement sessions and campaigns required for fulfilling the present thesis, a software application

Frequency Region	Param.	(1)	(2)	(3)	(4)	Combined uncertainty	Combined exc. (4)
0.5 - 10 GHz	ϵ_r'	0.61	0.40	0.05	0.21	0.67	0.66
	ϵ_r''	0.71	0.66	0.12	0.42	0.86	0.81
10 - 18 GHz	ϵ_r'	0.47	0.36	0.10	0.41	0.59	0.52
	ϵ_r''	0.46	2.19	0.28	1.96	1.94	1.35
18 - 26.5 GHz	ϵ_r'	1.84	0.78	0.20	0.95	2.01	1.89
	ϵ_r''	1.94	3.09	0.42	3.51	3.63	2.65

Table 2.2: Values of uncertainty in percentage terms of the relevant parameters averaged for three spectrum regions.

has been developed. This application is responsible of controlling the VNA, gathering the raw measurements, obtaining the related permittivity, represent it and store it. It has been developed in MATLAB, using Standard Commands for Programmable Instruments (SCPI) commands in order to communicate with the VNA. The interface of the software is presented in the Fig. 2.8.

The user interface is connected to the VNA by means of an Ethernet cable, and the SCPI commands are sent after establishing a TCP/IP connection. The interface has the following major features:

- **Configuration of the VNA.** The application allows configuring the acquisition frequencies, the output power and the bandwidth of the Intermediate Frequency (IF) filter of the VNA. One can make use of the default parameters or setting them manually.

- **Calibration of the system.** Once the system is configured and the temperature of the water is set, it guides to the user during the measurement of the calibration standards (air, short circuit, distilled water and methanol). Afterwards, it uses the acquired data to obtain the four unknowns of the Eq. 2.8 to relate a reflection measurement with its corresponding permittivity.

- **Permittivity measurement.** The application guides the user during the capture of reflection coefficient, then it processes the signal to obtain the permittivity and presents it in two figures, one for the dielectric constant and another for the loss factor (or the conductivity).

- **File options.** The interface allows storing measurements of the current session as well as loading previous measurements for comparison purposes. The calibration can be stored as well, in case a failure of the

VNA or the computer occurs preventing the necessity of repeating all the process.

2.4 Conclusion

In this chapter, the dielectric characterization system used for performing the measurements needed for fulfilling the objectives of the thesis is presented. The open-ended coaxial system has been selected, since it has many advantages with respect to the rest of dielectric characterization systems. Its non-destructive nature and its capability of measuring semi-solid materials are needed for developing a cancer detection application that could be applied on soft samples, even directly on living human tissues. The possibility of measuring wide bandwidths (from 0.5 to 26.5 GHz) is very interesting for research, as the frequencies in which a potential CRC detection application would work is unknown. And lastly, its capability of measuring in just a few seconds is of great importance.

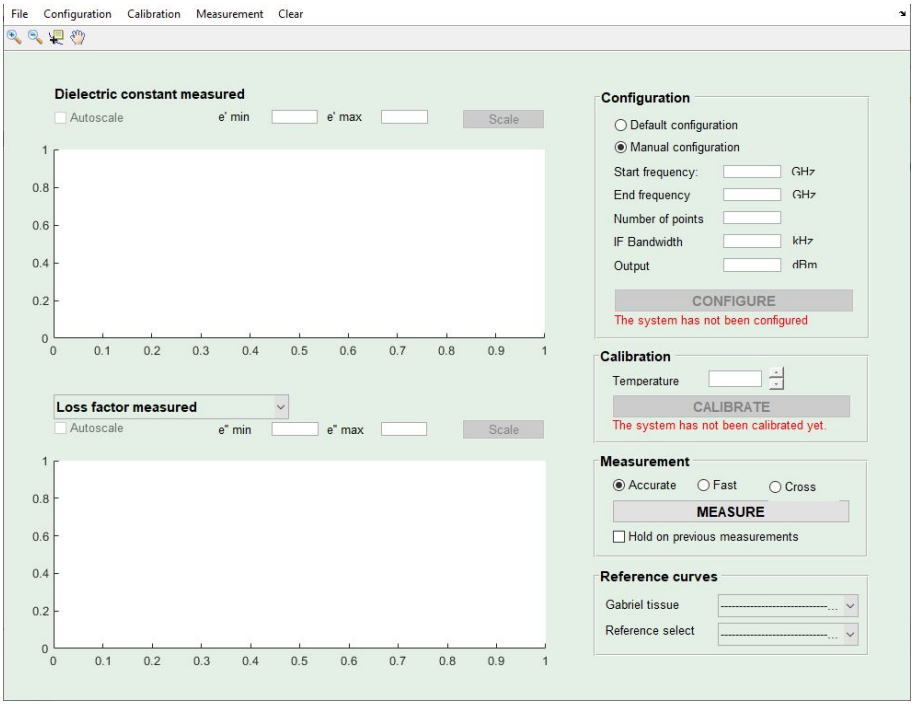

Figure 2.8: Measurement interface developed.

On the one hand, it prevents the issues related to tissue dehydration when measuring *ex vivo* samples. On the other hand, if used for measuring *in vivo*, it would avoid some discomfort for patients as measurements would take a very short amount of time.

The system consists of a VNA connected to a sensor, which is a coaxial with a flat cut end, and a computer for processing the data and obtaining the dielectric properties, as shown in the Fig. 2.1. Its performance is rather simple: the VNA sends a signal of the frequencies of interest through the sensor; then, part of this signal is reflected once it arrives to the material under test and travels back to the VNA; finally, the computer process this reflection in order to obtain its corresponding permittivity. In this chapter, a custom equation for calibrating the system and obtaining the electromagnetic properties has been developed (see Eq. 2.8). This "enhanced calibration" is based on three main principles: an equivalent circuit model used for relating the reflection produced by a particular material at the sensor's end with its dielectric properties, an error correction routine for translating the measurement from the VNA port to the sensor's end, and finally the measurement of four reference materials (two of them liquids) for solving the equation developed and thus being able to obtain the permittivity of a material from its particular reflection.

In general, this kind of systems are calibrated capturing previously the reflection of air, a short circuit and distilled water. Our approach allows measuring a fourth standard, which can provide a better accuracy of the method as we have proved. Besides, we have tested some liquids with the aim at investigating which of them could improve most the performance of the system. **Among the tested samples, methanol has proved to be the better choice as it improves the accuracy of the system regardless of the measured frequency and the permittivity of the tested material.** It should be highlighted that the accuracy of the system increases when measuring a material whose electromagnetic properties are close to those of one of the references. Methanol is a good choice as its properties complement quite well those of the rest of the standards (air, short circuit and distilled water), offering a better mapping between the reflection and the permittivity.

Once the calibration has been settled, the uncertainty of the system has been quantified, evaluating the sources involved: repeatability (related to random errors), errors due to instrumentation and methodology, drift of the system with time and cable movements. As expected, the uncertainty increases with frequency, being higher for loss factor than for the dielectric constant. Combining the different sources, the total uncertainty is around 1.89% and 2.65% for dielectric constant and conductivity, respectively. Considering cable movement (which occurs in those cases in which the sensor is moved after calibrating), these uncertainties increase up to 2.01% and 3.63%.

Lastly, the interface developed for automating these measurements has been presented. This interface, developed in the MATLAB framework and considering SCPI commands, is in charge of sending commands to the VNA, retrieving the captured data, process it and then presenting and storing the dielectric properties obtained. This application as well as the enhanced calibration with methanol are used within the rest of the dissertation, unless otherwise stated.

Chapter 3

Dielectric characterization of biological tissues

In this chapter, the *in vivo* dielectric properties of the tissues of the thoracic and the abdominal region are presented. These measurements are important for updating the most cited and used dielectric database of biological tissues, which was mostly performed on *ex vivo* conditions [87]. The main advantage of the campaign performed is the great number of characterized tissues, all of them measured *in vivo* in a wide frequency bandwidth and from the same animal species, making use of the measurement system described in the previous chapter.

3.1 Introduction

Nowadays, there is a great quantity of works in the literature addressing the dielectric properties of most of the biological tissues. Generally, these studies were performed on animals in diverse conditions: *in vivo*, in which living tissues are measured *in situ*, *ex vivo*, where samples are measured after being removed from the model's body, and *in vitro*, which are the same conditions that the latter approach but also emulating the temperature of the living tissues. There are measurements carried out on humans tissues as well, although the volume of studies is much lower than considering animals.

As many reports started to be carried out in the decade of the 80's, the technology was not so technologically advanced yet. Therefore, there is a lot of interesting works that were carried out without covering a wide bandwidth of the SHF band, and thus their results are limited mainly in frequency. Among

the many published works, the database from [87] is broadly used as a reference. The main reasons to use this work are the huge catalogue of tissues offered and the wide frequency bandwidth measured, from 1 MHz or below up to 20 GHz. However, since most tissues were measured in *ex vivo* conditions, the actual *in vivo* values are expected to be slightly higher because of structure changes in tissues and potential dehydration after death [88], as well as due to the lack of blood perfusion.

Regarding the published *in vivo* studies, some drawbacks can be highlighted. Firstly, the available works are focused on a few tissues or organs, amongst which skin, grey matter, kidney, liver, muscle and spleen are the most portrayed ones. On the contrary, without any apparent reason, other tissues such as esophagus and pancreas have not been measured at all above 500 MHz. In addition, there is a heterogeneity regarding the species chosen for characterization: apart from humans, there are works performed on cats, dogs, frogs, mice, pigs, rats and sheep, among others. This can lead to inconsistencies when comparing analogous or different tissues from different species. Another important problem is the diversity of frequencies at which the studies were carried out. On one hand, some authors measured from frequencies below the kilohertz range, while others started from hundreds of megahertz. On the other hand, some authors measured up to a few gigahertz, whereas others characterized up to millimeter-waves. A summary of the available dielectric studies performed on different tissues is presented in Appendix A.

As already commented in Chapter 1, a great knowledge of the electromagnetic properties is of great importance for developing different kinds of applications: Body Area Networks (BAN), WMD, in-body and wearable antennas, SAR and IPD evaluations, microwave imaging, hyperthermia etc. The number of applications is high and keeps rising, and therefore having a better knowledge of these properties can ease the design and it can even enhance the performance of the applications that rely on these data.

In the framework of this thesis, we aim at enlarging the data of electromagnetic properties at *in vivo* conditions, providing a large database of tissues, measured all from the same animal specie and in a wide bandwidth. The measurement campaign has been performed using the open-ended coaxial technique in the 0.5 - 26.5 GHz band, considering three different female porcine models of around 50 kilograms. These specimens were selected given the anatomical resemblance of their organs with the human ones. No significant differences are expected because of using female models instead of male ones, apart from the available tissues, since there are not reports in literature about the effect of gender over the dielectric properties. Measurements were carried out in an operating surgery room for animal experimentation of La Fe Research Foundation, room that was kept at a temperature of 21 °C during the three trials. In

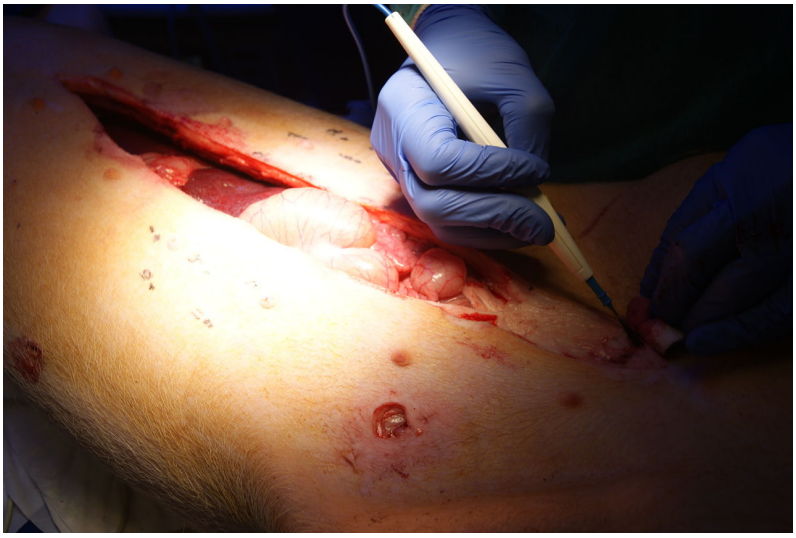

Figure 3.1: Photograph of the laparotomy performed on the animal model.

each of them, the animal was sedated and anaesthetized prior to the surgery, anaesthesia that was kept during the whole trial. The animal model was subjected to a continuous intravenous infusion of fentanyl and lactated Ringer as well. In order to correct possible excesses or shortages of anaesthesia, the animal's heart rate, blood pressure, respiratory frequency, and palpebral reflex were continuously monitored. The surgery consisted in a laparotomy and a thoracotomy, which are procedures to open both the abdominal and the thoracic cavities. A laparotomy performed in the trials is shown in the Fig. 3.1

3.2 Measurement protocol

Before preparing the measurement protocol, the trial was approved by the ethical committee of animal experimentation of the Hospital Universitari i Politècnic La Fe, Valencia, Spain, and approved as well by the ethical committee of the regional authority - Generalitat Valenciana (GVA). The experiment was in accordance with the animal-care guidelines set forth by the national government and the European Commission. The protocol considers the steps that have to be followed from the beginning of the trials up to their ends.

1. The animal model is anaesthetized and sedated at the beginning of the procedure. The animal is kept at this state during the whole trial.

2. Once started the current study, the surgeon performs the laparotomy on the animal's abdomen. At the same time, a set of three calibrations are applied and validated visually by means of a 0.1 M saline solution measurement (comparing the resulting permittivity with the one provided in [86]).

3. The biological tissues of the abdominal region are characterized. To this end, 3 measurements are carried out in 5 different points of each tissue, trying to separate the locations among them (having thus 15 measurements per tissue and animal). The temperature of the tissues is measured with a thermometer and then recorded.

4. The system is calibrated again after characterizing two tissues, using ethanol for cleaning the end of the sensor before recalibrating.

5. A lateral thoracotomy is performed once all the tissues of the abdominal region have been characterized. Meanwhile, a recalibration is once again performed and validated.

6. Once reachable, the biological tissues of the thoracic region are characterized, measuring and recalibrating in the same manner than for the abdominal ones.

7. Finally, all the instrumentation that has been in contact with the animal is cleaned with a solvent and stored. The probes are sterilized afterwards by means of an autoclave.

Two people were needed to perform the dielectric characterization of the biological tissues. One person had to move manually the probe from the calibration position to the measurement ones. The probe had to be held firmly against the tissues, applying enough pressure to avoid the presence of air between the sensor and the tissue but preventing tissue damage or fluid accumulation that can compromise the results [89]. A coaxial cable with high phase stability versus bending (Minicircuits FLC-1M-SMSM+) was used to connect the probe with the VNA. As a result, measurements were barely affected by cable movements, as one can appreciate from the uncertainty source added because of this factor in Section 2.3.3. Still, we tried to keep the curvature that the cable had in the calibration position. The second person was in charge of controlling the software interface and guiding the person that is measuring.

With the aim at speeding up the measurements, two modifications have been performed for this campaign with respect to the normal performance of the system. On the one hand, some changes have been performed on the software interface in order to facilitate the performance of the three calibrations,

guide the multiple measurements of each tissue and store these measurements automatically. On the other hand, 401 evenly-spaced frequencies have been captured in each measurements instead of 1601 points, since the trend of permittivity with frequency is kept.

3.3 Results

In this section the dielectric properties of the characterized tissues are presented. A minimum of 45 measurements of the following biological tissues has been performed: **aorta, bladder, blood, colon, fallopian tubes, fat, gallbladder, heart, kidney, liver, lung, muscle, oesophagus, ovary, pancreas, skin, small intestine, spleen, stomach, uterine matrix.** The temperature of the measured tissues varied between 37.2 °C and 38.5 °C, which are very close to the normal temperature of human tissues. It should be mentioned that despite the fact that the normal temperature of porcine models is around 40 °C, it is reduced because of the use of anesthesia and because both the abdominal and the thoracic cavities were opened and exposed to air.

For each characterized tissue, a **figure** with its **dielectric properties** is represented. The properties are shown by means of the Cole-Cole fitting of the average values (see Section 2.1, Eq. 2.3), presented jointly **with their respective total uncertainties.** The average is performed for each one of the measured frequencies, obtaining a resulting permittivity curve that is then fitted by means of a 2-pole Cole-Cole equation, whereas the uncertainty is evaluated considering the same sources shown previously in Section 2.3.3. The sources related to systematic errors due to the instrumentation and methodology, drift of the system with time and cable movement are common to all the measured tissues, but the repeatability term differs for each one of them. The SDM of the measured permittivities of each tissue is used as their respective repeatabilities, as done as well in [83]. The combined uncertainty of each part of the permittivity is combined as exposed previously in Section 2.3.3.

Apart from the figure, two extra **tables** are presented for each tissue. The first one presents the **fitted coefficients** of the **2-pole Cole-Cole equation** presented in the figure, along with their **fitting error** in relative terms. These coefficients are computed in MATLAB by minimizing the sum of squares and using the trust-region-reflective method, which is based on trust regions [90, 91]. The second one summarizes the **uncertainties** of the presented properties for **three different frequency bands** in relative terms (0.5 - 10 GHz, 10 - 18 GHz and 18 - 26.5 GHz). The uncertainty of conductivity is the same than that of loss factor, since conductivity can be obtained directly from the imaginary part of the permittivity (see Section 2.1, Eq. 2.2).

Aorta

The average permittivity obtained for aorta tissue is presented in the Fig. 3.2, along with its uncertainty. Besides, the fitted coefficients of the 2-pole Cole-Cole equation are listed in the Table 3.1, and both the repeatability and the uncertainty of its dielectric properties are summarized in the Table 3.2.

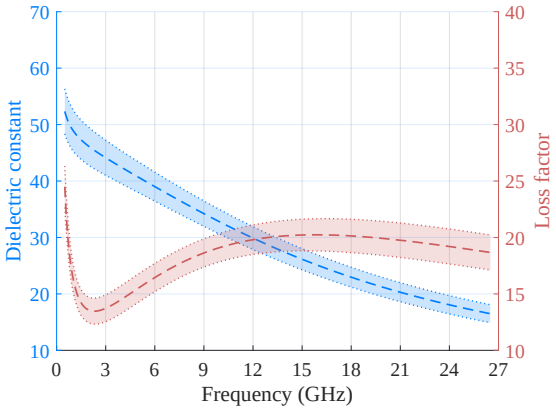

Figure 3.2: Cole-Cole fitted curve of the averaged permittivity of aorta tissue jointly with its combined uncertainty.

ϵ_∞	$\Delta\epsilon_1$	τ_1[ps]	α_1	$\Delta\epsilon_2$	τ_2[ns]	α_2	σ_s	Fitting error (ϵ'_r | ϵ''_r)
1.000	43.250	9.141	0.098	1360.509	439.155	0.377	0.291	1.535 % | 2.140 %

Table 3.1: Cole-Cole coefficients of the fitted permittivity of aorta tissue.

Freq. Band	**Parameter**	**Repeatability**	**Combined Uncertainty**
0.5 - 10	ϵ'_r	5.9 %	5.9 %
GHz	ϵ''_r	6.7 %	6.7 %
10 - 18	ϵ'_r	6.1 %	6.1 %
GHz	ϵ''_r	5.8 %	6.1 %
18 - 26.5	ϵ'_r	7.5 %	7.5 %
GHz	ϵ''_r	6.5 %	7.2 %

Table 3.2: Repeatability and combined uncertainty of aorta tissue for three spectrum regions. Values in relative terms of the relevant parameter.

Bladder

The average permittivity obtained for bladder tissue is presented in the Fig. 3.3, along with its uncertainty. Besides, the fitted coefficients of the 2-pole Cole-Cole equation are listed in the Table 3.3, and both the repeatability and the uncertainty of its dielectric properties are summarized in the Table 3.4.

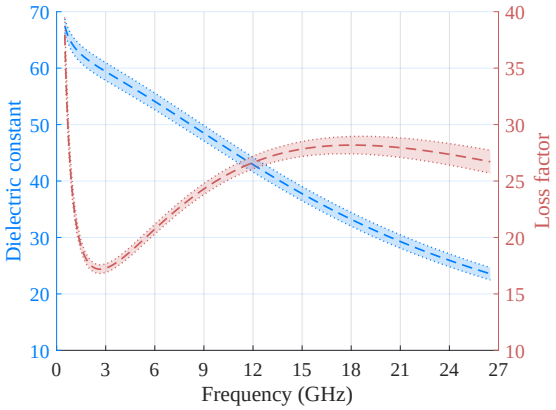

Figure 3.3: Cole-Cole fitted curve of the averaged permittivity of bladder tissue jointly with its combined uncertainty.

ϵ_∞	$\Delta\epsilon_1$	τ_1[ps]	α_1	$\Delta\epsilon_2$	τ_2[ns]	α_2	σ_s	Fitting error (ϵ'_r | ϵ''_r)
2.008	56.689	8.203	0.051	866.641	223.742	0.387	0.659	1.113 % | 1.688 %

Table 3.3: Cole-Cole coefficients of the fitted permittivity of bladder tissue.

Freq. Band	**Parameter**	**Repeatability**	**Combined Uncertainty**
0.5 - 10	ϵ'_r	2.3 %	2.3 %
GHz	ϵ''_r	1.9 %	2.0 %
10 - 18	ϵ'_r	2.8 %	2.8 %
GHz	ϵ''_r	1.6 %	2.5 %
18 - 26.5	ϵ'_r	3.6 %	3.7 %
GHz	ϵ''_r	1.8 %	3.6 %

Table 3.4: Repeatability and combined uncertainty of bladder tissue for three spectrum regions. Values in relative terms of the relevant parameter.

Blood

The average permittivity obtained for blood is presented in the Fig. 3.4, along with its uncertainty. Besides, the fitted coefficients of the 2-pole Cole-Cole equation are listed in the Table 3.5, and both the repeatability and the uncertainty of its dielectric properties are summarized in the Table 3.6.

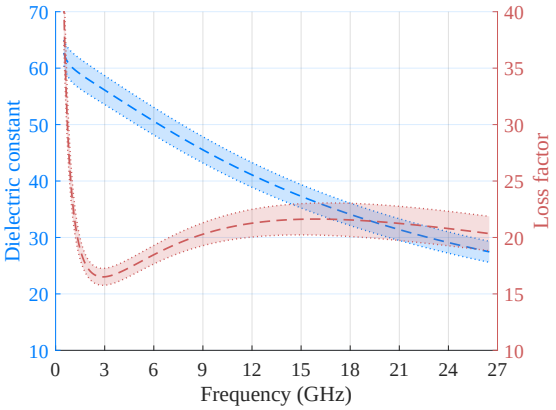

Figure 3.4: Cole-Cole fitted curve of the averaged permittivity of blood jointly with its combined uncertainty.

ϵ_∞	$\Delta\epsilon_1$	τ_1[ps]	α_1	$\Delta\epsilon_2$	τ_2[ns]	α_2	σ_s	Fitting error (ϵ'_r | ϵ''_r)
7.500	53.673	8.967	0.170	632.735	5.443	0.003	0.027	2.277 % | 3.490 %

Table 3.5: Cole-Cole coefficients of the fitted permittivity of blood.

Freq. Band	**Parameter**	**Repeatability**	**Combined Uncertainty**
0.5 - 10	ϵ'_r	4.1 %	4.1 %
GHz	ϵ''_r	4.2 %	4.2 %
10 - 18	ϵ'_r	4.7 %	4.8 %
GHz	ϵ''_r	5.2 %	5.5 %
18 - 26.5	ϵ'_r	5.4 %	5.5 %
GHz	ϵ''_r	5.9 %	6.6 %

Table 3.6: Repeatability and combined uncertainty of blood for three spectrum regions. Values in relative terms of the relevant parameter.

Colon

The average permittivity obtained for colon tissue is presented in the Fig. 3.5, along with its uncertainty. Besides, the fitted coefficients of the 2-pole Cole-Cole equation are listed in the Table 3.7, and both the repeatability and the uncertainty of its dielectric properties are summarized in the Table 3.8.

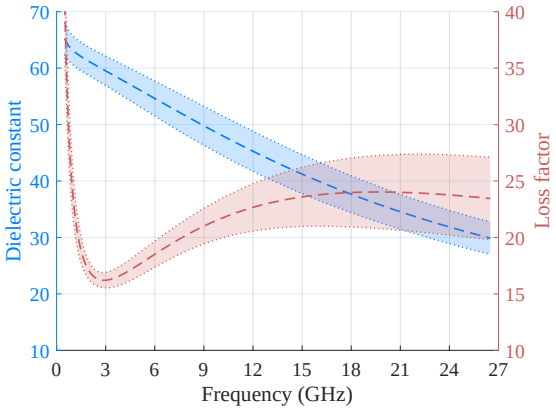

Figure 3.5: Cole-Cole fitted curve of the averaged permittivity of colon tissue jointly with its combined uncertainty.

ϵ_∞	$\Delta\epsilon_1$	τ_1[ps]	α_1	$\Delta\epsilon_2$	τ_2[ns]	α_2	σ_s	Fitting error (ϵ'_r | ϵ''_r)
5.575	57.408	7.500	0.142	1617.041	21.050	0.049	0.240	0.769 % | 2.954 %

Table 3.7: Cole-Cole coefficients of the fitted permittivity of colon tissue.

Freq. Band	**Parameter**	**Repeatability**	**Combined Uncertainty**
0.5 - 10	ϵ'_r	4.7 %	4.7 %
GHz	ϵ''_r	5.5 %	5.5 %
10 - 18	ϵ'_r	7.0 %	7.1 %
GHz	ϵ''_r	9.0 %	9.2 %
18 - 26.5	ϵ'_r	7.8 %	7.9 %
GHz	ϵ''_r	12.2 %	12.6 %

Table 3.8: Repeatability and combined uncertainty of colon tissue for three spectrum regions. Values in relative terms of the relevant parameter.

Fallopian tubes

The average permittivity obtained for fallopian tubes is presented in the Fig. 3.6, along with its uncertainty. Besides, the fitted coefficients of the 2-pole Cole-Cole equation are listed in the Table 3.9, and both the repeatability and the uncertainty of its dielectric properties are summarized in the Table 3.10.

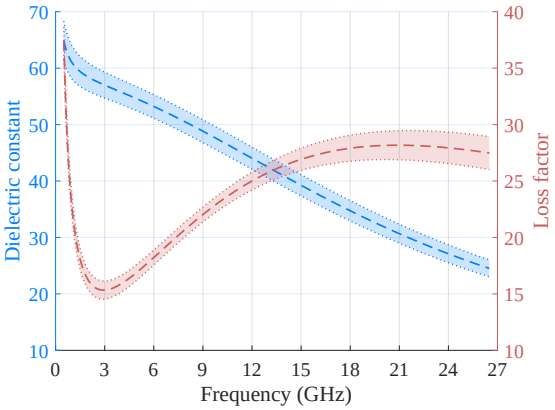

Figure 3.6: Cole-Cole fitted curve of the averaged permittivity of fallopian tubes jointly with its combined uncertainty.

ϵ_∞	$\Delta\epsilon_1$	τ_1[ps]	α_1	$\Delta\epsilon_2$	τ_2[ns]	α_2	σ_s	Fitting error (ϵ'_r | ϵ''_r)
2.022	53.699	7.229	0.007	391.079	17.225	0.267	0.496	1.371 % | 2.206 %

Table 3.9: Cole-Cole coefficients of the fitted permittivity of fallopian tubes.

Freq. Band	**Parameter**	**Repeatability**	**Combined Uncertainty**
0.5 - 10	ϵ'_r	3.6 %	3.6 %
GHz	ϵ''_r	3.5 %	3.5 %
10 - 18	ϵ'_r	4.1 %	4.1 %
GHz	ϵ''_r	2.8 %	3.4 %
18 - 26.5	ϵ'_r	4.8 %	4.9 %
GHz	ϵ''_r	3.5 %	4.7 %

Table 3.10: Repeatability and combined uncertainty of fallopian tubes for three spectrum regions. Values in relative terms of the relevant parameter.

Fat tissue

The average permittivity obtained for fat tissue is presented in the Fig. 3.7, along with its uncertainty. Besides, the fitted coefficients of the 2-pole Cole-Cole equation are listed in the Table 3.11, and both the repeatability and the uncertainty of its dielectric properties are summarized in the Table 3.12.

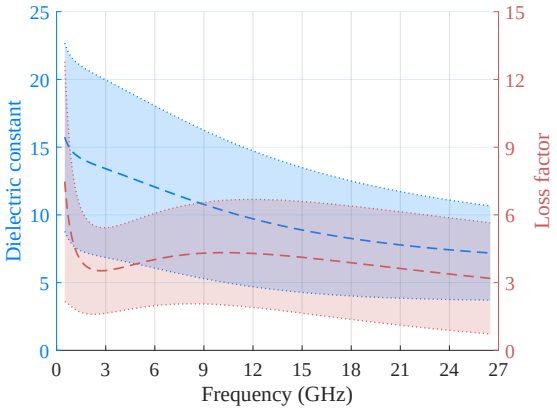

Figure 3.7: Cole-Cole fitted curve of the averaged permittivity of fat tissue jointly with its combined uncertainty.

ϵ_∞	$\Delta\epsilon_1$	τ_1[ps]	α_1	$\Delta\epsilon_2$	τ_2[ns]	α_2	σ_s	Fitting error (ϵ'_r | ϵ''_r)
5.587	8.293	13.500	0.042	5.011	0.435	0.094	0.139	1.782 % | 3.577 %

Table 3.11: Cole-Cole coefficients of the fitted permittivity of fat tissue.

Freq. Band	**Parameter**	**Repeatability**	**Combined Uncertainty**
0.5 - 10	ϵ'_r	42.6 %	42.6 %
GHz	ϵ''_r	46.4 %	46.4 %
10 - 18	ϵ'_r	44.1 %	44.1 %
GHz	ϵ''_r	49.3 %	49.3 %
18 - 26.5	ϵ'_r	43.0 %	43.0 %
GHz	ϵ''_r	57.1 %	57.2 %

Table 3.12: Repeatability and combined uncertainty of fat tissue for three spectrum regions. Values in relative terms of the relevant parameter.

Gallbladder

The average permittivity obtained for gallbladder is presented in the Fig. 3.8, along with its uncertainty. Besides, the fitted coefficients of the 2-pole Cole-Cole equation are listed in the Table 3.13, and both the repeatability and the uncertainty of its dielectric properties are summarized in the Table 3.14.

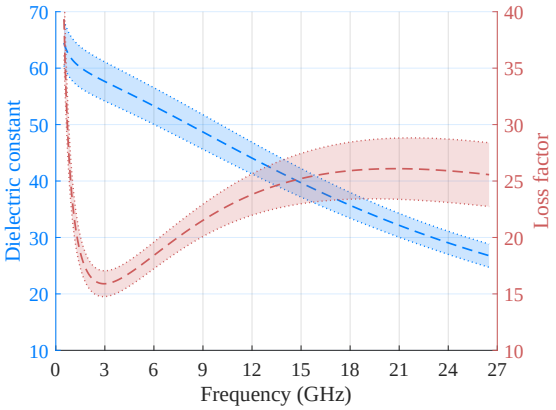

Figure 3.8: Cole-Cole fitted curve of the averaged permittivity of gallbladder tissue jointly with its combined uncertainty.

ϵ_∞	$\Delta\epsilon_1$	τ_1[ps]	α_1	$\Delta\epsilon_2$	τ_2[ns]	α_2	σ_s	Fitting error (ϵ'_r | ϵ''_r)
2.849	55.061	7.167	0.072	264.682	23.525	0.312	0.730	0.937 % | 1.691 %

Table 3.13: Cole-Cole coefficients of the fitted permittivity of gallbladder tissue.

Freq. Band	**Parameter**	**Repeatability**	**Combined Uncertainty**
0.5 - 10	ϵ'_r	5.3 %	5.3 %
GHz	ϵ''_r	5.9 %	6.0 %
10 - 18	ϵ'_r	5.5 %	5.5 %
GHz	ϵ''_r	7.2 %	7.4 %
18 - 26.5	ϵ'_r	5.9 %	6.0 %
GHz	ϵ''_r	8.9 %	9.4 %

Table 3.14: Repeatability and combined uncertainty of gallbladder tissue for three spectrum regions. Values in relative terms of the relevant parameter.

Heart

The average permittivity obtained for heart tissue is presented in the Fig. 3.9, along with its uncertainty. Besides, the fitted coefficients of the 2-pole Cole-Cole equation are listed in the Table 3.15, and both the repeatability and the uncertainty of its dielectric properties are summarized in the Table 3.16.

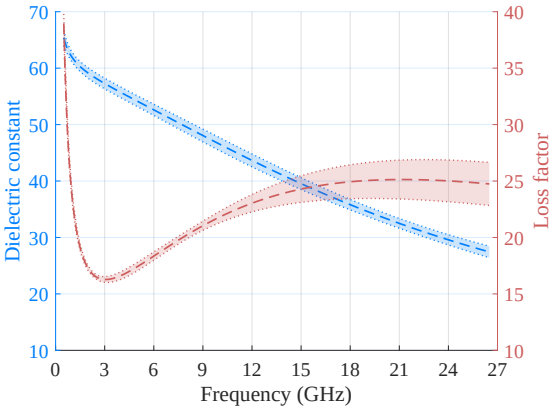

Figure 3.9: Cole-Cole fitted curve of the averaged permittivity of heart tissue jointly with its combined uncertainty.

ϵ_∞	$\Delta\epsilon_1$	τ_1[ps]	α_1	$\Delta\epsilon_2$	τ_2[ns]	α_2	σ_s	Fitting error (ϵ'_r | ϵ''_r)
2.511	54.178	6.914	0.096	1161.477	439.155	0.400	0.701	0.997 % | 1.565 %

Table 3.15: Cole-Cole coefficients of the fitted permittivity of heart tissue.

Freq. Band	**Parameter**	**Repeatability**	**Combined Uncertainty**
0.5 - 10	ϵ'_r	1.6 %	1.7 %
GHz	ϵ''_r	1.6 %	1.6 %
10 - 18	ϵ'_r	2.2 %	2.3 %
GHz	ϵ''_r	3.5 %	4.0 %
18 - 26.5	ϵ'_r	2.5 %	2.6 %
GHz	ϵ''_r	5.7 %	6.5 %

Table 3.16: Repeatability and combined uncertainty of heart tissue for three spectrum regions. Values in relative terms of the relevant parameter.

Kidney

The average permittivity obtained for kidney tissue is presented in the Fig. 3.10, along with its uncertainty. Besides, the fitted coefficients of the 2-pole Cole-Cole equation are listed in the Table 3.17, and both the repeatability and the uncertainty of its dielectric properties are summarized in the Table 3.18.

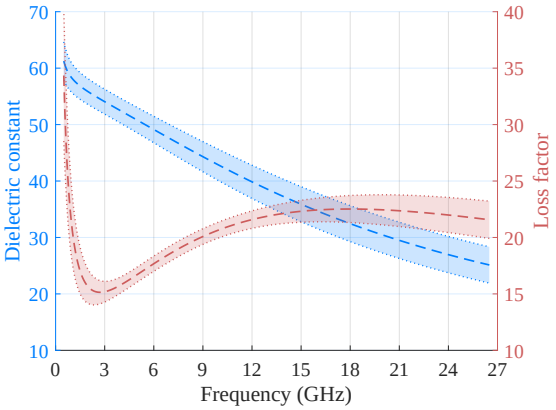

Figure 3.10: Cole-Cole fitted curve of the averaged permittivity of kidney tissue jointly with its combined uncertainty.

ϵ_∞	$\Delta\epsilon_1$	τ_1[ps]	α_1	$\Delta\epsilon_2$	τ_2[ns]	α_2	σ_s	Fitting error (ϵ'_r | ϵ''_r)
4.850	51.691	8.149	0.122	452.493	11.421	0.136	0.353	0.719 % | 1.157 %

Table 3.17: Cole-Cole coefficients of the fitted permittivity of kidney tissue.

Freq. Band	**Parameter**	**Repeatability**	**Combined Uncertainty**
0.5 - 10	ϵ'_r	4.2 %	4.2 %
GHz	ϵ''_r	5.0 %	5.0 %
10 - 18	ϵ'_r	7.1 %	7.1 %
GHz	ϵ''_r	3.4 %	3.9 %
18 - 26.5	ϵ'_r	9.7 %	9.8 %
GHz	ϵ''_r	5.3 %	6.1 %

Table 3.18: Repeatability and combined uncertainty of kidney tissue for three spectrum regions. Values in relative terms of the relevant parameter.

Liver

The average permittivity obtained for liver tissue is presented in the Fig. 3.11, along with its uncertainty. Besides, the fitted coefficients of the 2-pole Cole-Cole equation are listed in the Table 3.19, and both the repeatability and the uncertainty of its dielectric properties are summarized in the Table 3.20.

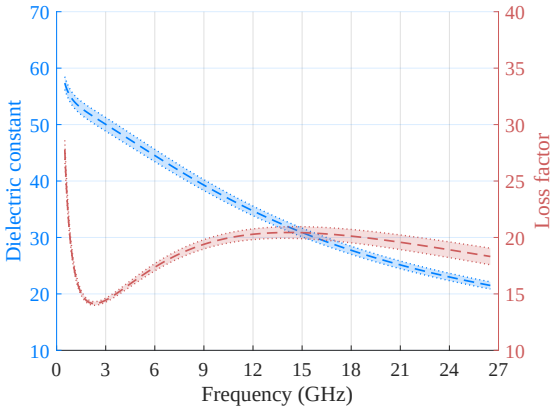

Figure 3.11: Cole-Cole fitted curve of the averaged permittivity of liver tissue jointly with its combined uncertainty.

ϵ_∞	$\Delta\epsilon_1$	τ_1[ps]	α_1	$\Delta\epsilon_2$	τ_2[ns]	α_2	σ_s	Fitting error (ϵ'_r | ϵ''_r)
6.639	47.545	10.329	0.126	8.939	0.375	0.000	0.587	0.597 % | 0.843 %

Table 3.19: Cole-Cole coefficients of the fitted permittivity of liver tissue.

Freq. Band	**Parameter**	**Repeatability**	**Combined Uncertainty**
0.5 - 10	ϵ'_r	2.1 %	2.1 %
GHz	ϵ''_r	1.5 %	1.6 %
10 - 18	ϵ'_r	2.1 %	2.2 %
GHz	ϵ''_r	1.8 %	2.6 %
18 - 26.5	ϵ'_r	2.3 %	2.5 %
GHz	ϵ''_r	2.1 %	3.7 %

Table 3.20: Repeatability and combined uncertainty of liver tissue for three spectrum regions. Values in relative terms of the relevant parameter.

Lung

The average permittivity obtained for lung tissue is presented in the Fig. 3.12, along with its uncertainty. Besides, the fitted coefficients of the 2-pole Cole-Cole equation are listed in the Table 3.21, and both the repeatability and the uncertainty of its dielectric properties are summarized in the Table 3.22.

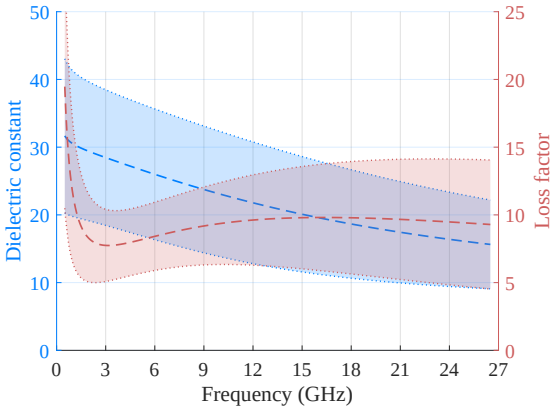

Figure 3.12: Cole-Cole fitted curve of the averaged permittivity of lung tissue jointly with its combined uncertainty.

ϵ_∞	$\Delta\epsilon_1$	τ_1[ps]	α_1	$\Delta\epsilon_2$	τ_2[ns]	α_2	σ_s	Fitting error (ϵ'_r | ϵ''_r)
6.373	23.958	8.569	0.168	2000.000	58.952	0.066	0.089	1.255 % | 2.435 %

Table 3.21: Cole-Cole coefficients of the fitted permittivity of lung tissue.

Freq. Band	**Parameter**	**Repeatability**	**Combined Uncertainty**
0.5 - 10	ϵ'_r	31.9 %	31.9 %
GHz	ϵ''_r	29.0 %	29.0 %
10 - 18	ϵ'_r	36.3 %	36.3 %
GHz	ϵ''_r	31.7 %	31.8 %
18 - 26.5	ϵ'_r	37.2 %	37.2 %
GHz	ϵ''_r	39.9 %	40.0 %

Table 3.22: Repeatability and combined uncertainty of lung tissue for three spectrum regions. Values in relative terms of the relevant parameter.

Muscle

The average permittivity obtained for muscle tissue is presented in the Fig. 3.13, along with its uncertainty. Besides, the fitted coefficients of the 2-pole Cole-Cole equation are listed in the Table 3.23, and both the repeatability and the uncertainty of its dielectric properties are summarized in the Table 3.24.

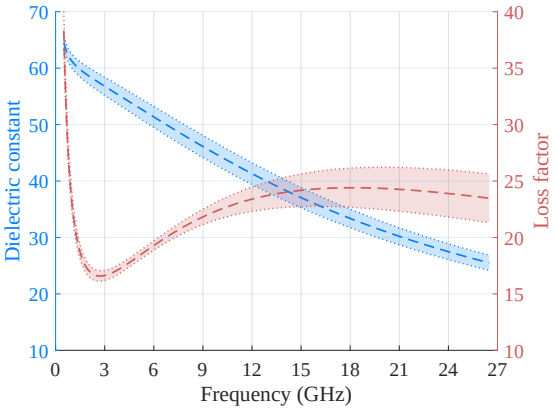

Figure 3.13: Cole-Cole fitted curve of the averaged permittivity of muscle tissue jointly with its combined uncertainty.

ϵ_∞	$\Delta\epsilon_1$	τ_1[ps]	α_1	$\Delta\epsilon_2$	τ_2[ns]	α_2	σ_s	Fitting error (ϵ'_r | ϵ''_r)
2.504	57.810	8.079	0.138	660.060	7.840	0.064	0.103	0.619 % | 1.052 %

Table 3.23: Cole-Cole coefficients of the fitted permittivity of muscle tissue.

Freq. Band	**Parameter**	**Repeatability**	**Combined Uncertainty**
0.5 - 10	ϵ'_r	2.9 %	2.9 %
GHz	ϵ''_r	2.4 %	2.4 %
10 - 18	ϵ'_r	4.1 %	4.1 %
GHz	ϵ''_r	4.6 %	5.0 %
18 - 26.5	ϵ'_r	4.3 %	4.4 %
GHz	ϵ''_r	6.8 %	7.5 %

Table 3.24: Repeatability and combined uncertainty of muscle tissue for three spectrum regions. Values in relative terms of the relevant parameter.

Oesophagus

The average permittivity obtained for oesophagus tissue is presented in the Fig. 3.14, along with its uncertainty. Besides, the fitted coefficients of the 2-pole Cole-Cole equation are listed in the Table 3.25, and both the repeatability and the uncertainty of its dielectric properties are summarized in the Table 3.26.

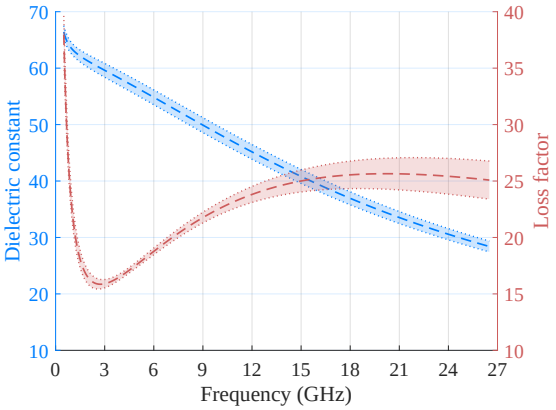

Figure 3.14: Cole-Cole fitted curve of the averaged permittivity of oesophagus tissue jointly with its combined uncertainty.

ϵ_∞	$\Delta\epsilon_1$	τ_1[ps]	α_1	$\Delta\epsilon_2$	τ_2[ns]	α_2	σ_s	Fitting error (ϵ'_r | ϵ''_r)
3.492	58.771	7.390	0.113	934.202	9.932	0.057	0.001	0.729 % | 1.296 %

Table 3.25: Cole-Cole coefficients of the fitted permittivity of oesophagus tissue.

Freq. Band	**Parameter**	**Repeatability**	**Combined Uncertainty**
0.5 - 10	ϵ'_r	1.9 %	2.0 %
GHz	ϵ''_r	2.0 %	2.0 %
10 - 18	ϵ'_r	2.6 %	2.6 %
GHz	ϵ''_r	2.9 %	3.4 %
18 - 26.5	ϵ'_r	2.7 %	2.8 %
GHz	ϵ''_r	4.5 %	5.5 %

Table 3.26: Repeatability and combined uncertainty of oesophagus tissue for three spectrum regions. Values in relative terms of the relevant parameter.

Ovary

The average permittivity obtained for ovary tissue is presented in the Fig. 3.15, along with its uncertainty. Besides, the fitted coefficients of the 2-pole Cole-Cole equation are listed in the Table 3.27, and both the repeatability and the uncertainty of its dielectric properties are summarized in the Table 3.28.

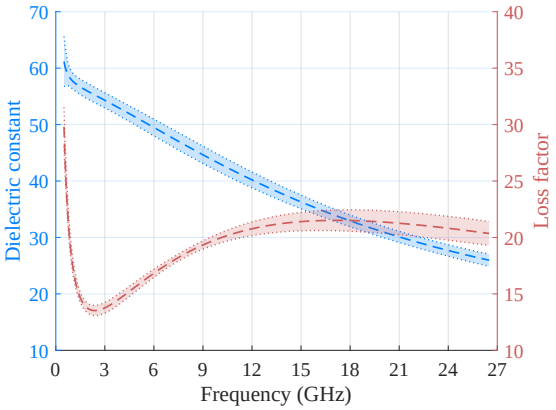

Figure 3.15: Cole-Cole fitted curve of the averaged permittivity of ovary tissue jointly with its combined uncertainty.

ϵ_∞	$\Delta\epsilon_1$	τ_1[ps]	α_1	$\Delta\epsilon_2$	τ_2[ns]	α_2	σ_s	Fitting error (ϵ'_r | ϵ''_r)
7.500	50.358	8.718	0.124	192.885	2.257	0.001	0.029	1.094 % | 1.697 %

Table 3.27: Cole-Cole coefficients of the fitted permittivity of ovary tissue.

Freq. Band	Parameter	Repeatability	Combined Uncertainty
0.5 - 10	ϵ'_r	2.5 %	2.6 %
GHz	ϵ''_r	2.2 %	2.3 %
10 - 18	ϵ'_r	2.9 %	2.9 %
GHz	ϵ''_r	2.7 %	3.3 %
18 - 26.5	ϵ'_r	3.0 %	3.0 %
GHz	ϵ''_r	3.6 %	4.7 %

Table 3.28: Repeatability and combined uncertainty of ovary tissue for three spectrum regions. Values in relative terms of the relevant parameter.

Pancreas

The average permittivity obtained for pancreas tissue is presented in the Fig. 3.16, along with its uncertainty. Besides, the fitted coefficients of the 2-pole Cole-Cole equation are listed in the Table 3.29, and both the repeatability and the uncertainty of its dielectric properties are summarized in the Table 3.30.

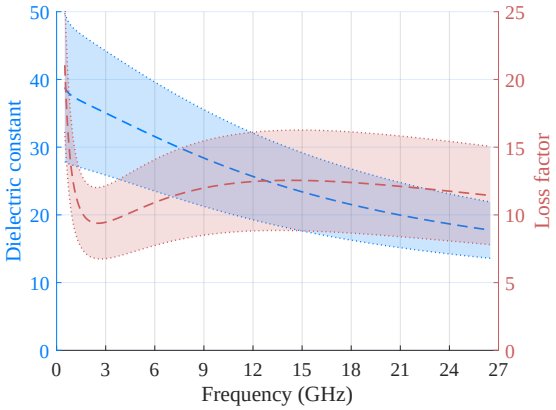

Figure 3.16: Cole-Cole fitted curve of the averaged permittivity of pancreas tissue jointly with its combined uncertainty.

ϵ_∞	$\Delta\epsilon_1$	τ_1[ps]	α_1	$\Delta\epsilon_2$	τ_2[ns]	α_2	σ_s	Fitting error (ϵ'_r | ϵ''_r)
7.500	30.676	10.045	0.160	247.513	4.687	0.000	0.076	1.791 % | 3.535 %

Table 3.29: Cole-Cole coefficients of the fitted permittivity of pancreas tissue.

Freq. Band	**Parameter**	**Repeatability**	**Combined Uncertainty**
0.5 - 10	ϵ'_r	22.4 %	22.4 %
GHz	ϵ''_r	24.5 %	24.5 %
10 - 18	ϵ'_r	21.4 %	21.4 %
GHz	ϵ''_r	25.6 %	25.6 %
18 - 26.5	ϵ'_r	20.7 %	20.7 %
GHz	ϵ''_r	26.8 %	27.0 %

Table 3.30: Repeatability and combined uncertainty of pancreas tissue for three spectrum regions. Values in relative terms of the relevant parameter.

Skin

The average permittivity obtained for skin tissue is presented in the Fig. 3.17, along with its uncertainty. Besides, the fitted coefficients of the 2-pole Cole-Cole equation are listed in the Table 3.31, and both the repeatability and the uncertainty of its dielectric properties are summarized in the Table 3.32.

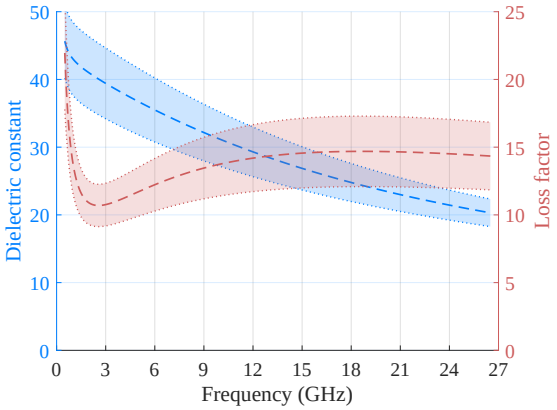

Figure 3.17: Cole-Cole fitted curve of the averaged permittivity of skin tissue jointly with its combined uncertainty.

ϵ_∞	$\Delta\epsilon_1$	τ_1[ps]	α_1	$\Delta\epsilon_2$	τ_2[ns]	α_2	σ_s	Fitting error (ϵ'_r | ϵ''_r)
2.843	40.665	7.725	0.229	135.310	3.072	0.053	0.129	0.628 % | 1.204 %

Table 3.31: Cole-Cole coefficients of the fitted permittivity of skin tissue.

Freq. Band	**Parameter**	**Repeatability**	**Combined Uncertainty**
0.5 - 10	ϵ'_r	11.4 %	11.4 %
GHz	ϵ''_r	13.7 %	13.8 %
10 - 18	ϵ'_r	10.5 %	10.5 %
GHz	ϵ''_r	15.1 %	15.3 %
18 - 26.5	ϵ'_r	9.2 %	9.2 %
GHz	ϵ''_r	15.1 %	15.4 %

Table 3.32: Repeatability and combined uncertainty of skin tissue for three spectrum regions. Values in relative terms of the relevant parameter.

Small intestine

The average permittivity obtained for small intestine is presented in the Fig. 3.18, along with its uncertainty. Besides, the fitted coefficients of the 2-pole Cole-Cole equation are listed in the Table 3.33, and both the repeatability and the uncertainty of its dielectric properties are summarized in the Table 3.34.

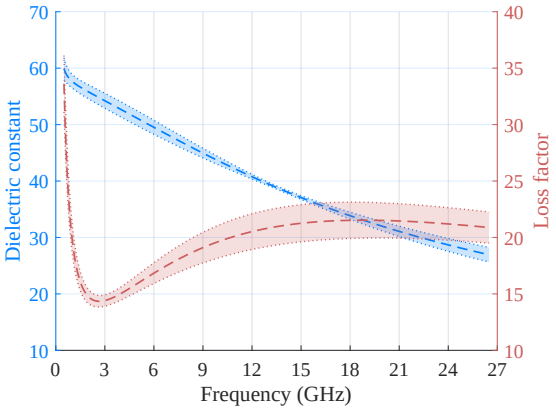

Figure 3.18: Cole-Cole fitted curve of the averaged permittivity of small intestine tissue jointly with its combined uncertainty.

ϵ_∞	$\Delta\epsilon_1$	τ_1[ps]	α_1	$\Delta\epsilon_2$	τ_2[ns]	α_2	σ_s	Fitting error (ϵ'_r | ϵ''_r)
6.097	57.200	7.777	0.152	997.973	17.630	0.069	0.425	1.364 % | 2.806 %

Table 3.33: Cole-Cole coefficients of the fitted permittivity of small intestine tissue.

Freq. Band	**Parameter**	**Repeatability**	**Combined Uncertainty**
0.5 - 10	ϵ'_r	2.6 %	2.6 %
GHz	ϵ''_r	4.5 %	4.5 %
10 - 18	ϵ'_r	3.1 %	3.1 %
GHz	ϵ''_r	3.9 %	4.3 %
18 - 26.5	ϵ'_r	4.1 %	4.2 %
GHz	ϵ''_r	5.7 %	6.5 %

Table 3.34: Repeatability and combined uncertainty of small intestine tissue for three spectrum regions. Values in relative terms of the relevant parameter.

Spleen

The average permittivity obtained for spleen tissue is presented in the Fig. 3.19, along with its uncertainty. Besides, the fitted coefficients of the 2-pole Cole-Cole equation are listed in the Table 3.35, and both the repeatability and the uncertainty of its dielectric properties are summarized in the Table 3.36.

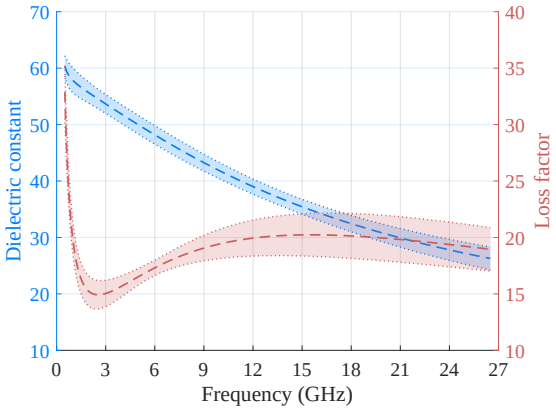

Figure 3.19: Cole-Cole fitted curve of the averaged permittivity of spleen tissue jointly with its combined uncertainty.

ϵ_∞	$\Delta\epsilon_1$	τ_1[ps]	α_1	$\Delta\epsilon_2$	τ_2[ns]	α_2	σ_s	Fitting error (ϵ'_r | ϵ''_r)
7.500	51.454	9.275	0.181	327.594	3.918	0.004	0.100	2.104 % | 3.619 %

Table 3.35: Cole-Cole coefficients of the fitted permittivity of spleen tissue.

Freq. Band	**Parameter**	**Repeatability**	**Combined Uncertainty**
0.5 - 10	ϵ'_r	3.0 %	3.0 %
GHz	ϵ''_r	5.2 %	5.2 %
10 - 18	ϵ'_r	3.2 %	3.2 %
GHz	ϵ''_r	8.0 %	8.2 %
18 - 26.5	ϵ'_r	5.1 %	5.2 %
GHz	ϵ''_r	9.2 %	9.7 %

Table 3.36: Repeatability and combined uncertainty of spleen tissue for three spectrum regions. Values in relative terms of the relevant parameter.

Stomach

The average permittivity obtained for stomach tissue is presented in the Fig. 3.20, along with its uncertainty. Besides, the fitted coefficients of the 2-pole Cole-Cole equation are listed in the Table 3.37, and both the repeatability and the uncertainty of its dielectric properties are summarized in the Table 3.38.

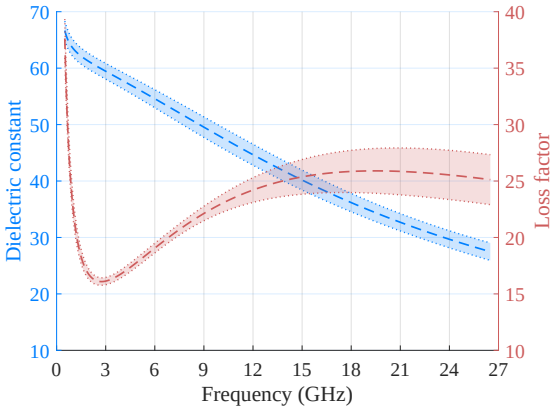

Figure 3.20: Cole-Cole fitted curve of the averaged permittivity of stomach tissue jointly with its combined uncertainty.

ϵ_∞	$\Delta\epsilon_1$	τ_1[ps]	α_1	$\Delta\epsilon_2$	τ_2[ns]	α_2	σ_s	Fitting error (ϵ'_r | ϵ''_r)
4.045	57.239	7.641	0.095	448.590	12.308	0.155	0.454	0.696 % | 2.826 %

Table 3.37: Cole-Cole coefficients of the fitted permittivity of stomach tissue.

Freq. Band	**Parameter**	**Repeatability**	**Combined Uncertainty**
0.5 - 10	ϵ'_r	2.4 %	2.5 %
GHz	ϵ''_r	2.2 %	2.3 %
10 - 18	ϵ'_r	3.6 %	3.6 %
GHz	ϵ''_r	4.3 %	4.7 %
18 - 26.5	ϵ'_r	4.2 %	4.3 %
GHz	ϵ''_r	6.2 %	6.9 %

Table 3.38: Repeatability and combined uncertainty of stomach tissue for three spectrum regions. Values in relative terms of the relevant parameter.

Uterine matrix

The average permittivity obtained for uterine matrix is presented in the Fig. 3.21, along with its uncertainty. Besides, the fitted coefficients of the 2-pole Cole-Cole equation are listed in the Table 3.39, and both the repeatability and the uncertainty of its dielectric properties are summarized in the Table 3.40.

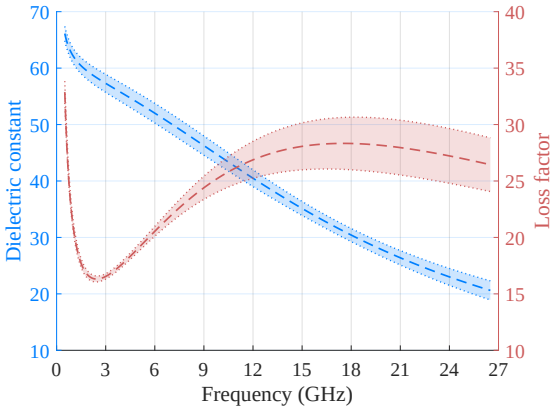

Figure 3.21: Cole-Cole fitted curve of the averaged permittivity of uterine matrix jointly with its combined uncertainty.

ϵ_∞	$\Delta\epsilon_1$	τ_1[ps]	α_1	$\Delta\epsilon_2$	τ_2[ns]	α_2	σ_s	Fitting error (ϵ'_r | ϵ''_r)
1.000	55.043	8.534	0.029	2000.000	407.500	0.351	0.417	2.041 % | 2.673 %

Table 3.39: Cole-Cole coefficients of the fitted permittivity of uterine matrix.

Freq. Band	**Parameter**	**Repeatability**	**Combined Uncertainty**
0.5 - 10	ϵ'_r	2.7 %	2.7 %
GHz	ϵ''_r	2.1 %	2.2 %
10 - 18	ϵ'_r	3.1 %	3.2 %
GHz	ϵ''_r	5.9 %	6.2 %
18 - 26.5	ϵ'_r	4.9 %	4.9 %
GHz	ϵ''_r	7.4 %	8.0 %

Table 3.40: Repeatability and combined uncertainty of uterine matrix for three spectrum regions. Values in relative terms of the relevant parameter.

To the best of the author's knowledge, this database is the largest *in vivo* collection presented so far. Some of the studied tissues, such as pancreas, oesophagous or fallopian tubes had never been characterized so far above 0.5 GHz, nor even at *ex vivo* conditions. Regarding the rest, most of them have been already measured at *ex vivo* conditions, whereas only some had been characterized *in vivo* but in campaigns with comprised studying a few organs.

As trivially expected, high water-content tissues have greater dielectric properties than those with a lower quantity, like skin or fat tissue. This kind of tissues have higher values of the fitting coefficient $\Delta\epsilon_1$ of the 2-pole Cole-Cole equation, which is related to the dielectric constant at the beginning of γ-dispersion (the most significant dispersion region within the acquisition frequencies). This coefficient has a value that varies approximately between 50 and 60 units for high water-content tissues, whereas tissues such as skin, lung or fat have a dielectric constant of around 41, 24 and 8, respectively.

All the results (Cole-Cole coefficients, uncertainty and figures) have been uploaded to an online source [92]. This web application, developed using the JavaScript library "React", provides as well the possibility of downloading the electromagnetic properties of the biological tissues for the frequencies selected by the users, if these are within the characterized frequencies of the study.

3.3.1 Uncertainty of the dielectric data

A large disparity among the uncertainty of the characterized tissues can be observed. Uncertainty is usually related to the reliability of the results returned by a system or instrument. For instance, the uncertainty analysis presented in Section 2.3.3 for the open-ended coaxial system used over the execution of this thesis has this purpose. However, apart form the uncertainty sources related to the system, the dielectric properties of biological tissues vary from their average to a greater or lesser extent. This variability, evaluated in the previous section as the repeatability source of the combined uncertainty, is particular for each tissue. Repeatability (or variability, we refer to the same phenomenon using both terms interchangeably) is evaluated as the SDM of the measured permittivities, and the following factors can affect it:

1. **Natural heterogeneity of the characterized tissue.** The biological structure of tissues is not completely homogeneous, and it causes changes in the measured properties. For instance, the water content of fat and skin tissue is not constant regardless of the body region being characterized.

2. **Pressure applied to the tissue with the open-ended coaxial probe.** An excess in the applied pressure can damage the tissue, whereas a short-

age can provoke the presence of air bubbles between the tissue and the probe [89].

3. **Age of the subjects.** It is known that the younger a particular model is, the higher dielectric properties it has within its particular species [93]. In general, this effect is more significant in immature subjects.

4. **Temperature of the tissue.** This factor also affects the resulting permittivity. For this reason, many authors aim at measuring either *in vivo* or *ex vivo* at normal body temperature (this is, *in vitro*).

Among these factors, tissue heterogeneity is the most impactful one on the obtained repeatabilities. The structure of most biological tissues is quite homogeneous, and hence their uncertainty is usually low. In general, for high-water content tissues, the uncertainty of the real part is below or around ±5 %, whereas the imaginary one is around ±10 %. However, there are a few exceptions. For instance, the uncertainty of kidney tissue is higher, but it is mainly due to the fact that its absolute properties are lower than those of many high water-content tissues, and thus the errors increase in relative terms.

A Kolmogorov-Smirnov test has been performed at each frequency testing several distribution functions in order to characterize the kind of distribution that better fits the measurements obtained of the characterized tissues in three specific frequencies distributed among the acquisition frequencies: 2.45 GHz, 12.5 GHz and 18 GHz. The following distributions have been tested with the MATLAB suite: beta, binomial, Birnbaum-Saunders, exponential, extreme value, Gamma, Gaussian, generalized extreme value, generalized pareto, logistic, loglogistic, lognormal, Nakagami, Poisson, Rayleight, Rice, t Location-Scale, uniform and Weibull. Results have shown that the logistic distribution (Eq. 3.1) is the one that fits better the scatter of the dielectric properties. It is a kind of distribution similar in shape to the gaussian one but with heavier tails.

$$PDF(x) = \frac{e^{\frac{x-\mu}{\sigma}}}{\sigma(1+e^{\frac{x-\mu}{\sigma}})^2} \tag{3.1}$$

where μ and σ are the mean and a scale parameter of the Probability Density Function (PDF).

Down below the probability densities of the dielectric properties at these frequencies are analyzed for 4 tissues: muscle, skin, fat and pancreas. These tissues have been chosen as representatives of different degrees of water content and a tissue with a large tissue heterogeneity. In the Figs. 3.22, 3.23 and 3.24 the probability densities of their dielectric properties are represented for

2.45, 12.5 and 18 GHz, respectively. Besides, the computed coefficients for the logistic distribution are listed in the Table 3.41.

In the Fig. 3.22, one can observe that pancreas tissue is the one with the highest variability, closely followed by fat tissue. On the contrary, since the heterogeneity of muscle tissue is significantly lower, the likelihood of measuring a dielectric property of muscle close to its average value is much higher. In absolute values, the variability in loss factor is much lower than in dielectric constant. This is due to the fact that, at 2.45 GHz, dielectric constant values are much greater than loss factors'. In fact, looking again the tables of uncertainty of each of the twenty characterized tissues, one can observe that the repeatability is fairly similar for both properties in all of them since values were computed in percentage terms from the relevant parameter.

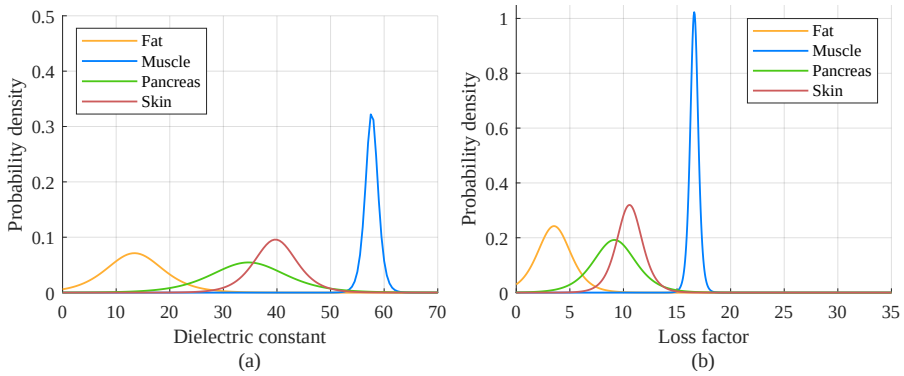

Figure 3.22: Probability distribution of the dielectric properties at f=2.45 GHz: (a) dielectric constant, (b) loss factor.

Observing the probability densities of the dielectric constants of the tissues at higher frequencies in the Figs. 3.23 and 3.24, one can observe that variability tend to decrease, at least in absolute values. On the contrary, in loss factor variability tends to increase. However, comparing the probability densities of a particular tissue among different frequencies is not completely accurate. For instance, the repeatabilities of the tissues shown at the different tables of the previous section show that, in general, they increase with frequency in relative terms. Therefore, comparing the probability densities of both properties or even of the same property at different frequencies is not an easy task since they are affected by the absolute values considered each time.

In general, regardless of the property and frequency considered, pancreas tissue is the one with the highest variability, followed by fat, skin and muscle. Most high water-content tissues have a similar distribution than that of the

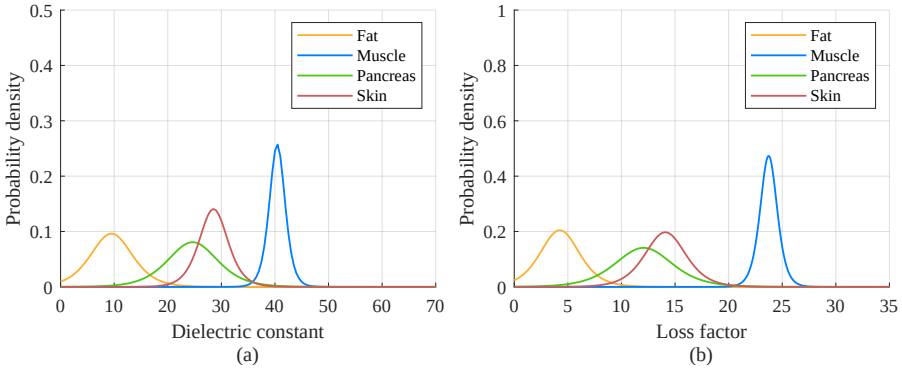

Figure 3.23: Probability distribution of the dielectric properties at f=12.5 GHz: (a) dielectric constant, (b) loss factor.

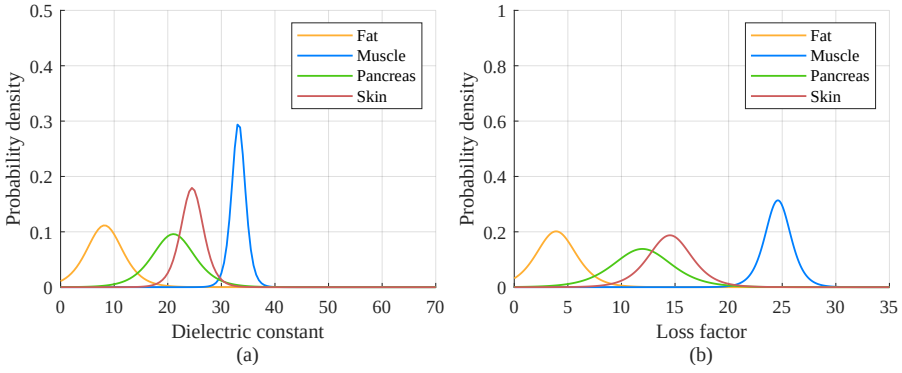

Figure 3.24: Probability distribution of the dielectric properties at f=18 GHz: (a) dielectric constant, (b) loss factor.

muscle. On the other hand, tissues with a lower quantity of water have more specific behaviours. For instance, the dielectric properties of skin and fat tissue vary greatly since the quantity of adipose tissue and water is not constant. These properties vary not only when measuring at different positions, but also within a particular region (although at a lower degree). Lung, particularly, has a large variability due to the breathing state. These large variabilities were previously reported in Gabriel's report [87]. However, the large variability obtained for pancreas tissue was not expected. Its dielectric properties were only previously presented in [94], and unlike our results, theirs were similar to those from high water-content tissues. This may be caused by their assumption that pancreas had the same dielectric properties than thyroid, originally measured in Gabriel's database [87].

Tissue	**Property**	**f = 2.45 GHz**		**f = 12.5 GHz**		**f = 18 GHz**	
		μ	s	μ	s	μ	s
Muscle	ϵ_r'	57.68	0.77	40.42	0.97	33.20	0.84
	ϵ_r''	16.61	0.24	23.74	0.53	24.60	0.80
Skin	ϵ_r'	39.72	2.61	28.54	1.78	24.54	1.39
	ϵ_r''	10.56	0.78	14.09	1.27	14.53	1.33
Pancreas	ϵ_r'	34.67	4.59	24.64	3.09	21.06	2.61
	ϵ_r''	9.16	1.30	12.07	1.77	11.95	1.81
Fat	ϵ_r'	13.41	3.51	9.49	2.60	8.20	2.24
	ϵ_r''	3.52	1.03	4.25	1.22	3.91	1.24

Table 3.41: Fitted coefficients of the logistic distribution for the selected tissues and frequencies.

Impact of dielectric uncertainty in WBAN systems

In the introductory chapter, we exposed that the electromagnetic properties of biological tissues are important for developing different types of applications, like SAR evaluations and development of electromagnetic phantoms, among others. Hence, the uncertainty of the measurements can compromise these developments. However, this uncertainty is inherent to biological tissues, and in some application designs it should be taken into account.

For instance, this phenomenon can have an impact in the development of antennas for Wireless Body Area Networks (WBAN). For the same working frequencies, this kind of antennas are much smaller than those that work for air, since the presence of a surrounding dielectric of much higher value shifts their resonant frequency to lower values [95] - apart from other effects

like changes in the radiation patterns. When designing a particular antenna for a particular WBAN system, the most common practice is to replicate the conditions in which it is intended to work in a simulated environment. This design is performed by using both an electromagnetic simulation software and a Computer-Aided Design (CAD) model that imitates the shape of the body or the part of the body to be simulated. This CAD model contains the shape of the different tissues that compose it and the dielectric properties related to these tissues.

The most common and straightforward practice is to assign the electromagnetic properties provided in Gabriel's database to the simulated tissues. Simulating just in this manner has some downsides: tissues are not completely homogeneous within all their shape, as we have proved; dielectric properties are usually measured using animal models, which vary among species [96]; the age of the subject and the measurement conditions in which these properties where gathered add an extra uncertainty to the values [53, 93] etc. Therefore, when designing a WBAN antenna, they should work not only for the typical and expected case, but they also should perform reasonably well within the variability range of the dielectric properties of the considered tissues. Indeed, it should be mentioned that some authors have designed WBAN antennas considering a potential detuning of these properties, or making them useful in the presence many different tissues [97, 98].

With the aim at proving the impact of tissue variability in the design of a WBAN channel, a set of simulations considering an In-Body to On-Body channel have been performed. Simulations were carried out with CST Microwave Studio, choosing part of the abdomen from the CAD Female Visible Human model (commonly known as "Nelly") and using different values of the dielectric properties of the tissues involved. In the model, only skin, fat and muscle tissues were considered, simulating the performance of two WBAN antennas as one can observe in the Fig. 3.25. Besides, the antenna presented in [99] was used as the on-body one, located almost in contact with skin tissue, whereas the antenna presented in [94] was used as the in-body one, placed inside muscle tissue.

Simulations were performed within the 3.1 - 5.1 GHz band despite antennas could work up to higher frequencies since the computational cost increases hugely with frequency. Even so, the particular performance of these two antennas is not important in itself but the conclusions that can be extrapolated from the obtained results. The overall dimensions of the simulated scenario were 22.7 cm x 18.7 cm x 19.7 cm, considering a mesh of around 158 million of cells for computation. The antennas were separated 5 cm, crossing layers of 5 mm of air, 2 mm of skin, 2.2 cm of fat and 2.1 cm of muscle tissue, approximately. The following cases were simulated:

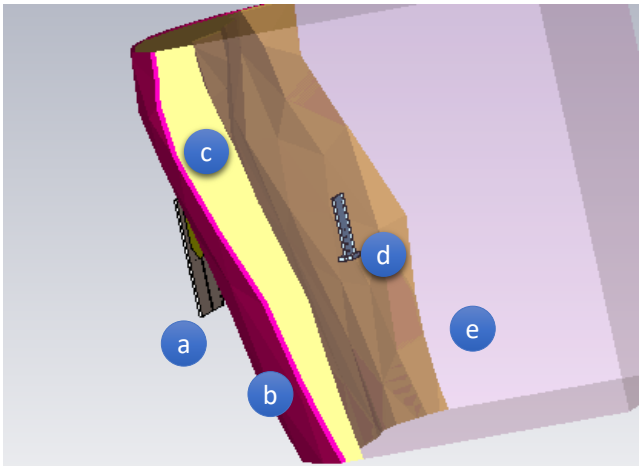

Figure 3.25: Instance of the simulation setup considered: (a) on-body antenna, (b) skin layer, (c) fat layer, (d) in-body antenna, (e) muscle layer.

1. **Minimum permittivity case.** In this first case, the average permittivities - 2 x SDM of each tissue were selected.

2. **Average permittivity case.** The second simulation consisted in using the average properties computed for each tissue.

3. **Maximum permittivity case.** Lastly, the setup was simulated considering the average permittivities + 2 x SDM of the tissues.

We chose twice the SDM to compute the edge cases since, considering a normal distribution (and the logistic is pretty similar to that one), the 95% of the possible permittivities would lie within these values. The maximum and minimum measured permittivities of the tissues were not considered since, in the other manner, we can minimize the effect of possible measurement outliers.

In the Fig. 3.26, the adaptation of the in-body (dashed) and the on-body (solid) antennas are represented for each case. Although both antennas seem to be matched (i.e., they have a reflection coefficient below -10 dB), the variability of the dielectric properties of the tissues affected more significantly to the external one. It could be due to the fact that skin tissue, which is the closest to this antenna, has much larger variability in the simulated frequencies than muscle, which is the tissue that surrounds the in-body one. With respect to the on-body antenna, the differences between the edge cases are around 2 dB in almost all the simulated bandwidth, which shows the importance of checking

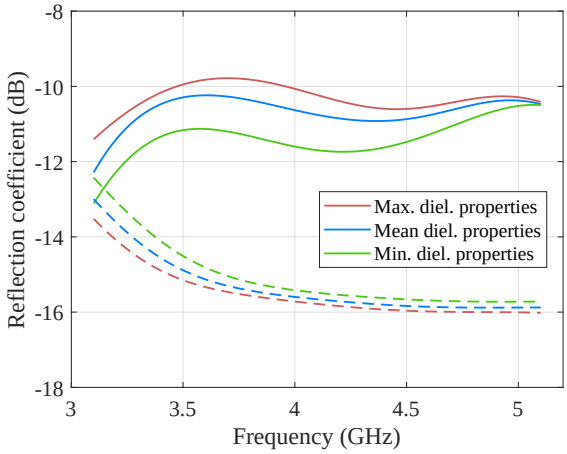

Figure 3.26: Reflection coefficients of the in-body antenna (dashed lines) and the on-body antenna (solid lines) in the three cases.

that antennas perform properly not just for the average permittivity properties. The differences were not as large for the in-body antenna, but still close to 1 dB at 3.1 GHz.

Besides, the dielectric properties of the tissue that surrounds an antenna defines its resonant frequencies, as also stated in [100]. This is not as critical for wideband antennas as for narrowband ones. For instance, one can observe that tissue variability causes a frequency shifting in both the local minimums and maximums of the reflection coefficient of the on-body antenna, although it remains matched. Nevertheless, considering a narrowband antenna, this shifting can be much more problematic. As aforementioned, some authors are already designing their antennas to work for different tissues [97, 98]. This approach can avoid collaterally the problems that the dielectric variability of the tissues involve.

It should be mentioned that the presented results are particular for the two considered antennas and does not represent all kinds of WBAN antennas, which could be affected to greater or lesser extents. We have made use of these antennas as we had available their CAD designs and they have been manufactured and used in real WBAN testings, and although these particular antennas were adapted at the three simulations, we wanted to show that the tissue uncertainty is indeed translated to the simulation results and therefore it could be disruptive for other devices.

3.3.2 Comparison with other studies

The presented results are particularly novel for pancreas and oesophagus, tissues that have not been characterized at any condition so far. Despite the fact that some dielectric properties have been reported for pancreas tissue in [94], authors assumed that the properties of the thyroid were identical than pancreas, which we have proved wrong given the large differences. This is also the first report in which dielectric data of *in vivo* stomach is presented, and the first time that heart tissue is measured *in vivo* above 8 GHz, extending the work performed in [101]. In addition, the latter work was carried out on frog tissues, which makes dielectric data difficult to be extrapolated since the temperature of the heart tissue measured was 22 °C. This occurred because the inner temperature of frog models adapt to that of the environment, and the implications of being around 15 °C less than human's normal temperature are not negligible. A summary of the differences in dielectric properties among the biological tissues characterized in the current dissertation and in previous studies is presented in the Table 3.42. For each tissue, differences are presented as shown in Eq. 3.2, in percentage terms and averaging within those frequencies shared with our study.

$$\Delta\epsilon'_r(\%) = \frac{1}{n}\sum_{f=f_1}^{f_{end}} \frac{\epsilon'_{ref}(f) - \epsilon'_r(f)}{\epsilon'_r(f)} * 100 \tag{3.2}$$

where $\Delta\epsilon'_r$ is the average difference of the relative differences computed for the dielectric constant, n is the number of shared frequencies from the first one f_1 to the last one f_{end} common to our study, $\epsilon'_{ref}(f)$ is the dielectric constant of the study to be compared and $\epsilon'_r(f)$ is the averaged dielectric constant of our study. The differences in loss factor $\Delta\epsilon''_r$ are calculated in the same way.

Reference	Source	Freq. (GHz)	Mean Differences (%) ($\Delta\epsilon'_r$ | $\Delta\epsilon''_r$)
Abdilla [102]	Bovine *Ex vivo*	0.5 - 26.5	Liver (3.16|-23.57), Muscle (-8.31|-18.20)
Andreuccetti [94]	Human *Ex vivo*	0.5 - 20	Pancreas (58.50|84.02)
Brady[1] [103]	Bovine *In vitro*	2 - 4	Aorta (-4.34|-8.29), Kidney (-11.74|-4.74), Liver (-15.04|-12.91), Muscle (-18.29|-10.34)
Burdette[1] [104]	Canine *In vivo*	0.5 - 11	Kidney (-9.49|13.16), Kidney (-18.50|-11.39)[2]
	Human *In vitro*	0.5 - 8	Muscle (-15.71|n.a.[3])

	Rat *In vivo*	0.5 - 11	Blood (10.13|8.11), Fat (-16.26|-29.03)[4], Muscle (-2.28|n.a.[3])
Farrugia [105]	Rat *In vivo*	0.5 - 26.5	Liver (2.96|-9.71)
Fornes [106]	Human *Ex vivo*	0.5 - 18	Colon (-14.70|-9.42)
Gabriel [87]	Bovine *In vitro*	0.5 - 20	Fat (-34.46|-47.87)
	Human *In vitro*		Aorta (1.88|-14.08), Bladder (-68.76|-73.21), Ovary (-23.31|-7.99), Skin (-0.17|13.35)[5], Small intestine (-13.74|9.50), Stomach (1.72|3.11), Uterine matrix (7.93|-8.86)
	Ovine *In vitro*		Blood (-0.77|15.74), Colon (-14.69|-6.02), Gallbladder (-1.16|-0.20), Heart (-9.75|-4.61), Kidney (-6.09|2.75), Liver (-14.45|-12.29), Lung (-32.17|-18.58), Muscle (-3.41|-13.69), Spleen (-5.36|8.76)
Guardiola [107]	Human *Ex vivo*	0.5 - 20	Colon (-16.36|-28.51)
Joines [51]	Human *Ex vivo*	0.5 - 0.9	Colon (-24.04|-32.76), Kidney (2.72|3.50), Liver (-7.93|-5.67), Lung (94.91|71.01), Muscle (-16.88|-30.01)
Kraszewski [108]	Feline *In vivo*	0.5 - 8	Kidney (-11.74|-18.50), Liver (-4.38|-18.40), Muscle (-9.98|-9.56), Spleen (-4.09|-10.60)
	Feline *In vitro*		Kidney (-12.30|-21.03), Liver (-1.48|-14.57), Muscle (-9.73|-11.33), Spleen (-3.10|-8.82)
	Rat *In vivo*	0.5 - 12	Kidney (-7.01|-12.69), Liver (-8.28|-15.30), Muscle (-3.62|-4.96), Spleen (-2.84|-1.93)
Lazebnik [109]	Bovine *Ex vivo*	0.5 - 20	Liver (-2.93|-12.86)
O'Rourke [53]	Human *Ex vivo*	0.5 - 20	Liver (-10.39|-15.65)

Peyman [93]	Rat *In vitro*	0.5 - 10	Kidney (-23.38|-14.17), Liver (-10.76|-10.26), Muscle (-19.58|-4.67), Skin (-24.91|-6.20), Spleen (-14.15|-6.32)
Porter [110]	Bovine *Ex vivo*	0.5 - 20	Bladder (-2.33|-1.74), Bladder (2.00|-3.16)[6]
Salahuddin [111]	Porcine *Ex vivo*	0.5 - 20	Kidney (-3.08|-4.50)
Schwartz [101]	Frog *In vivo*	0.5 - 8	Blood (21.33|-3.21), Heart (12.63|11.43), Muscle (-2.03|7.71)
	Frog *In vitro*		Heart (5.05|3.21), Skin (22.65|41.01)
Stuchly(A) [112]	Feline *In vivo*	0.5 - 1	Kidney (-26.55|-17.98), Liver (-13.06|0.84), Muscle (-6.71|8.95), Spleen (-13.84|-0.91)
Stuchly(B) [96]	Feline, Rat *In vivo*	0.5 - 8	Liver (-4.54|-22.49), Muscle (-10.42|-16.95), Spleen (-5.73|-14.23)
Xu [113]	Canine *In vitro*	0.5 - 11	Heart (-16.73|7.05), Kidney (-9.27|8.09), Liver (-4.16|4.10), Muscle (-9.72|12.03), Skin (-7.25|10.65)
Yilmaz [114]	Rat *In vivo*	0.5 - 6	Liver (-6.64|-15.08)

[1] Data extracted from figures
[2] Measurements performed *in vitro*
[3] Data could not be retrieved from figures with accuracy
[4] Measurements only up to 2 GHz
[5] Measurements performed *in vivo*
[6] Measurements performed on porcine samples

Table 3.42: Summary of the averaged differences with respect to previous studies. Values in relative terms of the relevant parameter.

The electromagnetic properties measured within the framework of this thesis are greater than those properties presented in many of the gathered *ex vivo* studies. In those studies in which different conditions were measured, the dielectric properties are higher if gathered *in vivo* than in any other condition [101, 104, 108], agreeing with our outcomes. The differences are lower with respect to dielectric characterization studies performed at *in vivo* conditions, although generally the values of this work are slightly higher than most of them. This can be due to the fact that many of the self-declared *in vivo* studies were

not conducted strictly at this condition, but rather considering freshly killed models. The latter approach facilitates the characterization, but the lack of blood perfusion can lower the measured properties. Still, our results agree generally well with most of the compared *in vivo* sources. It should be mentioned that the differences are higher comparing with the study of *Schwartz* [101], although as aforementioned it can be due to the fact that the temperature of the *in vivo* frog samples was much lower than that of the rest of the *in vivo* sources.

3.4 Conclusion

In this chapter, we have presented the *in vivo* electromagnetic properties found for the tissues of the abdominal and the thoracic regions, properties that enlarge the information that is currently available in literature. The key advantage of the presented collection with respect to other *in vivo* studies is the fact that a great quantity of tissues have been characterized under the same conditions: using the open-ended coaxial system, all of them characterized within a very wide bandwidth and taking samples from the same animal species.

To access the tissues of these regions, a laparotomy and a thoracotomy were performed on three sedated and anaesthetized female porcine models of 50 kg. **At least 45 measurements of the following tissues were carried: aorta, bladder, blood, colon, fallopian tubes, fat, gallbladder, heart, kidney, liver, lung, muscle, oesophagus, ovary, pancreas, skin, small intestine, spleen, stomach, uterine matrix.** Then, the average properties were computed, alongside their respective uncertainties and the Cole-Cole model of each averaged permittivity. A quantitative comparison with other *in vivo* and *ex vivo* studies is addressed, observing that generally *in vivo* properties are higher to their analogous *ex vivo* ones.

Results showed that high water-content tissues, apart from having higher permittivity values, had lower uncertainty than low water-content ones. Uncertainty is related to different factors, being the natural heterogeneity of the biological tissues the most significant one. As expected from Gabriel's studies, the variability of tissues like fat, skin and lung was higher than compared to the rest. However, pancreas also showed a large unexpected uncertainty, due to a natural inhomogeneity that has not been assessed so far. Finally, a set of simulations of an in-body and an on-body antenna have been run in order to show how the variability of tissues can impact their adaptation, always considering that these results are particular for these two antennas.

Chapter 4

Dielectric characterization of pathological human colon tissues

In this chapter, the dielectric data of the human colon tissues collected in this thesis are presented. Healthy, cancerous and different pathological states of colon tissue have been characterized. To this end, two different sources of human colon samples have been collected: samples gathered from colonoscopy procedures and samples taken from surgery resections. The main idea is to determine if it is possible to detect CRC or other pathologies making use of their dielectric properties. These measurements were carried out at Hospital Universitari i Politècnic La Fe, Valencia, Spain, in a conditioned room of its endoscopy unit and under the guidance and supervision of the medical experts.

4.1 Introduction

There are several differences between healthy cells and cancerous cells. Some of the differences are already understood, whereas others are not so well known yet. Mutations cause that cancerous cells keep growing when enough cells are present, irregularities in shape and size, a higher demand of blood supply etc. In essence, cancer mutations change the biological structure of the cells, which in turn has an effect on the interaction with the electromagnetic waves. Among other reasons, this is due to the fact that proteins acquire more surface charges in malignant tumours, and the attraction of these charges for water molecules results in the presence of more "bound water" [56].

This different interaction can be translated into changes in the electromagnetic properties of the cancerous states of the tissues. Many of them have found out significant differences between the properties of healthy and malignant tissues. In [51], several normal and malignant *ex vivo* human tissue samples were measured in the 50 - 900 MHz frequency band, showing that the dielectric properties of malignant tissues had larger values than those of healthy ones. In [52], similar differences were obtained up to 5 GHz. The xenograft model was used, in which human tumours were cultivated in mice, grown, extracted and measured just after resection. In [53], authors investigated the differences between normal, malignant and cirrhotic human liver from 0.5 to 20 GHz, concluding as well that statistically significant differences exist between the dielectric properties of *ex vivo* normal and malignant liver tissue. Besides, breast cancer has been one of the most investigated [54, 55]. This is due to the fact that the major electromagnetic differences between malignant and healthy cells have been obtained for this tissue, making it easier the development of cancer detection applications.

All these evidences prove that the electromagnetic properties can be used as cancer detection markers. Colon tissue was selected as a target of the present thesis as the open-ended coaxial system could be used during the colonoscopy procedure, by measuring either biopsy samples or *in situ* colon tissue if the system could be embedded within the colonoscope. Therefore, two sources of tissues in which human samples can be gathered have been considered: biopsies from colonoscopy procedures and samples from surgery resections.

For both measurement campaigns, the healthy and pathological colon samples of each patient have been measured. In order to develop a detection tool, it is important to find differences between the healthy and the pathological states within a patient. Obtaining the permittivity of a suspicious tissue and considering a decision threshold would not be valid since the permittivity of a particular pathology does not have identical values regardless of the patient studied. The following factors are mainly responsible for this:

- On the first place, it is known that the **age** of the patient can affect to the absolute values of the permittivity [115]. It should be highlighted that no large changes are expected among adult people.

- The **elapsed time** between samples' **extraction and measurement** is not identical. It means that the samples of some patients have been exposed to air more than others, which can alter the obtained values as exposed in [105]. In addition, the size of the samples can modify their dehydration rate.

- The **temperature** of the samples is another factor that can modify the dielectric properties of a biological tissues, and since measurements are performed *ex vivo* it depends on the ambient temperature.

- Finally, the **calibration** can affect differently between measurement sessions. Possible errors would be systematic within a calibration session, meaning that they would affect the measured samples of a particular patient in the same manner.

4.2 Measurement of biopsies

The protocol of sample gathering as well as the results obtained from the measurements of colonoscopy biopsies are detailed in this section. Even though the size of the biopsies is rather small, this source of samples was considered since other colon pathologies apart from CRC could be evaluated.

4.2.1 Sample collection protocol

The protocol for collecting and measuring the biological samples was prepared jointly with the medical supervisor and afterwards it was approved by the ethical committee of the hospital. The protocol considers all the steps that have to be followed from the first contact with the patient until the storage of the dielectric properties:

1. Before starting the colonoscopy procedure, patients are informed by the medical staff of the aim of the study and asked to participate in it. If they are willing to take part in it, they have to sign a consent form giving their permission.

2. The examination of the colon is performed. If suspicious tissues are found, they are resected to be sent to the anatomical pathology unit. In those cases in which suspicious tissues are large enough, a sample is collected for the present study as well. Tissues are resected by means of biopsy forceps and then they are placed in empty plastic receptacles.

3. If a suspicious colon tissue is resected for this study, then a healthy sample of the nearby area is taken as well and placed in another receptacle. Once both samples are collected, they are sent to the measurement room as soon as possible (ten minutes at most).

4. A calibration of the system is performed recurrently in order to be ready to measure when samples arrive to the measurement room. Then, both

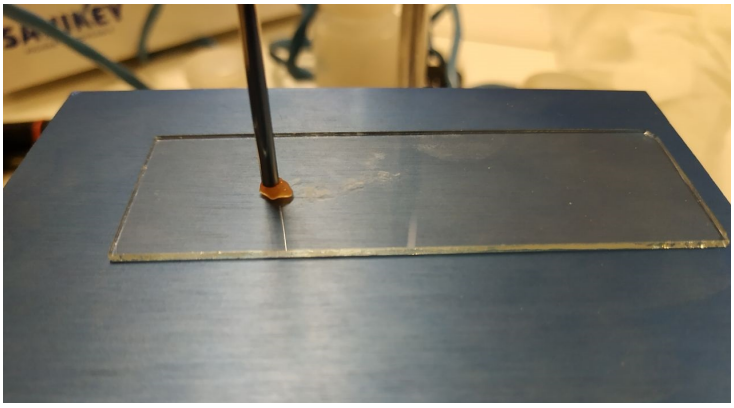

Figure 4.1: Measurement of a sample gathered from a colonoscopy procedure.

samples are placed in a glass sheet and pressed to the tip of the open-ended coaxial sensor, as can be seen in the Fig. 4.1. Three measurements are performed and stored, using a numerical code to relate them with their medical history.

5. Once the samples from a patient have been measured, all the equipment that has been in contact with the samples (i.e., sensor's tip, forceps to place the samples in glass sheets) is cleaned using either acetone or ethanol. Samples are put back into the plastic receptacles and dropped in a suitable container.

6. Biopsies are analyzed by the anatomical pathology unit, returning the results within a few weeks. Then, we are able to process the results in terms of their resulting pathological state. The protocol is summarized in the Fig. 4.2

At the beginning of the study, a healthy sample was collected from the willing patients regardless if they had suspicious polyps or not. As a result, a great volume of data from healthy tissues could be collected and then we were able to determine more accurately the average values of permittivity of these samples along with their deviation. Besides, six different pathologies have been being measured during the development of this thesis: Adenocarcinomas, adenomas without dysplasia, adenomas with Low-Grade Dysplasia (LGD), adenomas with High-Grade Dysplasia (HGD), hyperplastic polyps (hyperplasias) and hamartomatous polyps (hamartomas). A total of 71 paired samples (pathological and healthy from the same patient) have been currently analyzed. The volume of paired samples analyzed for each pathology is listed in the Table 4.1.

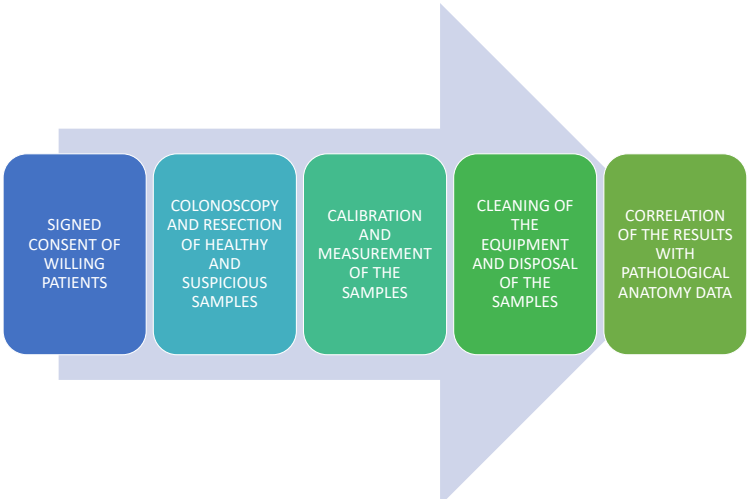

Figure 4.2: Summary of the protocol followed for gathering the dielectric data of the biopsies.

Pathology	Number of samples
Adenocarcinomas (CRC)	8
Adenomas without dysplasia	13
Adenomas with LGD	29
Adenomas with HGD	12
Hyperplastic polyps	7
Hamartomatous polyps	2

Table 4.1: Number of paired samples analyzed for each pathology.

4.2.2 Results of each pathology

In this section, the dielectric properties of the characterized pathologies are represented. The properties of their healthy tissues are depicted as well. To this end, first of all an average of the captured properties of each pathology is performed frequency by frequency (this is, if we have x measurements of one particular pathology, the mean of each captured frequency is computed). Then, the resulting permittivity curve of each pathology is fitted to a 2-pole Cole-Cole equation, which is presented jointly with their respective standard deviations (these deviations are shown just for a few frequencies for an easier visualization). The computed Cole-Cole coefficients of each pathology are listed later in the Table 4.2

CRC

Adenocarcinomas are the most common type of CRC by far, and it has been the only type of cancer assessed in this work. This cancer can appear after a series of mutations of colonic glands. At Fig. 4.3 one can observe that the dielectric properties of CRC are higher in average that those from their healthy tissues. Differences in dielectric constant are getting lower with frequency, unlike conductivity and loss factor. The larger differences in dielectric constant are found for the lower frequencies, between 2 and 5 GHz approximately. As shown in the figure, the variability of the dielectric properties of CRC is quite high, larger than that of the healthy tissues of patients with this pathology. It can be due to differences in the biological structure of cancerous cells among the different patients, although a higher volume of samples is needed to certify it.

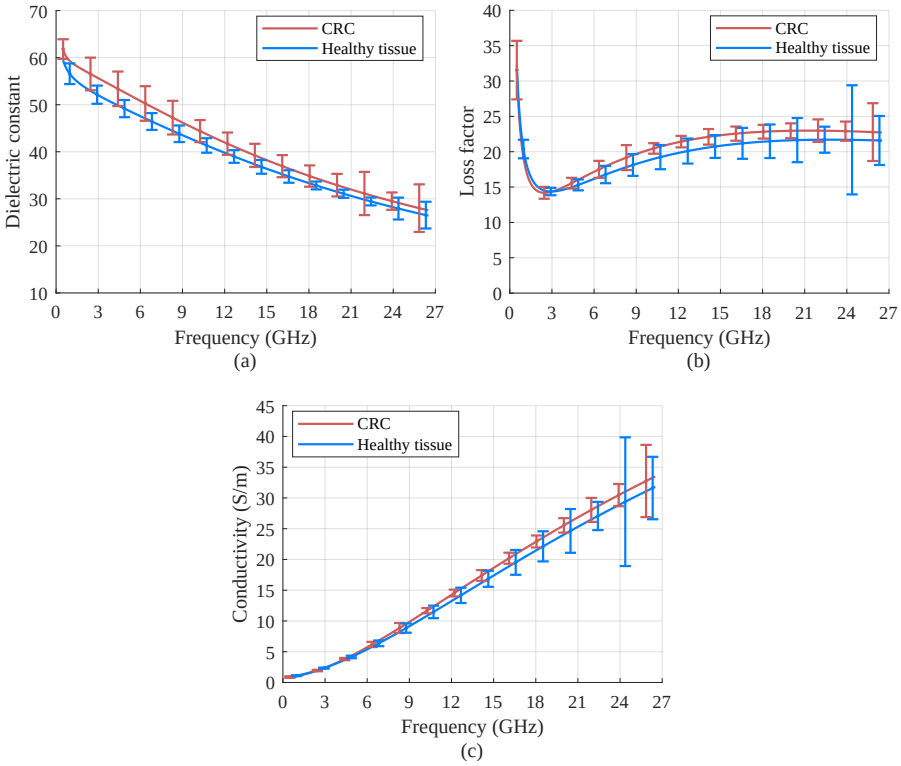

Figure 4.3: Averaged dielectric properties of the measurements of samples from patients with CRC jointly with their standard deviation.

Adenomas without dysplasia

Adenomas are benign tumours of epithelial tissue with glandular origin. However, they are considered a premalignant state of CRC. Its prevalence is quite high, and they are usually removed during colonoscopies because about in the 10% of individuals it becomes in CRC with time [116]. Observing Fig. 4.4, one can observe that the dielectric properties of the healthy and the adenomas without dysplasia of patients with this pathology are very similar. However, in this case, the average dielectric properties of the healthy tissue are above the pathological ones. Again, the variability of the pathological state is higher than of the normal one.

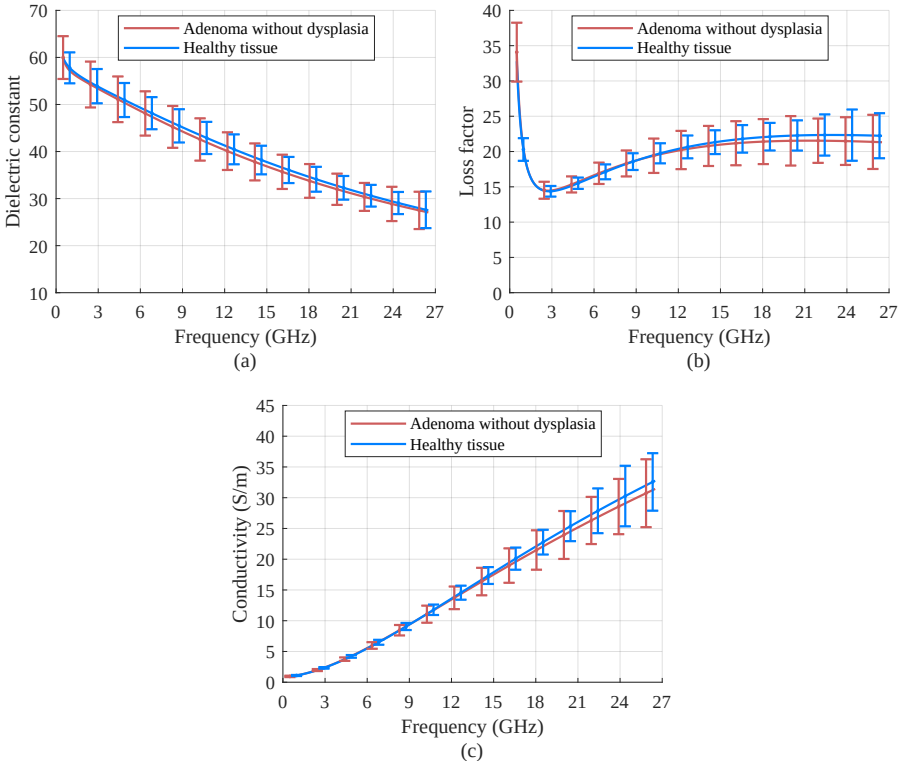

Figure 4.4: Averaged dielectric properties of the measurements of samples from patients with adenomas without dysplasia jointly with their standard deviation.

Adenomas with LGD

These are adenomas with an abnormal development of cells. In particular, the number of immature cells increases in contrast to the number of mature ones. It is often an indicative of an early neoplastic process. These kind of adenomas have been the most measured colon pathology. The average values of its dielectric properties are almost identical to those of the previous case. The variability of the properties of the pathological state is lower than that of the previous cases, being very similar to the normal one as one can observe in the Fig. 4.5. This could imply that the high variability observed for some of the other pathologies could be simply due to random errors, which effect was not reduced because of the lower number of measured samples.

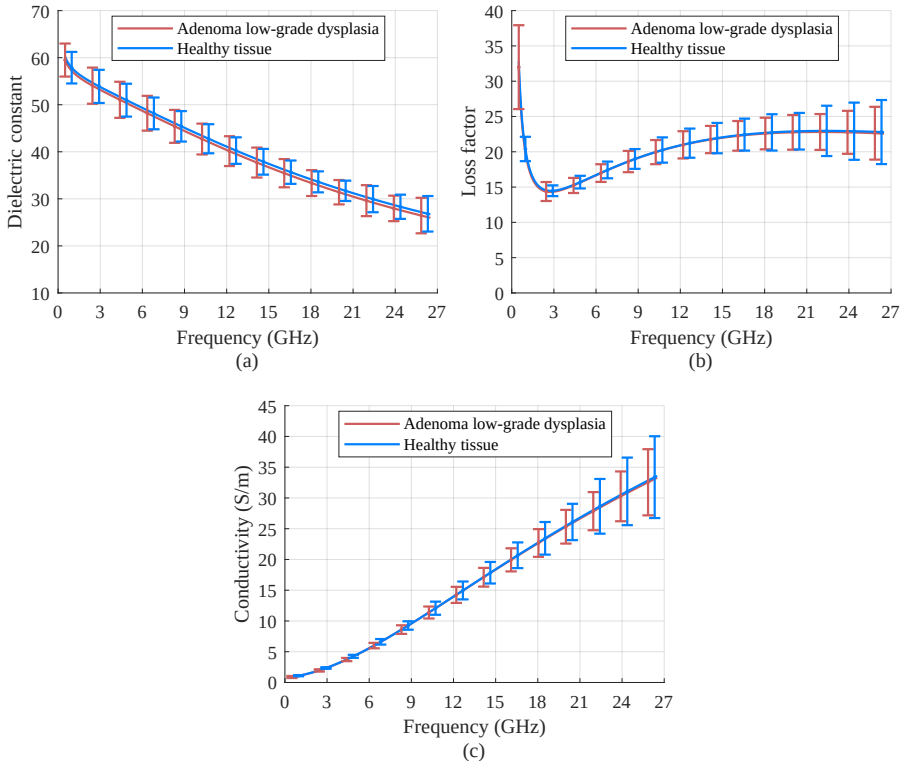

Figure 4.5: Averaged dielectric properties of the measurements of samples from patients with adenomas with LGD jointly with their standard deviation.

Adenomas with HGD

These are advanced states of adenomas with dysplasia, a more advanced state towards CRC. In the Fig. 4.6 are represented the averaged properties obtained for this kind of adenomas. Results are in agreement with the two previous cases: the electromagnetic properties of this kind of adenomas are very similar to the healthy tissues of the patients with this pathology. In addition, since the properties of the pathological state barely vary among the three kinds of adenomas, it seems that the degree of dysplasia is not affecting the dielectric properties. In this case, the variability of the pathological state is very similar to the normal one, having some outliers at frequencies above 21 GHz in the loss factor and the conductivity. This can be due to the greater noise of the measurements above 20 GHz, as the standard deviation is not following the trend observed for the lower frequencies.

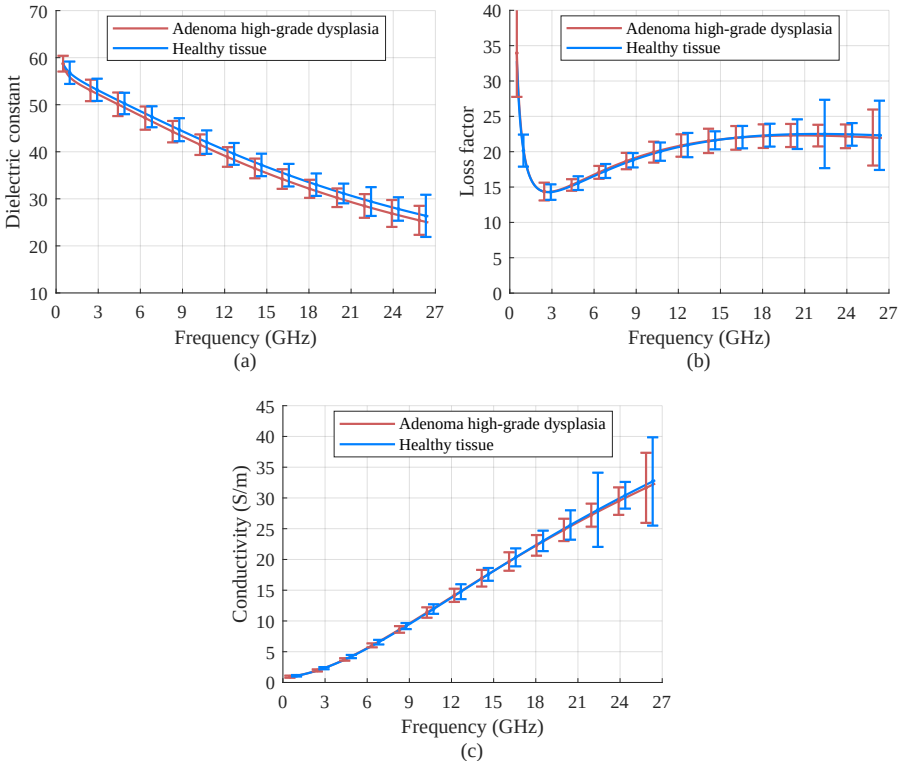

Figure 4.6: Averaged dielectric properties of the measurements of samples from patients with adenomas with HGD jointly with their standard deviation.

Hyperplastic polyps

Hyperplasia is a kind of benign polyp that, unlike the adenoma, is not usually considered to be premalignant. The properties obtained for hyperplastic polyps are depicted in the Fig. 4.7. One can observe that the dielectric properties of these polyps are almost the same than those of the normal tissues of the patients with this pathology. Still, the loss factor of the pathology is slightly higher than the normal state (and thus, the conductivity as well). The current case is the only one in which the variability shown by the properties of the normal state is significantly higher than that of the pathological ones. This reinforces the idea that some of the shown variabilities may not be very representative given the low pool of measurements performed, as occurred in the case of CRC measurements.

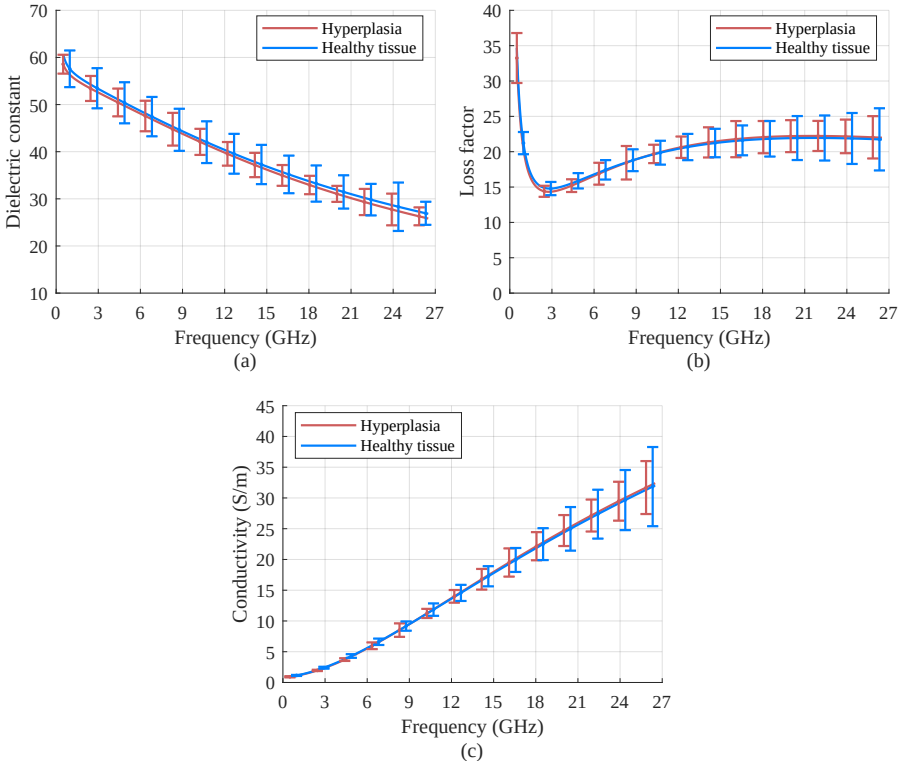

Figure 4.7: Averaged dielectric properties of the measurements of samples from patients with hyperplastic polyps jointly with their standard deviation.

Hamartomatous polyps

Hamartomas appear as a resulting of an increment of mature cells that have grown in a disorganized way, sometimes achieving a significant size. In the Fig. 4.8, the electromagnetic properties of this kind of colon polyps are plotted. Although this pathological state seems to have much lower properties than the normal state, it should be reminded that only samples from two patients were measured. In fact, the healthy properties are higher than in the previous case.

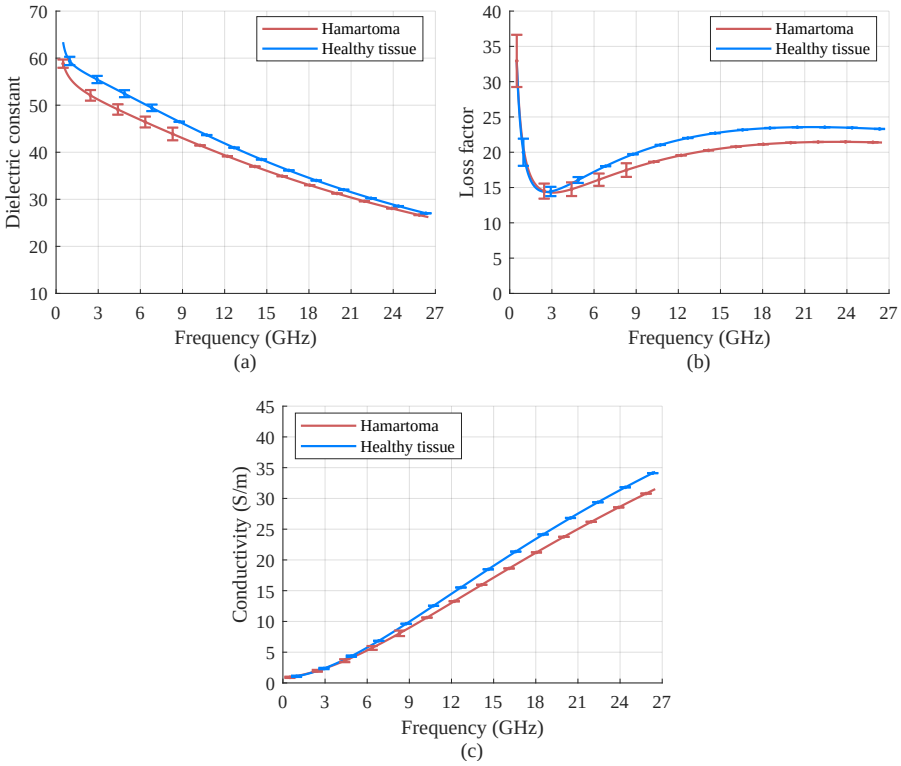

Figure 4.8: Averaged dielectric properties of the measurements of samples from patients with hamartomatous polyps jointly with their standard deviation.

As a general conclusion of the results presented so far, the cancerous tissues seem to have higher electromagnetic properties that the normal state, in contrast with the rest of pathologies, in which their properties are identical or even lower than those of the normal one. The Cole-Cole coefficients of the average

	ϵ_∞	$\Delta\epsilon_1$	τ_1[**ps**]	α_1	$\Delta\epsilon_2$	τ_2[**ns**]	α_2	σ_s
CRC	1	59.137	7.039	0.177	343.943	3.735	0.000	0.001
Healthy	1	51.654	6.384	0.152	943.856	439.155	0.400	0.575
Adenoma	1	57.074	6.920	0.198	146.148	2.279	0.000	0.323
Healthy	1	54.574	6.427	0.160	636.370	439.155	0.400	0.674
Ad. LGD	1	53.363	6.752	0.135	723.844	439.155	0.400	0.629
Healthy	1	53.889	6.595	0.138	750.889	439.155	0.400	0.644
Ad. HGD	1	54.668	7.206	0.152	449.323	4.784	0.028	0.001
Healthy	1	54.074	6.726	0.147	734.728	439.155	0.368	0.684
Hyperplasia	1	54.433	6.881	0.155	190.569	9.738	0.178	0.573
Healthy	1	55.962	6.803	0.179	664.180	7.682	0.056	0.001
Hamartoma	1	50.293	6.240	0.145	1032.396	439.155	0.400	0.571
Healthy	1	57.832	7.002	0.150	239.442	2.551	0.024	0.001

Table 4.2: Cole-Cole coefficients of the fitted permittivity of both the presented pathologies and the healthy samples of patients with these pathologies.

permittivity of the shown pathologies and the normal tissues of the patients with these pathologies are listed in the Table 4.2.

Due to the acquisition frequencies of the measurements performed in this thesis, only the poles related to the dispersions δ and γ are computed, since any effect of α and β dispersions are noticeable within them. Hence, eight terms of the Cole-Cole equation are provided for each fitting shown in this dissertation. The most important ones are the coefficients of the γ-dispersion, indicated by the subscript "1", since they have an effect almost at all measured frequencies (their weight is higher from 2 GHz). In particular, the term $\Delta\epsilon_1$ quantifies the initial dielectric constant of the dispersion, whereas τ_1 and α_1 describe the decreasing trend of the dielectric constant with frequency. Besides, τ_1 is related to the relaxation frequency of this pole, meaning that around that frequency $f_1 = 2\pi/\tau_1$ [Hz] there is a local maximum in the loss factor and a maximum of the slope of the dielectric constant.

Regarding δ-dispersion, its coefficients describe the change of trend of the dielectric constant in the lower measured frequencies (below 2 GHz). Combined with the conductivity term σ_s, they also quantify the values of loss factor below 4 GHz. It should be mentioned that the computed coefficients for the second pole are not physically significant and they only serve for fitting purposes, since many frequencies of this dispersion region are not measured. The same occurs with ϵ_∞, related to the permittivity when frequency tends toward infinity, since not enough high frequencies have been measured.

4.2.3 Differences between healthy and pathological states

As already commented at the beginning of the chapter, it is important to compute the differences between the suspicious and the healthy samples of a patient since measuring just the suspicious tissue would not give enough data to diagnose it: the variability in the absolute values is quite high, and therefore is not possible to establish a threshold in the absolute values of dielectric constant to determine whether a suspicious sample is cancer or not (due to the reasons explained at the beginning of the present chapter).

For each characterized pathology, the differences in dielectric constant, loss factor and conductivity are presented by means of box and whisker plots. They represent the median of the differences, the upper and lower quartiles, the highest and lowest differences and the measurement outliers. The differences in dielectric constant were particularized at 2.45 GHz. On the one hand, we chose this frequency since the larger differences in this property between CRC and normal tissues appear below 5 GHz, as we showed in the previous section. On the other hand, future detection systems could operate in this frequency, since it belongs to the Industrial, Scientific and Medical (ISM) bands available for current and future application deployments. With respect to the loss factor, larger differences between healthy and cancerous cells are found around 12.5 GHz. This frequency is selected since, unfortunately, no ISM bands are allocated close to this frequency. Regarding the conductivity, 18 GHz was chosen despite the differences in higher frequency bands are greater since noise becomes an altering factor at computing the standard deviation above this frequency.

The differences in dielectric constant $\Delta\epsilon'_r$ are computed just with a trivial subtraction, as shown in the Eq.4.1, being the differences in loss factor $\Delta\epsilon''_r$ and in conductivity $\Delta\sigma$ [S/m] computed in the same manner.

$$\Delta\epsilon'_r = \epsilon'_{pathlogy} - \epsilon'_{healthy} \tag{4.1}$$

Dielectric constant

The box and whisker plot of the differences on dielectric constant at 2.45 GHz is shown in the Fig. 4.9, for the characterized pathologies. Positive differences are found only for the CRC case, as was expected from the previous section. The median of this difference is 4.8 units, which is quite significant. On the other hand, the adenomas (regardless their degree of dysplasia) and hyperplastic polyps show almost the same median, slightly below 0 units. One can observe that the boxes are a bit large, meaning that the difference varies significantly among patients. Hamartomas have not been included in this analysis given the scarcity of measurements performed regarding this pathology.

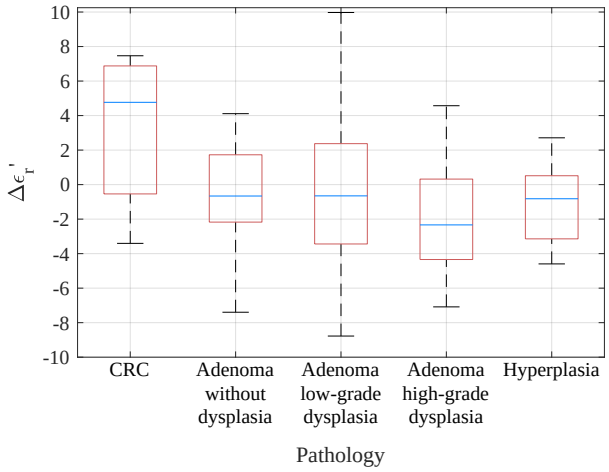

Figure 4.9: Box and whisker diagram of the difference between pathological and healthy tissues in dielectric constant at $f = 2.45$ GHz.

Loss factor

In the Fig. 4.10 is represented the box and whisker plot of the differences on loss factor at 12.5 GHz. The differences are positive not only for CRC, but also for adenoma without dysplasia and hyperplasia. Once more, larger differences are found for CRC, having a median of 2.25 units. Regarding the adenomas, their boxes are quite similar, meaning that their loss factors usually lie within the same units regardless their degree of dysplasia. As expected from Fig. 4.7, the difference between hyperplastic and healthy samples within patients has a median of almost zero units. Again, boxes are quite large, implying that the obtained differences change significantly among patients.

Conductivity

Lastly, the box and whisker diagram of the differences on conductivity at 18 GHz is shown in the Fig. 4.11. If we had presented these differences in the same frequency than loss factor, their distribution would have been identical, only changing the scale (since the same factor would have applied to all the data, see the Eq. 2.2). However, we chose to present the differences at a higher frequency since the differences in conductivity between CRC and healthy tissues are higher at larger frequencies. One can observe that, again, the larger

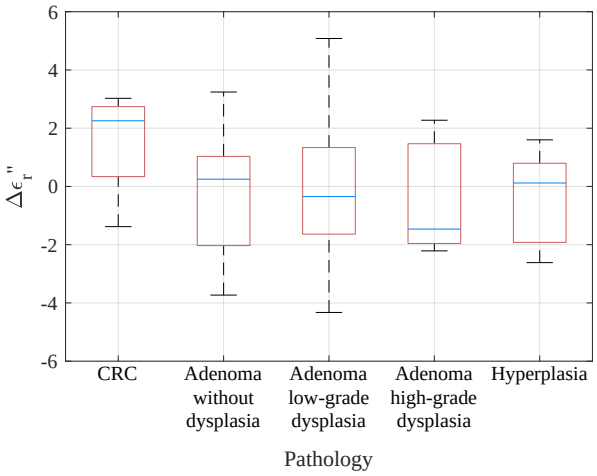

Figure 4.10: Box and whisker diagram of the difference between pathological and healthy tissues in loss factor at $f = 12.5$ GHz.

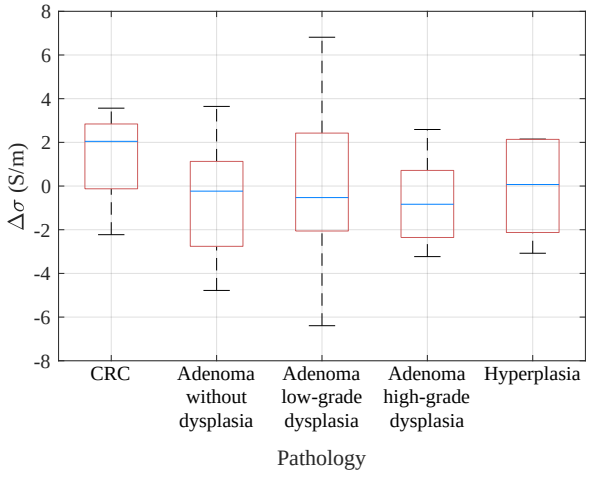

Figure 4.11: Box and whisker diagram of the difference between pathological and healthy tissues in conductivity at $f = 18$ GHz.

differences are found for CRC. Adenomas have similar differences with respect to healthy tissues, with a median of zero units (as the hyperplastic polyps).

4.2.4 Detection performance

With the aim at studying the validity of the open-ended coaxial technique for detecting the presence of CRC, the markers of performance of the system considering the dielectric data gathered in the previous sections have been computed. Since the maximum differences are found in the lower frequencies of the dielectric constant, we chose the unlicensed 2.45 GHz ISM frequency of this property to carry out the analysis of diagnostic capability. It should be mentioned that, apart of being greater differences, the significance of them is higher as the error bars are less superimposed (see Fig. 4.3). Therefore, a threshold of 3.1 units in the difference in dielectric constant between the suspicious and the healthy (control) samples has been selected, as this value maximizes the accuracy of the system (maximizes its capability to identify correctly both cancerous and non-cancerous samples). According to the diagnosis, this system can return the following kind of results:

- **True Positive (TP)**: The disease has been correctly diagnosed for an ill patient.
- **True Negative (TN)**: The disease has not been diagnosed for a healthy patient.
- **False Positive (FP)**: The disease has been diagnosed for a healthy patient.
- **False Negative (FN)**: The disease has not been detected for an ill patient.

From these for kind of results, five markers of performance of the system can be computed. The sensibility (Eq. 4.2) is the probability of classifying correctly an ill patient, this is, the probability of getting a positive value from a patient that suffers from CRC. The specificity quantifies the probability of classifying correctly a healthy patient, which is the probability of having a negative result for a patient without CRC (Eq. 4.3). The Positive Predictive Value (PPV) reflects the proportion of positive results that corresponds to truly sick patients (Eq. 4.4), whereas the Negative Predictive Value (NPV) states the proportion of negative results that corresponds to truly healthy patients (Eq. 4.5). Finally, the Global Predictive Value (GPV), which can be identified as the accuracy of the system, reflects the proportion of correct results among the totality of cases assessed (Eq. 4.6).

$$Sensibility = 100 * \frac{True\ positives}{Number\ of\ positive\ cases} = 100 * \frac{\mathrm{TP}}{\mathrm{TP} + \mathrm{FN}} = 75.0\% \quad (4.2)$$

$$Specificity = 100 * \frac{True\ negatives}{Number\ of\ negative\ cases} = 100 * \frac{\mathrm{TN}}{\mathrm{TN} + \mathrm{FP}} = 88.7\% \quad (4.3)$$

$$PPV = 100 * \frac{True\ positives}{Total\ of\ positives} = \frac{\mathrm{TP}}{\mathrm{TP} + \mathrm{FP}} = 46.2\% \quad (4.4)$$

$$NPV = 100 * \frac{True\ negatives}{Total\ of\ negatives} = 100 * \frac{\mathrm{TN}}{\mathrm{TN} + \mathrm{FN}} = 96.5\% \quad (4.5)$$

$$GPV = 100 * \frac{True\ diagnosis}{Number\ of\ cases} = 100 * \frac{\mathrm{TP} + \mathrm{TN}}{\mathrm{TP} + \mathrm{TN} + \mathrm{FP} + \mathrm{FN}} = 87.5\% \quad (4.6)$$

As the permittivity values of healthy and pathological samples decrease with frequency more or less at the same level, these detection markers are kept even if a potential system is designed for upper frequencies. For instance, at 10 GHz the markers remain identical if the threshold is moved accordingly (as the absolute differences are reduced). For the same value of sensitivity, considering either the loss factor or the conductivity reduces the overall performance of the system to an accuracy (or GPV) of less than 85% whatever the frequency considered.

Although we have found out differences between healthy and cancerous samples, we did not find significant differences to diagnose any other pathology. Hence, two major actions can be performed with the open-ended coaxial system. On the one hand, it can be utilized to discard samples that the colonoscopist already thought were not malignant, avoiding thus any additional burden to the pathology unit. In the detection markers we appreciate a NPV of 96.5%, that is in accordance with the threshold of $\geq 90\%$ established by the Preservation and Incorporation of Valuable Endoscopic Innovation document written by the American Society of Gastrointestinal Endoscopy (ASGE), which gives an interesting approach to our system [117]. On the other hand, it could be used to speed up the pathological analysis of suspicious samples, if both the visual inspection and the electromagnetic processing suggest the likelihood of being malignant.

In future deployments, systems should consider a safety margin from the selected threshold as results always have a certain amount of uncertainty. In this case, uncertainties are related to factors such as the measurement system and calibration (Section 2.3.3), tissue dehydration and measurement errors. In any case, the performance markers provided could change with a larger volume of results. For instance, the number of cancerous biopsies is low and thus the addition of more results could affect the performance in terms of sensibility substantially.

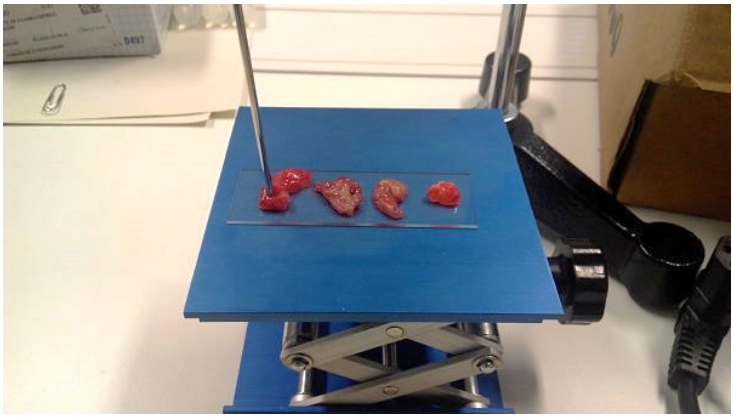

Figure 4.12: Measurement of colon samples gathered from a surgery procedure.

4.3 Measurement of surgery samples

The protocol of sample gathering as well as the results obtained from the measurements of surgery resections are detailed in this section. This source was considered given the large size of the measurement samples and the certainty of being characterizing cancerous samples. A total of 20 paired samples (pathological and healthy from the same patient) from this source have been analyzed.

4.3.1 Sample collection protocol

As occurred with the previous campaign, the protocol for collecting and measuring the biological samples was prepared by the medical supervisor and then approved by the ethical committee of the hospital. The protocol guides through the steps that have to be followed from the first contact with the patient until the storage of the dielectric properties:

1. Before starting the surgical procedure, patients that carry CRC are informed by the medical staff of the aim of the study and asked to participate in it. If they are willing to take part in it, they have to sign a consent form giving their permission.

2. The colon surgery is performed. In this operation, the part of the colon that contains the cancer is removed. Part of the surrounding healthy tissue is extracted as well to ensure that no cancerous cells remain. Then, one sample of healthy tissue and a malignant one are cut, placed in empty

receptacles and sent to the measurement room as soon as possible (between 20 and 30 minutes from excision).

3. In the measurement room, a calibration of the system is performed recurrently in order to be ready to measure when samples arrive. Both samples are placed in a glass sheet and pressed to the tip of the open-ended coaxial sensor, as it can be seen in the Fig. 4.12. Five measurements are performed and stored, using a numerical code to relate them with their medical history.

4. All the equipment that has been in contact with a biological sample (i.e., sensor's tip, forceps to place the samples in glass sheets) is cleaned using either acetone or ethanol. Samples are put back into the plastic receptacles and dropped in a suitable container.

4.3.2 Results

The dielectric constant, loss factor and conductivity of the healthy and the cancerous tissues are represented in the Fig. 4.13 jointly with their respective standard deviations. As performed as well with the results from the biopsies campaign, these properties have been obtained after applying a 2-pole Cole-Cole fitting to the average properties computed. Comparing the dielectric constant of both states, one can observe that the dielectric constant of malignant colon tissue is around five points higher than that of healthy tissue at lower frequencies (5.06 averaging the first 4 GHz), whereas above this frequency the difference tends to decrease. **Analyzing the entire frequency band in relative terms, the mean of the dielectric constant of malignant tissues is 8.40% higher averaging all the measured frequencies.** As commented in the introduction chapter, [118] explained that this significant difference is due to the higher water content that cancerous tissues have. Moreover, since proteins acquire more surface charges in cancerous tissues, water molecules are attracted to them causing an increment of "bound water" [56]. On the other hand, error bars show a lower standard deviation of the dielectric constant of malignant tissues with respect to healthy ones in the whole frequency band, showing thus a narrower dispersion of the measurements of this kind of tissue. This effect was also noticed in the liver *ex vivo* report of [53].

Loss factor differences are slightly higher in relative terms (10% averaging all the acquisition frequencies), but the standard deviation is much greater as one can observe from the error bars. Regarding the conductivity, the differences between normal and cancerous cells are small and noticeable above 6 GHz, but they have less statistical significance since the error bars are highly superimposed in almost all of the studied frequency band. These differences increase

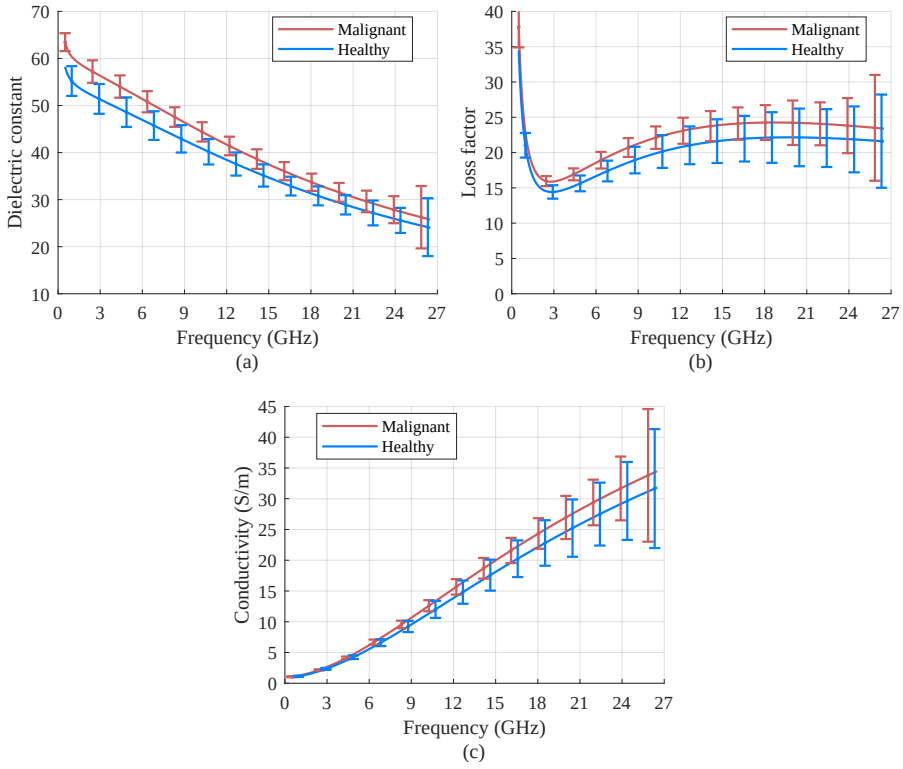

Figure 4.13: Averaged dielectric properties of the measurements of samples from surgery resections jointly with their standard deviation. (a) Dielectric constant, (b) loss factor, (c) conductivity.

with frequency due to the frequency factor that multiplies the imaginary part of the permittivity, as one can see in the Eq. 2.2. Again, the standard deviation of malignant tissues is lower than that of healthy ones, as one can observe from the error bars.

Results have been particularized for six frequencies: 500 MHz, 900 MHz, 2.45 GHz, 5 GHz, 8.5 GHz, 12.5 GHz and 18 GHz. These frequencies have been chosen in order to give specific values of our measurements and analyze them in the following sections. Besides, the 500 MHz, 900 MHz and 5 GHz bands facilitate comparing our results with literature data. The particular data for 900 MHz and 2.45 GHz can be useful in the design of devices that work in the the already available 915 MHz and 2.45 GHz ISM bands (the electromagnetic properties of 900 and 915 MHz are almost identical). The upper frequencies

(8.5, 12.5 GHz and 18 GHz) have been chosen for showing specific data at higher frequencies. The mean and the standard deviation of the dielectric parameters for the seven discrete frequencies are presented in the Tables 4.3 and 4.4 for healthy and malignant tissues, respectively. In general, it can be seen that for any dielectric parameter and frequency, the values of the malignant state are higher and their deviation lower than the healthy ones.

Frequency	ϵ_r'	ϵ_r''	σ[**S/m**]
0.5 GHz	63.16 ± 2.05	37.81 ± 2.91	1.06 ± 0.08
0.9 GHz	60.80 ± 2.27	24.00 ± 1.65	1.20 ± 0.09
2.45 GHz	57.19 ± 2.46	15.95 ± 0.70	2.17 ± 0.10
5 GHz	53.10 ± 2.49	17.52 ± 0.93	4.87 ± 0.28
8.5 GHz	47.25 ± 2.22	20.87 ± 1.39	9.89 ± 0.74
12.5 GHz	40.97 ± 2.01	23.22 ± 1.91	16.14 ± 1.33
18 GHz	33.75 ± 1.86	24.25 ± 2.43	24.29 ± 2.43

Table 4.3: Dielectric data of malignant tissues particularized for discrete frequencies. Mean and standard deviation values.

Frequency	ϵ_r'	ϵ_r''	σ[**S/m**]
0.5 GHz	57.86 ± 2.96	34.46 ± 2.89	0.97 ± 0.08
0.9 GHz	55.55 ± 3.06	22.01 ± 1.86	1.10 ± 0.09
2.45 GHz	52.14 ± 3.11	14.53 ± 0.96	1.98 ± 0.12
5 GHz	48.46 ± 3.12	15.75 ± 1.14	4.38 ± 0.30
8.5 GHz	43.35 ± 2.94	18.74 ± 1.83	8.86 ± 0.84
12.5 GHz	37.80 ± 2.53	20.96 ± 2.69	14.57 ± 1.87
18 GHz	31.33 ± 1.94	22.10 ± 3.42	22.14 ± 3.42

Table 4.4: Dielectric data of healthy tissues particularized for discrete frequencies. Mean and standard deviation values.

The Cole-Cole fitting coefficients are presented in the Table 4.5. As already commented at the end of Section 4.2.2, one of the most characteristic parameters is $\Delta\epsilon_1$, since it quantifies approximately the dielectric constant at the initial frequencies of γ-dispersion, above 1 GHz. The other coefficients of that pole describe the decreasing trend of the dielectric constant with frequency as well as the values and frequency of the local maximum of the loss factor. The second pole is less significant, but jointly with the conductivity term it is useful for fitting the properties at the lower measured frequencies.

	ϵ_∞	$\Delta\epsilon_1$	$\tau_1[\mathbf{ps}]$	α_1	$\Delta\epsilon_2$	$\tau_2[\mathbf{ns}]$	α_2	σ_s
Malignant	3.690	55.268	7.915	0.114	983.172	10.900	0.065	0.005
Healthy	2.746	50.580	7.487	0.116	1196.854	16.090	0.085	0.005

Table 4.5: Cole-Cole coefficients of the fitted permittivity of the cancerous and the healthy samples from surgery resections.

4.3.3 Differences between healthy and malignant states

In this section, we evaluate the change in dielectric properties between the healthy and the cancerous tissues of each patient, and then we analyze how these differences vary among the 20 patients (in terms of its probability distribution and standard deviation). Although the average of this difference can be computed directly from the wideband data, its standard deviation should be calculated in order to assess the reproducibility of this difference among patients.

In the Fig. 4.14, the averaged differences in the dielectric properties between the healthy and the malignant tissues within the same patient are presented jointly with their standard deviation (in error bar format). As expected from the previous results, and agreeing well with the results provided in Section 4.2.3 for the biopsies campaign, the larger differences are found in the lower frequencies of the dielectric constant. In addition, this difference is the most significant considering the error bars, since even considering the standard deviation it remains greatly above zero units: considering the particular frequency of 2.45 GHz, the difference is above 3.1 units for 19 out of the 20 patients considered. This difference in dielectric constant is reduced gradually when the frequency is increased, in both absolute and relative terms. This decrease could be explained by the information presented in [49, 50]. These works expound that the difference between the electromagnetic absorption of healthy and malignant tissues has its maximum peak between 100 and 800 MHz, centered approximately on 400 MHz, which can be related to the maximum differences of permittivity among them.

Regarding the standard deviation, it slightly decays with frequency in the dielectric constant, whereas in contrast it increases in loss factor. For both properties, there is an increase above 18 GHz due to the rise of the measurement noise above this frequency. The average and the standard deviation of the computed differences have been particularized in the Table 4.6 for the discrete frequencies selected in the previous section.

Besides, a Kolmogorov−Smirnov test has been performed at each frequency in order to characterize the kind of distribution that fits better the differences between tissues of the same patient (the kind of functions are the same than

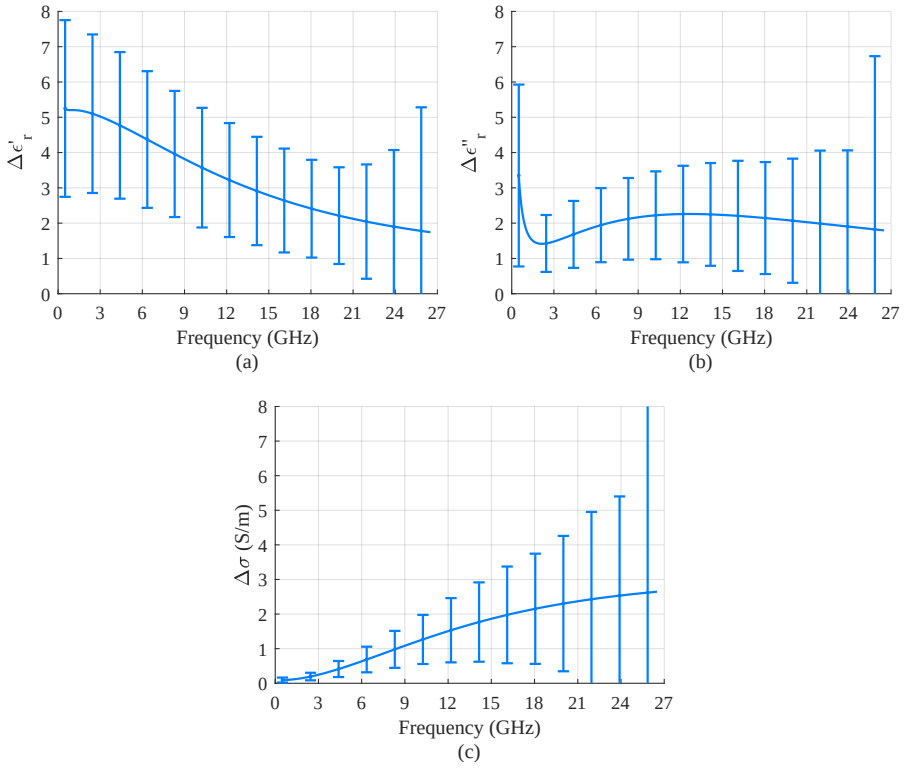

Figure 4.14: Mean and standard deviation of the differences in the dielectric properties of the measurements of surgery samples: (a) dielectric constant, (b) loss factor, (c) conductivity.

Frequency	$\Delta\epsilon'_r$	$\Delta\epsilon''_r$	$\Delta\sigma$[**S/m**]
0.5 GHz	5.25 ± 2.58	3.35 ± 2.58	0.09 ± 0.08
0.9 GHz	5.25 ± 2.57	1.98 ± 1.49	0.10 ± 0.09
2.45 GHz	5.04 ± 2.61	1.42 ± 0.81	0.19 ± 0.12
5 GHz	4.63 ± 2.54	1.77 ± 0.97	0.49 ± 0.29
8.5 GHz	3.90 ± 2.42	2.14 ± 1.16	1.03 ± 0.65
12.5 GHz	3.17 ± 1.59	2.26 ± 1.38	1.57 ± 0.96
18 GHz	2.42 ± 1.39	2.15 ± 1.57	2.15 ± 1.58

Table 4.6: Difference between the dielectric properties of malignant and healthy tissues particularized for discrete frequencies. Mean and standard deviation values.

those tested in Section 3.3.1). The test has shown that the logistic distribution is the one that better fits this difference at most frequencies (see the Eq. 4.2). In the Fig. 4.15 the logistic distributions of the difference in dielectric constant at 2.45 GHz, in loss factor at 12.5 GHz, and in conductivity at 18 GHz are represented. The motivation of selecting these frequencies is the same as in Section 4.2.3.

One can observe that the distribution of the difference in dielectric constant at 2.45 GHz is more relaxed than the other two distributions. It means that, for a particular measurement session, the probability of obtaining a difference in dielectric constant close to the mean value is lower than in the other two dielectric properties (e.g., the spread of the data is higher). Still, it can be observed that the probability density of a difference of zero units is much lower in dielectric constant at 2.45 GHz than for the differences in loss factor at 12.5

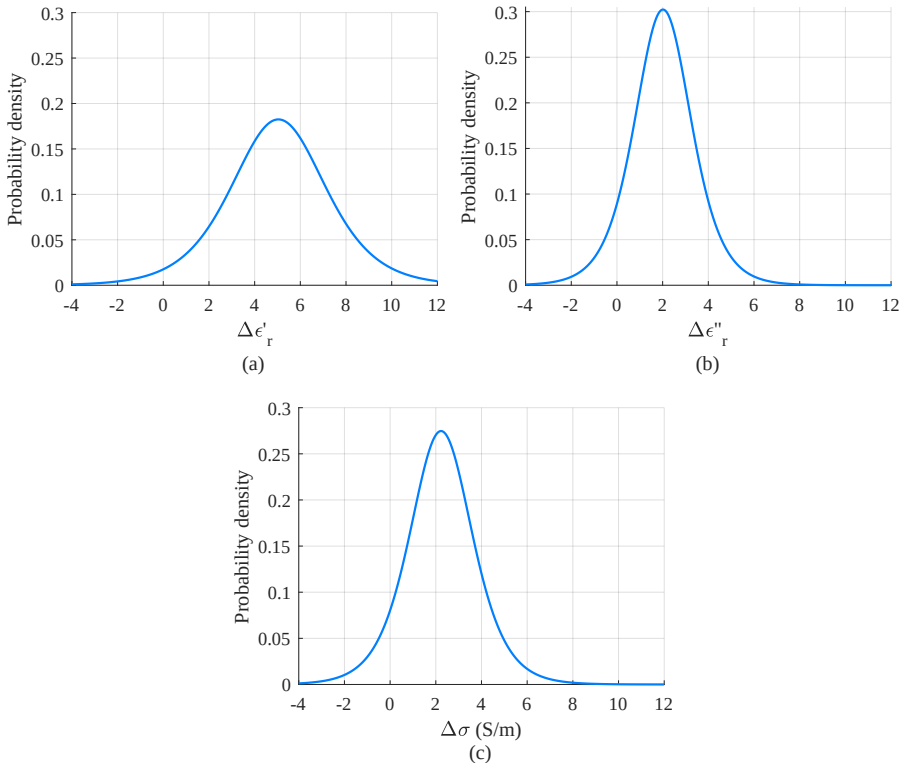

Figure 4.15: Probability densities of the differences in dielectric constant at 2.45 GHz (a), in loss factor at 12.5 GHz (b) and in conductivity at 18 GHz (c).

GHz and in conductivity at 18 GHz (0.018 vs 0.089 and 0.080, respectively), and thus the likelihood of having positive differences is much higher in this property.

4.4 Comparison with other studies

The electromagnetic properties of the healthy and the pathological colon tissues obtained through the previous measurement campaigns are compared to previously published data from other sources (if their data are within our acquisition frequencies). The gathered information is listed in the Table 4.7.

Source	Type	Frequency	Reference
Human	H,M,P	0.5 - 26.5 GHz	This thesis
Human	H,M,P	0.5 - 20 GHz	Guardiola [107]
Human	H,M	500 - 900 MHz	Joines [51]
Ovine	H	10 Hz - 20 GHz	Gabriel [87]
Mice	M	200 MHz - 5 GHz	Yoo [52]

Table 4.7: Sources of dielectric properties of colon tissues. H=Healthy, M=Malignant, P=Pathological.

The dielectric properties of healthy colon tissues gathered from the different sources are represented in the Fig. 4.16. As one can observe, the properties obtained from human biopsies and surgery samples of the present study have very similar values. On the other side, the measurements performed *in vivo* in porcine models have larger values, although keeping the same trend that the other sources. These measurements are presented in the chapter devoted to *in vivo* measurements (Chapter 3), and the properties are more than 11% higher than the other *ex vivo* sources.

Regarding the other sources, the properties of healthy colon measured *ex vivo* by Gabriel [87] have the same trends with frequency than ours, although with lower values. The same could be stated for the measurements performed by Joines [51]. On the contrary, the properties of healthy colon measurements performed by Guardiola *et al.* do not follow the same trend than the rest of the sources [107]. Two reasons can explain this divergence: firstly, they only used a single pole to model the permittivity, which causes fitting errors at the lower frequencies, especially in the dielectric constant since the effect of one dispersion region is not model; secondly, the relaxation frequency that they obtained was around 28 GHz, which is much higher than water's and hence it seems unrealistic. The latter can be due to possible measurement errors,

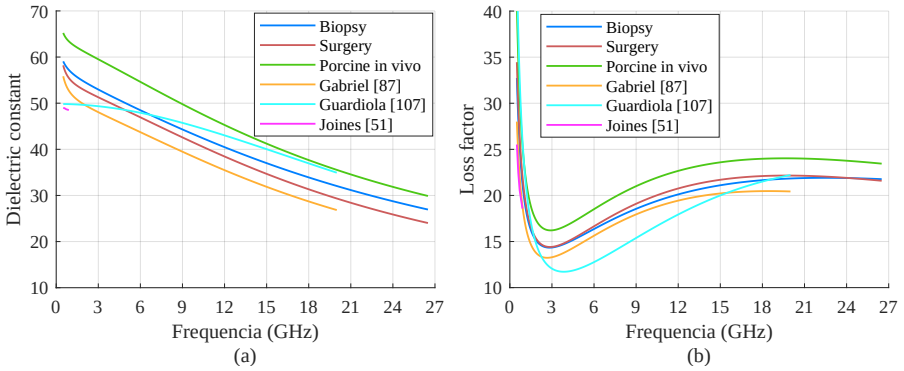

Figure 4.16: Dielectric properties of healthy colon tissue measured in this thesis and in literature: (a) dielectric constant, (b) loss factor.

since in their study it can be appreciate that the dielectric constant of their healthy measurements did not decreased continuously with frequency, as it should have. A miscalculation of the relaxation frequency affects to the trend of the dielectric constant as well as to the local maximum of the loss factor related to the γ-dispersion.

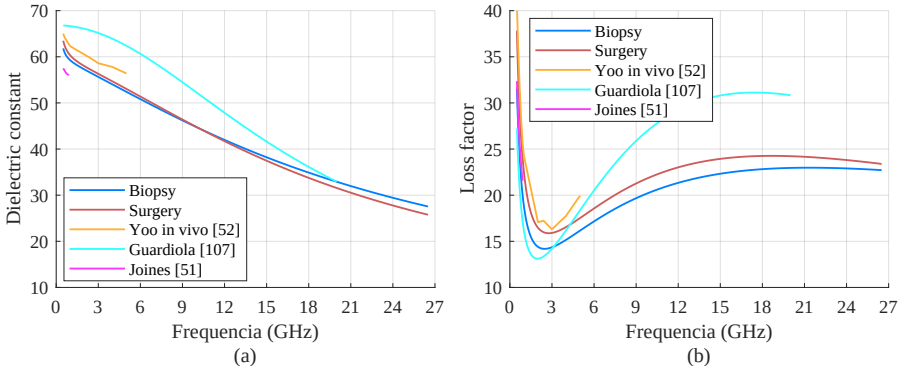

Figure 4.17: Dielectric properties of malignant colon tissue measured in this thesis and in literature: (a) dielectric constant, (b) loss factor.

The dielectric properties of malignant colon tissues gathered from the different sources are depicted in the Fig. 4.17. As occurred with the healthy colon, the properties obtained from human biopsies and surgery samples of the present study have very similar values, although in this case surgery's loss factor is slightly higher. Again, an *in vivo* study showed higher values than

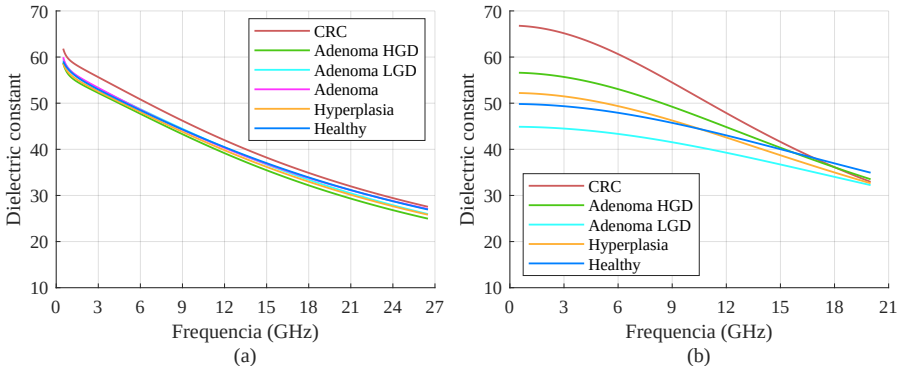

Figure 4.18: Dielectric properties of pathological colon tissue measured in: (a) this thesis (biopsy samples), (b) Guardiola *et al.* [107].

our *ex vivo* campaigns, but keeping as well the trend of the properties with frequency. The study of Guardiola *et al.* showed again an inconsistency with respect to the rest of the studies [107]. Observing the raw measurements that they performed on this kind of samples, it seems that in this case the strange trend of the properties may be due to a bad fitting of the measurements.

The dielectric constants of pathological colon tissue of the present thesis are compared to those presented in Guardiola *et al.* [107]. One can observe immediately that our results are much more pessimistic for diagnostic purposes, since the dielectric constants of most pathologies are almost identical. The only significant differences can be found between healthy and CRC samples, as it was exposed in Section 4.2.3, but these are anything comparable to the values presented in [107].

Still, we consider that the results published in Guardiola *et al.* are not very reliable. Colon is a high water-content tissue, and then it must have a large dielectric constant. It should have similar values as the rest of the organs of the gastrointestinal system and not like cartilage or skin, which have less content of water, for instance. Even though the results presented by our study make the development of a CRC detection application more challenging, they are in agreement with the studies listed in Appendix A and with the rest of colon sources presented previously, having thus higher credibility.

4.5 Conclusion

In this chapter is presented all the data concerning the dielectric properties of colon tissues. Two different campaigns have been carried out, both of them

aiming at obtaining the properties not only of healthy but also of cancerous and pathological states. The first one consisted in measuring the electromagnetic properties of colon tissues obtained from colonoscopy procedures, whereas in the second one tissues were characterized by taking samples from surgery procedures.

In both experiments, the enhanced calibration with methanol was used. Apart from the absolute dielectric properties of the tissues, the differences between healthy and malignant tissues (and pathological, when applicable) have been analyzed, presenting the 2-pole Cole-Cole fitting coefficients computed for each tissue type. In summary, potential applications of cancer detection should find differences between both states (cancer and control) rather than analyzing the properties of malignant samples independently. This is due to the fact that absolute properties of colon tissue, either healthy or not, vary for different reasons (patient itself, elapsed time between extraction and measurement, temperature and incineration of the system), affecting both states in a similar way.

On the one hand, the healthy and the pathological **biopsies from 71 patients have been analyzed** within the first measurement campaign. Eight colorectal cancer (CRC) samples, 13 adenomas without dysplasia, 29 adenomas with HGD, 12 adenomas with LGD, 7 hyperplastic polyps and 2 hamartomatous polyps have been measured. In addition, a total pool of 250 healthy samples has been measured as well. Results showed that, except for CRC samples, the dielectric properties of the pathological tissues were - in average - almost identical to those of healthy tissues. **Regarding CRC, the median of the difference in dielectric constant between healthy and malignant tissues was higher at lower frequencies, being of 4.8 units at ISM 2.45 GHz band.** The differences in conductivity were lower than in dielectric constant, and those increased with frequency. At 18 GHz, the median of the difference was of 2 units. However, it should be mentioned that the variability of the results is quite high, due to factors like varying tissue dehydration rates between healthy and pathological samples, and small sample size. Finally, selecting a threshold in the difference in dielectric constant between cancer and control tissues that maximizes the performance of a CRC detection system, the diagnostic markers are of 75%, 88.7%, 46.2%, 96.5% and 87.5% for the sensitivity, specificity, PPV, NPV and GPV (accuracy).

On the other hand, a total of **20 paired samples from surgery samples have been characterized**. The differences calculated between healthy and malignant tissues are in agreement with those obtained from the biopsies. **The difference in dielectric constants is higher at lower frequencies, with a mean of 5.04 points.** In this case, the variability is a bit lower than in the case of the biopsies, probably because the size of the samples was higher and,

then, tissue dehydration affected to a lesser extent. A Kolmogorov-Smirnov test was applied on the dielectric data in order to find the distribution that fits better the variability of the differences, being the logistic the best option. Finally, results have been compared to other studies in which colon tissue has been assessed, obtaining similar values to those presented in Gabriel's database, the most widespread one.

Chapter 5

Proposed systems for colon cancer detection

This chapter aims at presenting two approaches of colon cancer detection system based on making use of the electromagnetic differences presented in the previous chapter. The first approach involves analyzing biopsies right after their removal, similarly to the manner in which biopsies were characterized in Section 4.2 but with a few modifications. The second approach involves designing a flexible sensor capable of measuring colon tissues both *in vivo* and *in situ*. Among other features, the sensor must be large and thin enough to be embedded into a channel of a colonoscope. Before presenting these two approaches in higher detail, an alternative calibration that facilitates the use and the implementation of both systems is explained.

5.1 Introduction

As explained in Chapter 1, population screening programs are of huge importance to detect and diagnose cancer. If cancer is found soon, the survival probability increases and treatments can be less expensive. CRC screening tests can be classified into two main groups: invasive and non-invasive.

Colonoscopy and flexible sigmoidoscopy are the invasive tests available for CRC detection. These tests allow direct observation of the colonic wall. Nowadays, colonoscopy is the primary screening tool in many countries. This technique allows not only detecting cancerous tissues or other pathologies, but also offers the possibility of resecting some lesions or at least estimate their locations for a future surgery. Although being quite safe, this technique require

previous patient preparation and sedation. Some studies have estimated that the CRC mortality of people that go through a colonoscopy procedure is reduced between a 68% and an 88% with respect to people that do not [119–121]. However, it is worth mentioning that depending on the size of the polyps and the expertise of the medical doctor, some lesions may not be detected. Many technological advances have been made throughout the last years in order to optimize the detection of precursor lesions, mostly focused on improving the quality of the images of the colonoscopy or applying some processing over them. Examples of these techniques are High definition Colonoscopy (HC), Narrow Band Imaging (NBI), or Flexible Imaging Color Enhancement (FICE), to name a few [122].

The flexible sigmoidoscopy is quite similar to colonoscopy. It consumes less time than the colonoscopy and requires fewer patient preparation, although it is not as used as colonoscopy since it only examinates about one third of the colon.

The non-invasive tests include stool, blood and radiological tests include [123]:

- **Gualac-based Fecal Occult Blood Test (gFOBT)**. This economic test is performed to detect the presence of blood in faeces through a chemical reaction. Its use is being discarded by some countries since their results are not optimal, mainly because its results can be affected by patients diets. Its sensitivity for CRC detection may be approximately a 50% [124], being some reports that even reduce this value [125]. This test can miss many polyps and some cancers, and in case of abnormal results a colonoscopy needs to be performed.

- **Fecal Immunochemical Test (FIT)**. This test is similar to gFOBT, but with the advantage that its results are not as compromised by patients diets because of the nature of the chemical reaction. The sensitivity and specificity of this test are around the 79% and the 94%, respectively [126]. This test can miss many polyps and some cancers, and in case of abnormal results a colonoscopy needs to be performed.

- **Stool Deoxyribonucleic Acid (DNA) tests**. These tests aim at finding abnormal DNA malignancies in stool. A study performed on 10 000 patients comparing FIT and Cologuard® DNA test using colonoscopy as the gold standard showed that DNA tests had higher a sensitivity (92% vs 74%), but lower specificities (88.5% vs 95.5%) [127]. The big disadvantage of this test is its low capacity to detect advanced adenomas (42%). This test can miss many polyps and some cancers, and in case of abnormal results a colonoscopy needs to be performed.

- **Methylated SEPT9**. The presence of abnormalities of the gene SEPT9 in blood is being investigated as an indicator for CRC. In the review performed by [128], the sensitivity and specificity of using this marker is currently around 71% and 92%, respectively. For now, this test can miss many polyps and some cancers, and in case of abnormal results a colonoscopy needs to be performed.

- **Double Contrast Barium Enema (DCBE)**. It uses barium to outline the colon on a x-ray, and requires a previous patient preparation. It is being discarded because of its low sensitivity [123]. This test can miss many polyps and some cancers, and in case of abnormal results a colonoscopy needs to be performed.

- **Computed Tomographic Colonography (CTC)**. Also known as virtual colonoscopy, it is a radiographic test without need of sedation but with the same patient preparation as colonoscopy. Its sensitivity is estimated in 66.8%, whereas its specificity is around 80.3% [123]. Its capacity to find large polyps is similar to colonoscopy, but is lower to detect polyps lower than 8 mm. This test can miss small polyps, and in case of abnormal results a colonoscopy needs to be performed.

- **Capsule endoscopy**. It is a procedure that consists in swallowing a capsule with a camera that transmits images of the digestive tract. Its detection capabilities are similar to colonoscopy when polyps are larger than 6 mm [129], and has a slightly higher performance than CTC [130]. As CTC, a previous patient preparation is required and in case of abnormal results a colonoscopy needs to be performed.

In this chapter, we aim at proposing two applications based on the open-ended coaxial system that aid in the detection of CRC. These systems would work jointly with colonoscopy procedures, and thus the overall performance of this technique could be improved as it would rely not only on a visual examination, but also on the dielectric spectroscopy of suspicious tissues. As it has been shown, non-invasive tests are not as accurate as colonoscopy, and even if some anomalous marker is found a colonoscopy should be carried out anyways. Hence, improving this procedure - not only by means of enhancing the quality of the images - can provide larger benefits rather than developing an independent detection method.

5.2 Alternative calibration of the system

The enhanced calibration used so far, although quite accurate, is too complex to be used in a medical environment. Calibrating with air and a mechanical short circuit could be done without major problems, but measuring distilled water and methanol could compromise the performance of the whole system. On the one hand, medical experts may not have those liquids always available at their facilities. On the other hand, calibrating with liquids require checking that air bubbles are not present at the sensor's end. In addition, the current calibration takes too much time, making it less suitable for being used during a medical procedure, and most importantly for an *in vivo* approach, a sterile condition cannot be kept in this manner.

The alternative calibration proposed in this section is quite simple to execute as it only requires measuring the reflection of two elements: air and a healthy colon. The use of this calibration (hereinafter referred to it as "alternative calibration") has some implications that should be evaluated carefully. On one hand, the enhanced calibration proposed in Section 2.3.1 requires measuring four known elements, whereas the alternative calibration needs measuring only two. This fact by itself implies that the system will be less accurate. Towards the end of Section 2.3.1, it was exposed that the term G_n can be neglected if the system is not radiating (i.e., $G_n = 0$). Even so, an extra reference is needed, and for this reason an approximation of the reflection of a short circuit will be used. On the other hand, the dielectric properties of colon tissues vary among patients because they depend on factors such as the calibration accuracy, the temperature of the environment and the patient itself. Hence, relating any measurement of healthy colon tissue to a fixed permittivity adds a certain amount of error that has to be evaluated. As exposed in the previous chapter, the absolute values of the properties of colon tissue are not as important as the difference between the dielectric properties of the pathological and the control (healthy) sample. It must be checked if these differences are kept by comparing the performance of both calibrations.

5.2.1 Short circuit approximation

The possibility of using an approximation of the reflection caused by a short circuit in the sensor's end instead of measuring a physical one is evaluated. This approach greatly simplifies the calibration procedure, as any additional physical element is needed to carry it out. However, it adds an extra uncertainty to the obtained results. After measuring the reflection coefficients of both open circuit (air) and short circuit during the realization of this thesis, we observed that

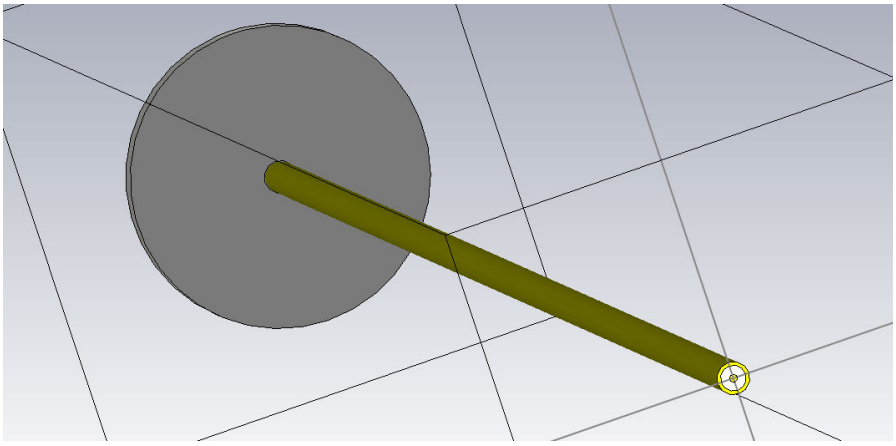

Figure 5.1: Simulation setup for evaluating the performance of an open-ended coaxial sensor with a short circuit at its end.

their modules are almost identical, despite the fact that air has a permittivity of $\epsilon_r = 1 + 0j$ whereas a short-circuit has ideally an infinite permittivity.

The relationship between the reflection coefficients of both standards has been investigated through electromagnetic simulations performed on CST (Computer Simulation Technology) Microwave Studio. To this end, an open-ended coaxial probe has been simulated considering both standards at its end. We have selected Keysight's N1501A slim form probe as the simulated sensor since it has been the most used one for measuring within the framework of the current thesis. The dimensions of the different layers were taken from [131]: a coaxial cable of 20 cm considering an external conductor with a diameter of 2.16 mm, having center conductor and insulator diameters of 0.51 mm and 1.68 mm, respectively. The simulated model can be seen in the Fig. 5.1, with a cylinder at its end that simulates a short circuit (i.e., a perfect conductor with a diameter of 5 cm and 2 mm of width). Simulations were performed within the 0.5 - 26 GHz band, the same bandwidth evaluated throughout the framework of the present thesis, considering a high accuracy simulation mesh (around 42.5 million cells for simulating the setup).

The reflection coefficients obtained after simulating the probe with both air and short circuit at its end are represented in the Fig. 5.2. One can observe that the module of both reflection coefficients is almost identical at all frequencies. However, it is trivially noticed from the remainder plots that their real and imaginary components are shifted by 180 degrees. These other views of the reflection coefficients are represented just up to 8.5 GHz in order to show

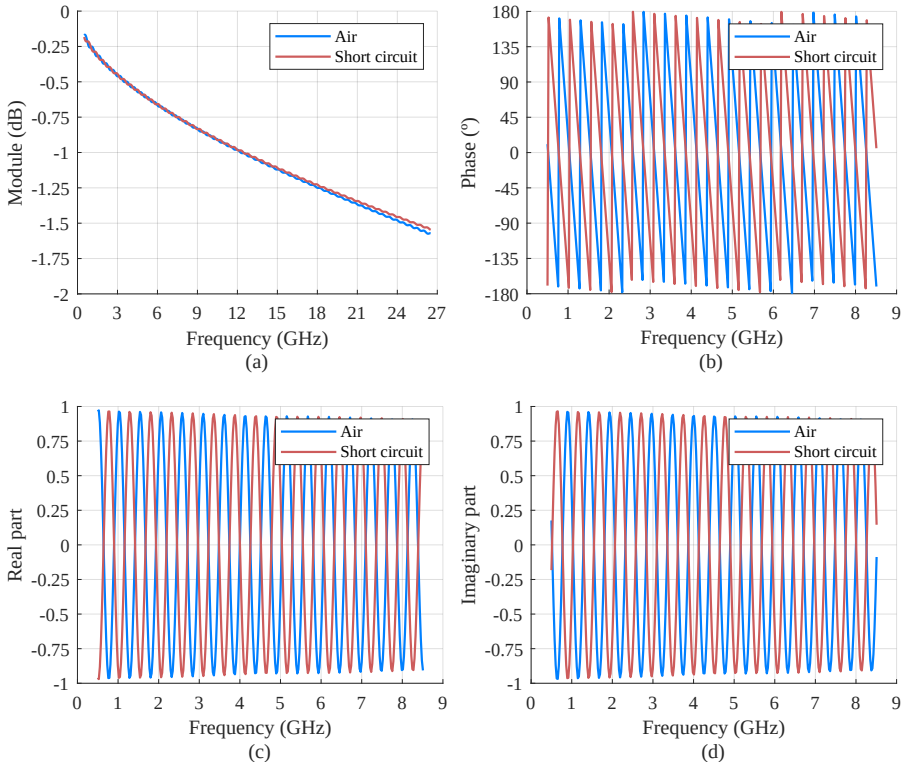

Figure 5.2: Simulated reflection coefficient of air and a short circuit: (a) module in dB, (b) phase in degrees, (c) real part, (d) imaginary part.

better the effect of sweeping both standards, since the trends are kept at upper frequencies.

Therefore, the proposed approach consists in measuring the reflection caused by the air and then change its sign in order to obtain an approximation of the short circuit. Using directly the reflection returned by simulations is not a viable option since, in reality, reflections are affected by several factors: temperature of the environment (as the electromagnetic response of the insulator of the sensor changes it), manufacturing defects of the sensor, performance of the VNA etc. The reflection caused by the MUT would be affected by these factors as well, so they should be considered in the calibration procedure in order to minimize their effect on the results.

5.2.2 Assessment of the alternative calibration

As aforementioned, the alternative calibration adds more uncertainty with respect to the enhanced calibration with methanol due to three reasons: less calibration standards are used, an approximation of short circuit is used instead of measuring a real one and the measurement of the reflection of healthy colon tissue is related to a permittivity that is not its real one. However, the key idea is to keep the differences between the properties of the pathological and healthy colon samples within a patient rather than obtaining an accurate value of the absolute properties.

In the remainder of this section, we evaluate whether the differences are either kept or not with respect to the enhanced calibration. To this end, the data collected from the campaign of surgery samples is utilized. Thanks to the fact that the reflection coefficients captured by the measurement system were stored (i.e., the S_{11} of the calibration standards, the healthy and the cancerous samples are available), we can obtain the permittivity returned by the alternative calibration mathematically. The unknowns A_1, A_2 and A_3 of the Eq. 2.8 are computed by solving a system of three equations with three unknowns, as it can be seen in the system of equations 5.1 (with $G_n = 0$). For setting up the system of equations, short's S_{11} is substituted by open's but in opposite sign, whereas the average permittivity obtained for healthy colon tissue is used as the reference value (presented in the Table 4.5).

$$\begin{cases} S_{11\_open} = \dfrac{A_2 + A_3}{A1 + 1} \\ -S_{11\_open} = \dfrac{A_2 + A_3\epsilon_{short}}{A1 + \epsilon_{short}} \\ S_{11\_healthy} = \dfrac{A_2 + A_3\epsilon_{healthy}}{A1 + \epsilon_{healthy}} \end{cases} \tag{5.1}$$

The estimated permittivity of cancerous tissues is computed, after recalibrating with the alternative method. In the Table 5.1 are listed the dielectric constants of seventeen of the twenty paired samples computed with both the enhanced and the alternative calibration (the reflection coefficients of the first three paired samples were not stored and thus could not been calculated with the alternative calibration). Values are presented for $f = 2.45$ GHz, since as already mentioned in the previous chapter the larger differences in this property are found in the lower frequencies. Selecting this frequency also accounts for the fact that it belongs to an ISM band, meaning that future cancer detection systems could be designed to work at this specific frequency.

	Enhanced calibration			Alternative calibration		
Patient	$\epsilon'_{healthy}$	$\epsilon'_{malignant}$	$\Delta\epsilon'$	$\epsilon'_{healthy}$	$\epsilon'_{malignant}$	$\Delta\epsilon'$
1	48.55	55.19	6.64	-	-	-
2	51.01	61.53	10.52	-	-	-
3	54.50	57.86	3.36	-	-	-
4	56.12	61.01	4.89	52.11	56.11	4.00
5	50.83	51.94	1.12	52.11	53.51	1.39
6	55.51	58.08	2.57	52.11	54.27	2.15
7	51.67	56.46	4.79	52.11	57.52	5.41
8	53.05	59.40	6.34	52.11	57.90	5.79
9	51.38	56.44	5.06	52.11	56.43	4.32
10	54.86	60.50	5.64	52.11	58.10	5.99
11	52.95	58.43	5.48	52.11	58.51	6.39
12	55.66	59.82	4.16	52.11	55.98	3.87
13	51.63	54.45	2.83	52.11	54.42	2.31
14	49.56	55.25	5.69	52.11	58.38	6.26
15	44.67	54.69	10.02	52.11	63.09	10.98
16	49.40	55.64	6.24	52.11	58.77	6.66
17	50.43	58.03	7.60	52.11	60.40	8.29
18	50.52	55.79	5.27	52.11	57.91	5.80
19	58.20	58.88	0.70	52.11	53.04	0.92
20	52.04	55.11	3.07	52.11	54.73	2.62

Table 5.1: Dielectric constant of healthy and malignant colon tissues and the differences between them at $f = 2.45$ GHz, with both the enhanced and the alternative calibration.

One can observe that the differences in dielectric constant between both malignant and healthy states are kept quite well using the alternative calibration. The larger discrepancy was obtained in patient 15, and this could be explained by the fact that the true dielectric constant of its healthy tissue (the one obtained with the enhanced calibration) differ greatly from the average one, almost eight units. Hence, the alternative calibration is relating the reflection of this tissue to a value that differs too much with respect to its actual one. In general, taking the difference obtained with the enhanced calibration as reference, the absolute error committed at computing the difference between both states with the alternative calibration is below to one unit. Although it seems small in absolute terms, this error is not negligible since it would add a significant amount of uncertainty in the performance of a cancer detection

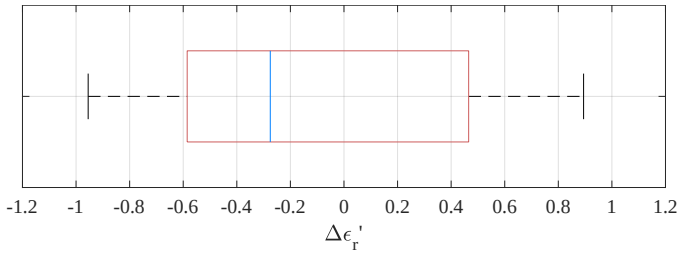

Figure 5.3: Box and whisker diagram of the error committed at computing the difference between malignant and healthy surgery samples with the alternative calibration.

application. A summary of the error committed is presented by means of a box and whisker diagram in the Fig. 5.3, having a median of -0.28 units.

5.3 Detection system of analysis of biopsies

The dielectric characterization system, as conceived in Chapter 2, is an accurate solution to find the electromagnetic properties of biological tissues. However, it has some drawbacks that makes it unsuitable for being used in a medical environment:

1. The system is quite big and requires of two connectors and a coaxial cable to connect the VNA with the sensor, hampering both the set-up and the storage of the system in an endoscopy room.

2. Since there is a flexible cable in the system, additional care must be taken since moving this element could compromise the measurements.

3. Calibrating with liquids is not an easy task. On one hand, the presence of air bubbles at the sensor's end during the calibration can compromise the performance of the system. On the other hand, distilled water and methanol may not be at disposal of the medical experts.

The issues related to the calibration procedure can be minimized by using the alternative calibration proposed in the previous section. With the aim at solving the other problems, the size of both the current sensor and the VNA should be reduced. For instance, the VNA can be substituted by a frequency reflectometer (1-port VNA) and a much smaller and thinner sensor could be used, like those shown in the Fig. 5.4. Ideally, with the aim of facilitating both the setup and the use of the system, all the elements should be embedded within a single equipment.

Figure 5.4: Elements considered to reduce the size of the dielectric characterization system: Reflectometer (left) and thin sensor (right).

Currently, the reflectometers commercially available work only up to 6 or 14 GHz depending on the manufacturer, although this would not be a problem since we confirmed in the previous chapter that the larger differences in dielectric constant between malignant and healthy tissues appear far below those frequencies. In addition, the shorter the sensor, the better, as the system would become even more compacted. Using these sensors has the additional advantage of allowing the measurement of much smaller biopsies.

As performed with the surgery samples in the previous section, the alternative calibration can be applied to the data gathered for biopsies and then analyze how it would affect the results. The box and whisker plot of the difference in dielectric constant between pathological and healthy tissues at $f = 2.45$ GHz is presented in the Fig. 5.5, with the results acquired with the alternative calibration in contrast to those presented in the Fig. 4.9 that were obtained with the enhanced one.

The boxes are almost identical than those computed with the enhanced calibration with methanol, with some minor discrepancy in the median value of adenomas with HGD. In fact, the values of the detection markers presented in Section 4.2.4 (i.e., sensitivity, specificity and predictive values) remain identical considering both calibrations, if the detection threshold in the difference in dielectric constant between the suspicious and the healthy (control) sample is kept at 3.1 units. As performed in the previous section with the surgery samples, the committed error at computing the difference of the dielectric constant with the alternative calibration is presented in the Fig. 5.6. Since both the inferior and superior limits of the box are closer to zero, one can notice that the error committed by the alternative calibration in biopsies is lower than in surgery samples. In this case, the committed error has a median of -0.08 units,

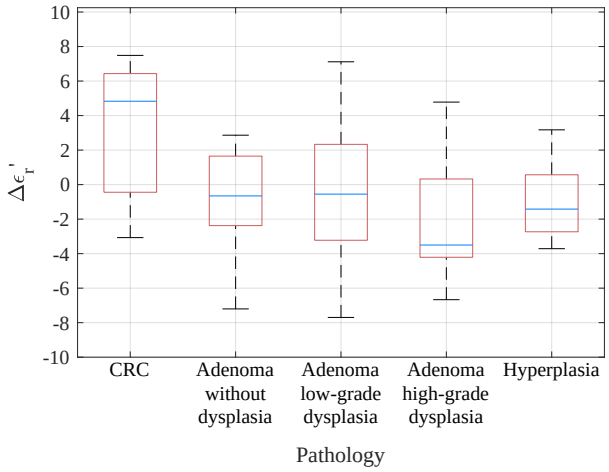

Figure 5.5: Box and whisker diagram of the difference in dielectric constant between pathological and healthy tissues at $f = 2.45$ GHz, with the alternative calibration.

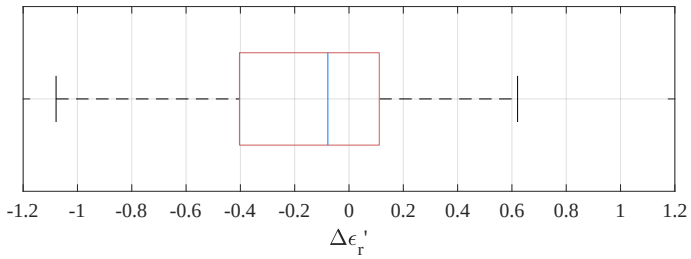

Figure 5.6: Box and whisker diagram of the error committed at computing the difference between malignant and healthy biopsy samples with the alternative calibration.

although the whiskers (or extreme differences) are similar between both colon sample sources.

The combined uncertainty presented in Section 2.3.3 is no longer valid since a new source of uncertainty has been added. The new total uncertainty could have been assessed with the surgery data in the previous section, although we have used the data from biopsies since the pool of measurements is four times higher and then the uncertainty can be analyzed with more accuracy. Therefore, we have used the error caused by the alternative calibration at computing the differences in dielectric constant between healthy and pathological

Frequency Band	(1)	(2)	(3)	(4)	Combined uncertainty
0.5 - 10 GHz	0.61	0.40	0.05	17.04	17.05
2.45 GHz	0.39	0.26	0.05	17.91	17.91

Table 5.2: Values of uncertainty in percentage terms of the relevant parameters averaged for three spectrum regions.

tissue and combined it with the rest of sources as explained in [83], excluding the uncertainty related to cable movements as this system is intended to be completely rigid.

The new uncertainty source has been treated like a source of random errors with normal distribution, as the mean error is almost zero and the probability density seems to follow that distribution after observing the histogram. Thus, the SDM of the errors caused by this calibration has been taken as the uncertainty component, and then it has been combined with the rest of sources. The updated system uncertainty is presented in the Table 5.2, being component number 4 the one related to the alternative calibration (whereas 1, 2 and 3 are related to system's repeatability, systematic error due to calibration and methodology and drift with time). We have presented only the uncertainty in the difference of dielectric constant of the lower band, as the CRC detection application would work at these frequencies - likely at 2.45 ISM band. It should be noticed that the uncertainty related to the enhanced calibration with methanol is kept as the difference is computed with data that also contains that source of uncertainty.

As expected, the alternative calibration adds a huge amount of uncertainty, being the only significant source to the combined uncertainty. This uncertainty is mainly due to the reference taken for the healthy tissue, as it can deviate greatly from the real value from a particular patient and location. In summary, the difference obtained between the dielectric constant of suspicious and healthy tissue obtained has an uncertainty of almost a 20%, which has to be accounted in the diagnosis. For instance, selecting a threshold of 3.1 units in the difference at 2.45 GHz, the uncertainty region would extent from 3.1 ± 0.62, meaning that from 2.48 units suspicious samples should be considered as malignant for further analysis in anatomical pathology unit.

The implementation of this solution is rather simple, being essentially a task of selecting smaller components and a sensor with a smaller diameter. Ideally, a short sensor could be embedded within the reflectometer, having thus a single piece of equipment. The application of control and diagnosis could be implemented for tablet Android devices, enabling

the possibility of managing the reflectometer wirelessly and avoiding then the presence of annoying extra cables.

5.4 Detection system embedded into a colonoscope

One of the objectives behind the development of this thesis is presenting a system capable of increasing the CRC detection capability of colonoscopy procedures. The previous approach is based on of measuring biopsies right after their removal, analyzing the differences in dielectric constant between a healthy sample and a suspicious one. This second approach goes a step beyond that one. It makes use of colonoscopes with two working channels, the first one for the usual endoscopy tools (like biopsy forceps) and the second one for embedding the dielectric probe. This system has the following challenges:

- The dielectric probe (or sensor) has to be both flexible and large. Besides, it needs to have an outer diameter lower than that of the working channel of the colonoscope, which generally vary from 2.8 mm to 3.8 mm depending on the considered model.
- The sensor must be watertight. The sensor's end should not let any kind of leakage into the coaxial, since it can affect to its performance.
- Possibility of sterilization. Ideally, the prototype should be capable of bearing a sterilization process so it can be used in many colonoscopy procedures. Single-use sensors could be an alternative, but it would require them to be more economic and then they might not have enough phase stability against bendings.
- The sensor should comply with the biocompatibility regulation. As it is going to be in brief contact with living human tissue, the materials of the coaxial end should comply with current regulation.
- The calibration cannot be performed prior to the insertion of the sensor in the colonoscope, since bendings alter the performance of the cable and thus calibration would not be valid after them.
- The electromagnetic differences computed between healthy and malignant colon samples may not be valid. Research should be performed at *in vivo* conditions.

Achieving a watertight, sterilizable and biocompatible sensor with such a small outer diameter is a challenging task. The conductors and the insulator of

Figure 5.7: Instance of an autoclave for carrying out steam sterilization.

commercially available flexible coaxial cables are generally made of copper and Polytetrafluoroethylene (PTFE). Unlike the dielectric, copper is not usually considered biocompatible. However, those cables in which copper is silver-plated may fulfil the minimum biocompatibility requirements, as the contact with human tissues lasts a few seconds. Besides, watertightness is not achieved with those cables. The external conductor is braided in order to grant an acceptable degree of bending, and this braiding can cause leakages of body fluids that alter the performance of the sensor with time. For this reason, sealing the coaxial end as performed in [132] is necessary. Moreover, preventing the leakage of body fluids would facilitate the cleaning of the sensor and its later sterilization. Sterilization could be performed using steam sterilization (i.e., using an autoclave like the one shown in the Fig. 5.7), chemical or dry heat methods etc.

The greater advantage that provides the alternative calibration is the possibility of calibrating with the sensor already embedded within the working channel of the colonoscope, since liquids nor short circuits are needed in this procedure. This calibration, despite it increases the uncertainty of the results, solves the issues that an external calibration involve. Still, moving the sensor also involves an increase of the measurement error - and it will have to be moved from the calibration position (control tissue) to the location of suspicious ones. The reflection of a coaxial sensor depend not only on the material placed at its end, but also on the losses that appear within its whole length. The error

correction procedure included in the calibration (see Section 2.3.1) translates the measurement plane from the VNA port to the coaxial end, meaning that the losses from the path are compensated. However, when moving the colonoscope and the sensor, their bendings and thus their losses change, altering the performance of the calibration. Therefore, the distance that the sensor can be moved from the calibration position must be evaluated for any potential flexible prototype, reminding that this distance will vary depending on their phase stability against bendings.

Before implementing this solution, the study of the dielectric properties of healthy and malignant colon human tissues should be performed again, but at *in vivo* conditions. Properties are expected to increase, as *ex vivo* tissues are influenced by tissue dehydration, lack of blood perfusion and change of the temperature, among other factors during their handling [89]. However, measuring human colon tissue *in vivo* is a challenging task since they could be accessed only during surgery procedures. Surgeries are critical procedures in which risks should be minimized, making this kind of studies unfeasible to be carried out. An alternative that some authors have explored is the possibility of using mouse xenograft models. It consists in transplanting human tumour into immunocompromised mice, as they will not reject human cells [133]. These models are usually used for testing cancer therapies, although there are studies in which these subjects have been used for cancer dielectric characterization [52, 134]. It should be reminded that healthy human colon tissue should be characterized *in vivo* as well in order to have a better reference for the alternative calibration.

This second approach is technologically more challenging to implement than the first one, mainly due to the several features that the coaxial sensor must possess. On the other hand, it has two major advantages over the first system: it can prevent performing some biopsies, and results are not influenced by the issues (dehydration, elapsed time, size...) related to *ex vivo* tissues.

5.4.1 Mechanical performance

The fact of using a bended open-ended coaxial sensor do not restrain the obtainment of the permittivity of a material from the gathered reflection. However, since the sensor has to be large enough to cover the entire colonoscope length and be connected to the VNA, movements or minor bendings after the calibration procedure can alter the relationship between reflection and permittivity. In this section, we present the measurements performed with a flexible prototype of an open-ended coaxial sensor with the aim at assessing how movements or bendings after calibrating affect the gathering of the permittivity of a colon tissue.

Figure 5.8: Flexible coaxial sensor considered.

The flexible sensor considered is presented in the Fig. 5.8. It is a 3 meter coaxial cable of the model Storm Flex® 086 from Teledyne Storm Microwave, having a SMA connector on one end and finished cut flat on the other. Its small outer diameter, 2.2 mm, made it suitable to fit inside the working channel of a colonoscope. This cable was considered due to its good phase stability against bendings, although more stable cables are commercially available.

The experiments consisted in measuring the inner colon tissues of porcine specimens *in vivo* using the flexible sensor, after performing a colonoscopy on them. Two were the main objectives of the trials. On the one hand, we wanted to assess whether the technique had enough repeatability for being used as a detection method. Essentially, we needed to know if measuring healthy tissues we obtain the same permittivity values, or how much can the sensor be moved from the calibration position for characterizing tissues. On the other hand, we aimed at evaluating if the method was comfortable enough for the medical experts, and how could we improve this process. It should be highlighted that no cancer was present on the specimens, and thus the detection capability by itself could not be assessed.

For the fulfilment of these goals, the software application presented in Section 2.3.4 needed some modifications:

- The alternative calibration was implemented, due to the reasons commented previously.

- The software was adapted for running in Android tablets, facilitating its use through the simplification of options.

- The application was able to be connected to the VNA wirelessly, reducing the inconveniences of having additional cables in the surgery room.

Measurement protocol

Two photographs of the experiments are presented in the Figs. 5.9 and 5.10. The procedure followed for performing the measurements is listed down below. Three different trials were done, and the differences among them are commented as well.

- The VNA was turned on two hours before the trial. Once started, the animal is sedated prior to the colonoscopy.

- A colonoscopy was performed on the animal specimen. The large intestine of porcine specimens has spiral shape, in contrast to humans' which it has a shape of a reversed "u". Due to the great curvature present, only 70 cm of endoscope were entered instead of the whole device.

- The sensor is inserted through the working channel of the colonoscope, preventing it from going out by the opened end of the colonoscope (e.g, the sensor is inserted up to around a centimetre from this edge).

- The alternative calibration starts, measuring the reflection at that position (air reference). Once captured, the sensor is moved forward until touching colon tissue, and then its reflection is captured (healthy reference). To achieve this, the medical expert made use of the video provided by the inner camera of the colonoscope, as one can see in the Fig. 5.10.

- On the first trial, the colonoscope (and the sensor with it) was moved backwards in steps of approximately 2.5 cm from the calibration procedure. On the second trial, the step was reduced to 1 cm, again moving backwards from the calibration position. Finally, the last trial consisted in moving the sensor within a circle of 1 cm of radius from the calibration position.

Figure 5.9: Instance of the experiment. The medical expert controls the sensor while looking at the screen that shows the real time video of the camera of the colonoscope.

Figure 5.10: Instance of the experiment in which are shown both the video captured by the camera of the colonoscope and the developed software.

Results

In this section the mechanical assessment of the detection system embedded within the colonoscope is exposed. It should be highlighted that the assessment is particular for the flexible coaxial considered as a sensor, meaning that with other cables results would have been different to a greater or lesser extent. The alternative calibration was used, but using an *in vivo* permittivity of healthy colon tissue as reference instead of those computed from the *ex vivo* experiments. This reference was obtained from the *in vivo* experiment that will be detailed in the following section.

The results of the first trial are presented in the Fig. 5.11. They are presented up to 12.4 GHz despite the fact that measurements were carried out up to 26.5 GHz since the SMA connector of the sensor had this maximum frequency of operation. As it can be seen, when the sensor within the colonoscope is moved backwards (this is, part of the colonoscope is pulled out), the dielectric properties of healthy tissues change. The more the cable is pulled out, the greater the differences with the reference position are. The change in dielectric constant at 2.45 GHz when the distance from the calibration position is of around 2.5 cm is of 0.57 units, which could be acceptable. In this particular trial, the changes when moving backwards around 5, 7.5 and 10 cm were of 1.05, 3.18 and 4.80 units, respectively.

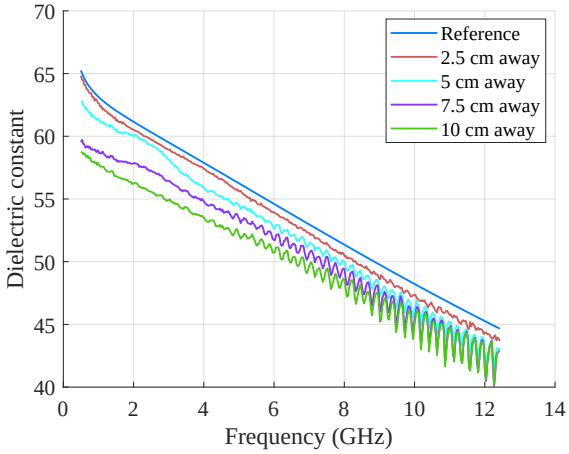

Figure 5.11: Dielectric constant of the measurements made with the detection system embedded within the colonoscope, moving backwards in steps of 2.5 cm from the calibration position.

Looking at the figures, one can observe that moving backwards 5 cm adds to much uncertainty. Despite in this case the change at 2.45 GHz was not very high, it was just a coincidence looking at the changes occurred in the rest of frequencies. Moving more than 5 cm is completely discarded, at least with the considered sensor.

The results of the second trial, in which the sensor was moved backwards in steps of 1 cm, are depicted in the Fig. 5.12. It can be seen again the tendency that greater distances from the calibration position implies higher differences from the reference healthy. At 2.45 GHz, the changes in dielectric constant were of 0.67, 1.40, 0.65, 1.25, 2.03 and 2.82 when moving backwards 1, 2, 3, 4, 5 and 6 cm, respectively. Although changes are not very large, even the changes when moving 2 cm are significant, giving the magnitude of the differences in dielectric properties between healthy and malignant colon tissues. Hence, only distances equal or below 1 cm from the calibration position should be considered for this application, at least with this flexible sensor, since the uncertainty with higher distances is unbearable.

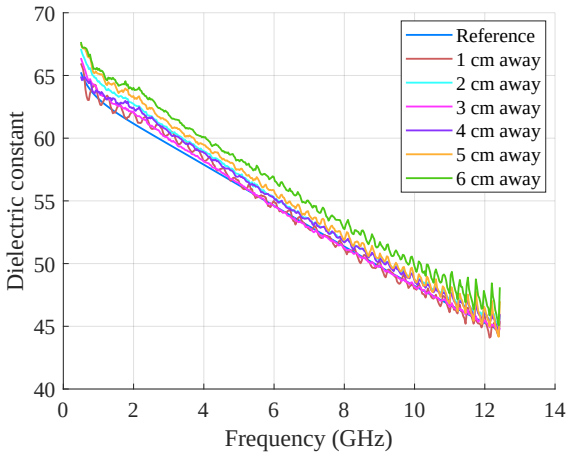

Figure 5.12: Dielectric constant of the measurements made with the detection system embedded within the colonoscope, moving backwards in steps of 1 cm from the calibration position.

Lastly, the results of the third trial are represented in the Fig. 5.13. In this case, the dielectric constants are very close to that of the reference. At 2.45 GHz, the differences were of 0.34, 0.23, 0.71, 0.61, 0.56 and 2.48 units. The discrepancy of the last result seems due to an error during the measurement, given the disparity with the rest of the values. This trial confirms that the flex-

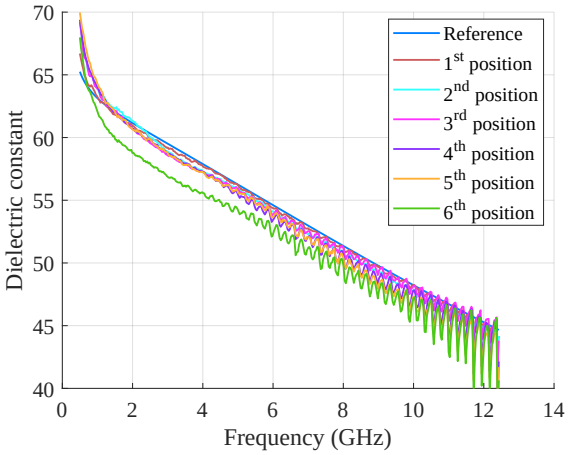

Figure 5.13: Dielectric constant of the measurements made with the detection system embedded within the colonoscope, moving within a circle of approximately 1 cm of radius from the calibration position.

ible sensor utilized could be used for measuring up to 1 cm from the calibration position.

This experiment has confirmed that the detection system embedded into a colonoscope can provide enough repeatability to be developed in further depth, if the restrictions in movement are respected. The results presented are particular for the coaxial cable selected, and they could be improved or worsened with other models. For instance, if flexible coaxial cables of High Speed Interconnects are selected as sensors, results could be more accurate given its excellent performance regardless of the bending degree that it undergoes (on the other hand, this model is much more expensive).

5.5 Testing tools

Due to obvious reasons, testing prototypes of these applications directly on human subjects is not feasible, at least until their final stage. Still, there are two different approaches for testing prototypes of the applications presented in the previous sections. The first one is based on making use of animal models for testing specific features of the applications, whereas the second is related to the use of electromagnetic *phantoms*.

Two kinds of trials can be performed with animal models. On the one hand, human colon samples (healthy, pathological and cancerous) can be cultivated for testing the detection capabilities of the systems, as samples from human subjects are scarce and difficult to gather in large volumes. As aforementioned, it could be done by means of the xenograft model, enlarging greatly the number of available samples and enabling as well the possibility of measuring *in vivo*. On the other hand, the mechanical performance of the second proposal (the one embeddable in the colonoscope) can be assessed in larger animal subjects, like porcine models.

However, animal experimentation is rather expensive and it is subjected to rigorous ethical constrains, which implies that researchers cannot make use of them continuously. A feasible alternative is the employment of electromagnetic phantoms. These are materials that mimic the electromagnetic properties of biological tissues, and depending on their manufacture they could also imitate the shape and even the texture of biological tissues. Thanks to a parallel research performed between our research group at the Institute for Telecommunications and Multimedia Applications (ITEAM) and the Centre for Biomaterials and Tissue Engineering (CBIT), both under the umbrella of the Universitat Politècnica de València (UPV), an intensive work for developing tissue phantoms has been carried out [135]. These phantoms have been developed using polar liquids, distilled water and salts as main ingredients. A proper relationship among the quantities of these materials can provide an outstanding imitation of the electromagnetic properties of tissues for very wide frequency bandwidths. For instance, the properties of cancerous and healthy colon tissue obtained in the surgery measurements of the previous chapter have been imitated with liquid phantoms obtaining great accuracy [136], as one can observe in the Fig. 5.14. The composition of these phantoms is listed in the Table 5.3.

Despite the great use that these liquid phantoms may have for other systems, the proposed applications need of solid or semi-solid ones for being usable as testing tools. For this reason, a gelification procedure of the liquid phantoms is being carried out. Novel synthetic hydrogels that imitate some particular tissues have already been presented [137]. One key advantage of these hydrogels is the possibility of conforming them with specific shapes. They could be potentially used to design a synthetic colon wall that has both the shape and

Tissue	**Phantom composition**
Colorectal cancer CRC	42% Acetonitrile, 1% NaCl
Healthy colon	48.5% Acetonitrile, 3% Ethanol, 1% NaCl

Table 5.3: Phantom composition to fit the permittivity of the surgery samples.

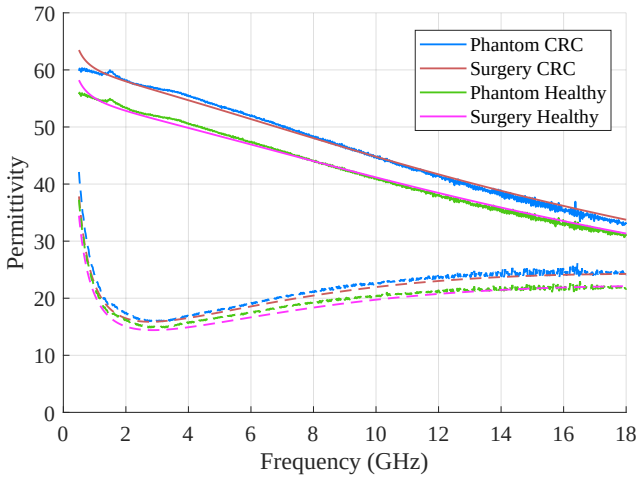

Figure 5.14: Permittivity of the colon surgery measurements and of the electromagnetic phantoms.

the electromagnetic properties of the tissue, even with spots with cancerous properties.

5.6 Conclusion

This chapter aims at proposing two applications for colorectal cancer detection that aid during colonoscopy procedures. **Both solutions require a colonoscopy, being thus complementary to this procedure rather than independent ones.** The first approach involves analyzing colonoscopy biopsies right after their removal, in *ex vivo* conditions. The second approach is related to embedding a flexible coaxial sensor within the colonoscope, enabling an *in vivo* analysis.

Before exposing both proposals, an alternative calibration for these systems has been explained. This calibration has three goals, aiming at facilitating the implementation of the proposed systems in medical environments: avoid the use of liquids, simplify the process and reduce the calibration time. It consists in calibrating just with air and a measurement of healthy colon tissue, emulating a short circuit from the measurement of air. Besides, using the data from the *ex vivo* surgery campaign, we have compared the differences between the properties of healthy and malignant tissues obtained with this alternative calibration and with the enhanced one. Results showed that this calibration

adds an extra amount of uncertainty that should be respected, since it changes these differences with a median of 0.53 units (always below that one unit).

The first approach is a simplification of the system used so far, not only in the calibration procedure but also in the size of its components. It involves using a much shorter and thinner sensor, allowing characterizing samples with a lower size, as well as utilizing a reflectometer instead of a bigger VNA. Taking the data from the *ex vivo* biopsies campaign, the alternative would change the difference between cancer and control tissues only with a median of 0.22 units, and almost always less than a unit. In fact, with this calibration, the diagnostic performance of the system (i.e., sensitivity, specificity and predictive values) would remain identical. This system would be used in the endoscopy room, within less than a minute from tissue extraction, with the main objective of discarding polyps that the medical expert already thought were not cancerous.

The second approach involves adapting the open-ended coaxial system to be embeddable into the working channel of a colonoscope. A flexible sensor is needed, requiring additional features such as watertightness, sterilization and biocompatibility. This solution is based on measuring a sample of healthy colon tissue adjacent to the suspicious ones, and if the differences between both states are great enough it could be due to the presence of cancer. However, before its potential deployment in real conditions, the dielectric properties of healthy, malignant and pathological colon human tissues must be characterized at *in vivo* conditions, since the differences presented in the previous chapter may not remain identical.

The mechanical performance of a preliminary system based on the latter approach was tested in an almost real environment. The idea of the experiment was to evaluate the conditions in which the permittivity of healthy colon remained almost constant from the calibration position (considering the alternative method). To this end, a colonsocopy was performed on porcine specimens, introducing a flexible sensor by the working channel of the colonsocope. Then, three set of trials were performed. In the first one, the permittivity was measured in backward steps of approximately 2.5 cm from the calibration position. Results showed that only in the first measurement the permittivity obtained was acceptable. The second trial was identical, just changing the steps to around 1 cm. Results showed that going more than 1 cm further from the calibration position was not recommended. The third trial, in which measurements were performed within a circle of 1 cm of radius from the calibration position, supported the previous conclusion. **This campaign showed that, with the coaxial cable considered as sensor, the cancer detection application embedded within a colonoscope should be calibrated in a healthy tissue located next to the suspicious tissues, ideally not longer than 1**

cm. This restriction could be relaxed considering a cable with higher stability against bendings.

Chapter 6

Conclusions and future work

This dissertation has been focused on investigating the electromagnetic properties of biological tissues for two major objectives. The first goal involved developing a new collection of electromagnetic properties of biological tissues measured *in vivo*. The currently available databases are limited mainly in the number of characterized tissues, although there are other issues related to the characterized frequencies and animal species chosen.

Measurements have been carried out on tissues from the thoracic and abdominal tissues of porcine specimens, making use of the open-ended coaxial technique within the 0.5 - 26.5 GHz band. This technique is based on translating reflective measurements performed with a VNA into electromagnetic properties. To this end, a previous calibration to relate measurement with properties has to be performed. In the framework of this thesis, we have found out that adding methanol to the typical calibration (i.e., using just air, a short circuit and distilled water) enhances significantly the accuracy of the technique. It has been shown that, if measured *in vivo*, tissues tend to show greater properties than in *ex vivo* conditions.

Besides, the second objective was related to present potential applications that aid in the detection of CRC based on the differences that appear in the electromagnetic properties between healthy and malignant tissues. Prior to proposing any application, the electromagnetic properties of healthy, pathological and malignant colon tissues have been investigated. Again, the open-ended coaxial technique has been used for obtaining these properties. Measurements have been performed on *ex vivo* tissues gathered from both colonoscopy and surgery procedures. Results have shown that, between healthy and malignant

colon tissues, differences in dielectric constant are in average of 5 units approximately (at the spectrum region where differences are higher, below 4 GHz). In conductivity differences are lower, and even though they increase with frequency only around 2 units in average are achieved. Results agreed quite well regardless of the source of data considered. However, no significant differences have been obtained between healthy colon tissue and other non-cancerous colon pathologies, meaning that the used technique may not be useful for diagnosing other pathologies.

Two systems that make used of the differences on dielectric properties have been proposed, being one of them *in vivo*. An alternative calibration procedure has been proposed for these systems, and despite adding a certain amount of uncertainty it is more simple and usable in a medical environment. The *ex vivo* approach consists simply on making use of a much smaller and compact version of the open-ended coaxial system, without any flexible part and measuring in the endoscopy room right after tissue extraction. On the other hand, the second approach is based on developing a large, flexible sensor that can be embedded within a colonoscope and allow direct *in vivo* measurements. A preliminary *in vivo* test has shown that the latter approach could be implemented with some restrictions, but several improvements should be still performed. Still, before deploying any kind of *in vivo* system, it should be assessed whether the differences obtained *ex vivo* are kept at *in vivo* conditions as well. This concluding chapter summarizes the main contributions of this thesis and suggests further topics of research beyond the results of this work.

6.1 Concluding remarks

6.1.1 Calibration algorithms

The calibration procedure has two main purposes. On the one hand, it translates the measurement plane from the VNA port to the end of the coaxial sensor, minimizing the effect of the intermediate hardware on the results. On the other hand, it relates reflection measurements to their corresponding electromagnetic properties. For fulfilling both purposes, we have made use of an equivalent circuit model previously proposed in literature and we have applied an error correction technique. Then, for applying this calibration, the reflection of materials with well-known electromagnetic properties have to be measured. Typical calibrations make use of air, a short circuit and distilled water.

First of all, we have evaluated an "enhanced" calibration consisting in adding a forth standard to the typical one for improving the accuracy of the system and thus obtaining results with lower uncertainties. Different liquids have been analyzed testing some samples, being methanol the most suitable

	Ethylene glycol		DMSO		Butanol	
	$\Delta\epsilon_r'$	$\Delta\epsilon_r''$	$\Delta\epsilon_r'$	$\Delta\epsilon_r''$	$\Delta\epsilon_r'$	$\Delta\epsilon_r''$
Typical calibration	1.98%	2.27%	1.15%	1.74%	4.71%	5.74%
With methanol	0.43%	0.60%	0.14%	0.62%	3.13%	3.24%
With ethanol	2.71%	2.66%	1.88%	1.45%	1.04%	1.13%
With isopropanol	2.52%	1.72%	1.45%	1.21%	1.10%	2.43%

Table 6.1: Averaged errors made by each calibration at measuring the tested liquids.

Frequency Region	Param.	(1)	(2)	(3)	(4)	Combined uncertainty	Combined exc. (4)
0.5 - 10	ϵ_r'	0.61	0.40	0.05	0.21	0.67	0.66
GHz	ϵ_r''	0.71	0.66	0.12	0.42	0.86	0.81
10 - 18	ϵ_r'	0.47	0.36	0.10	0.41	0.59	0.52
GHz	ϵ_r''	0.46	2.19	0.28	1.96	1.94	1.35
18 - 26.5	ϵ_r'	1.84	0.78	0.20	0.95	2.01	1.89
GHz	ϵ_r''	1.94	3.09	0.42	3.51	3.63	2.65

Table 6.2: Values of uncertainty in percentage terms of the relevant parameters averaged for three spectrum regions.

one as it improves significantly the performance of the typical calibration for any permittivity considered. In the Table 6.1 are averaged the errors performed considering each calibration, in percentage terms of the relevant parameter.

Once selected the optimal calibration, its total uncertainty has been assessed. To this end, the different sources of uncertainty have been evaluated and combined: repeatability of the measurements, systematic errors due to the instrumentation and methodology, drift of the system with time, and cable movements (when these occur). The combined uncertainty calculated for the system with the enhanced calibration is presented in the Table 6.2. One can observe that the uncertainty increase with frequency, being higher for the imaginary part of the permittivity than for the real one.

The enhanced calibration has been used in the characterization of the different kinds of colon samples, as the differences between healthy tissue and other pathologies - including cancer - had to be evaluated with the higher possible accuracy. However, this calibration is not suitable for medical environments, as it has a certain complexity and it makes use of liquids that may be not be accessible nor advisable in an endoscopy room. For this reason, an "alternative" calibration that could be used in future systems has been developed as

well. It is based on measuring air and healthy colon samples as references, simulating the short-circuit reflection and neglecting measuring a forth standard. Although much more simple, this calibration adds a certain amount of uncertainty. From post-processing the data from the *ex vivo* biopsy and surgery campaigns with the alternative calibration, the errors in dielectric constant were of around 0.2 and 0.4 in the average of dielectric constant respectively, with maximum deviations of 1 unit. However, modifications on this calibration or even major changes in the basics of the process should be studied in order to achieve lower errors.

6.1.2 Database of *in vivo* electromagnetic properties of biological tissues

To the best of the author's knowledge, the largest database of *in vivo* electromagnetic properties of biological tissues has been presented in the framework of this thesis. It has been focused on the tissues of both the abdominal and the thoracic regions: aorta, bladder, blood, colon, fallopian tubes, fat, gallbladder, heart, kidney, liver, lung, muscle, oesophagus, ovary, pancreas, skin, small intestine, spleen, stomach, uterine matrix. Still, this collection could be complemented with further measurements, especially from head tissues. In comparison to Gabriel's database - the most used and widespread one, the presented results are slightly higher, probably caused by the fact that Gabriel's database was performed considering mostly *ex vivo* tissues.

As trivially expected, high water-content tissues have greater permittivity values than low water-content ones. Most importantly, the properties of high water-content tissues have in general lower uncertainty than those with a lower water content. Larger uncertainties are related mainly to a greater natural heterogeneity of the biological tissues, as the uncertainty added by the measurement system is common to all the tissues. As expected from Gabriel's report, the variability of tissues like fat, lung and skin was much greater in comparison to the others. Unexpectedly, pancreas showed as well a high uncertainty, due to a natural heterogeneity that has not been previously addressed in literature. Further research should be performed in order to understand this behaviour properly.

6.1.3 Differences in dielectric properties between healthy and malignant colon tissues

In this work, we have focused on the differences in the electromagnetic properties between a healthy and a malignant sample from a patient rather than in analyzing only the absolute properties of suspicious samples. It is due to the

fact that absolute values vary significantly between patients and calibration sessions. Factors such as dielectric variability among subjects, tissue temperature, age of the subjects, tissue dehydration after tissue removal and random errors of the measurement system affect to the absolute values, making them unsuitable for being used as detection markers just by themselves. However, this factors affect to healthy tissues in essentially the same manner, and then the electromagnetic differences between suspicious and healthy samples are much more appropriate as detection markers.

Several pathologies have been analyzed from biopsy samples: Adenocarcinomas (CRC), adenomas without dysplasia, adenomas with both low and high levels of dysplasia, hyperplastic and hamartomatous polyps. Results have shown that non-cancerous lesions, regardless of their potential becoming into cancer, have almost identical properties to healthy ones in both dielectric constant and conductivity. In contrast, significant differences have been found out between cancer and healthy tissues. The larger differences in dielectric constant were found below 4 GHz, selecting 2.45 GHz as diagnostic frequency given its potential use in future systems as this frequency belongs to the reserved spectrum for Industrial, Scientific and Medical (ISM) applications. On the contrary, although lower in magnitude, differences in conductivity increase with frequency. In this case, we selected 18 GHz as any ISM frequency was available within the frequencies of interest (although ISM 24.125 GHz band could be selected, the measurement noise at this frequency is too high). The median of the differences were of 4.8 units and 2 S/m in dielectric constant and conductivity, respectively. Selecting the threshold in the difference between healthy and suspicious sample that maximizes the accuracy of the open-ended coaxial technique as a CRC detection system, we obtained the performance shown in the Table 6.3.

It should be mentioned that the overall accuracy of the system, 87.5%, could be increased if some modifications in the measurement system and protocol are applied, as those presented in Chapter 4. Still, observing the NPV, the system

Detection Marker	**Result**
Sensibility	75.0%
Specificity	88.7%
Positive Predictive Value (PPV)	46.2%
Negative Predictive Value (NPV)	96.5%
Accuracy or Global Predictive Value (GPV)	87.5%

Table 6.3: Performance of the open-ended coaxial technique for detecting cancer using biopsy samples.

seems quite good for assessing the negative cases, which is interesting for a particular application of the system. When a medical expert performs the visual inspection of a suspicious tissue that thinks of it as healthy with high probability, instead of sending it for pathological analysis, it could be discarded if the open-ended coaxial system agrees with the medical expert, lowering the burden to the anatomical pathology unit.

On the other hand, healthy and malignant colon samples from surgery procedures have been analyzed as well. Results are very similar to those obtained from biopsies, although a bit lower in magnitude. This was likely caused by the fact that surgery tissues were measured above 20 minutes after tissue extraction, which was higher than for biopsies and thus implies an increment of tissue dehydration. Still, differences between healthy and malignant were significant, agreeing quite well with the result from biopsies: the differences in dielectric constant had a mean of 5.04 units, whereas in conductivity they were of around 2.15 S/m. The probability densities of the differences follow a logistic distribution, very similar in shape to the Gaussian one. From all the observed differences, the development of CRC detection systems based on this properties seems feasible. Besides, future systems should analyze the differences in dielectric constant rather than in loss factor or conductivity since they are greater and, in addition, have lower variability.

6.1.4 Proposed systems for detecting colon cancer

Two different approaches can be followed for developing CRC detection systems. The *ex vivo* solution consists in compacting the system as much as possible, using a small reflectometer instead of a VNA and a much shorter and thinner sensor, ideally all compacted within a single device. This approach must be used inside the endoscopy room, measuring within seconds right after tissue removal (first a control tissue, for applying the alternative calibration, and then the suspicious one). It could make use of the differences obtained in the *ex vivo* measurement campaigns, and the variability of results could be minimized due to the lowered influence of both tissue dehydration and sample size. Still, there is room for improvement in the calibration procedure, as the proposed alternative calibration adds a significant uncertainty to the process that has to be always taken into account. After processing the data of the suspicious and healthy biopsies, we computed a combined uncertainty of around 18% on the difference in dielectric constant obtained owing to the use of the alternative calibration. This high uncertainty has to be considered when fixing the detection threshold.

The second solution evaluated relies on direct *in vivo* measurements. In this case, the VNA could be compacted as well for facilitating the handling of the

system, although the big breakthrough lies on the development of the sensor: it should be a large coaxial of more than 2.5 meters, with an outer diameter lower than 3.8 mm, watertight, biocompatible, with a very good stability in phase with bendings and, if possible, sterilizable. Summarizing, it should be completely harmless for human tissues, its performance should be affected by bendings and leakage of body fluids as low as possible, and must be embedded within the working channel of commercial colonoscopes. In one *in vivo* campaign with porcine models, we tested a prototype of flexible sensor in order to evaluate its repeatability. The prototype complied with the dimensions of the working channel of the colonoscope and had a good phase response with bendings, although it was not biocompatible and complete watertightness was not assured. It was shown that moving more than 1 cm from the position of the alternative calibration was not recommended, since the uncertainty burden is increased.

The *in vivo* approach seems easier to integrate within real colonoscopy procedures, although technologically is much more challenging than the *ex vivo* one. In addition, apart from the uncertainty sources presented in Section 2.3.3, both the use of the alternative calibration and the movement from the calibration position adds a by no means negligible amount of uncertainty. Still, before a potential implementation of this system, additional knowledge of the difference between *in vivo* healthy and malignant colon tissues is required, as no data is currently available.

6.2 Future work

6.2.1 Dielectric characterization of the colon healthy, malignant and pathological tissues at *in vivo* conditions

In the framework of this dissertation, measuring both healthy and malignant human colon tissues at *in vivo* conditions has not been possible. There are several restrictions to measuring this tissues directly: measurements must be performed at surgery procedures for allowing direct contact with tissues, the clinical trial has to be approved by the relevant committees, and last but not least sterile and biocompatible sensors must be used, which are not currently available commercially. Evidently, the probability of performing these measurements in basic research stages is almost zero. On the one hand, surgery procedures are risky and therefore adding unnecessary steps in the process is far from trivial. On the other hand, developing a custom sensor for having a sterilizable and biocompatible sensor takes a huge amount of time, not only

because of its design and manufacturing but also because certification processes for new medical devices are very time-consuming.

A more feasible alternative lies in the use of mouse xenograft models, which is a technique that consists in transplanting human cells into immunocompromised mice, which do not reject human cells. In this manner, human colon cells can be cultivated and measured at *in vivo* conditions. Then, once characterized the properties of cancerous and healthy cells in this condition, the differences can be obtained with much higher accuracy and used for calibrating the CRC detection system embedded within a colonsocope as well as for determining the optimal detection threshold.

6.2.2 Development of the proposed systems for colon cancer detection

The deployment of the two systems for CRC detection depends greatly on solving technological challenges, although there is room for improving the proposed calibration as well. Besides, the software interface has to be adapted for being used by medical experts. Apart from controlling the system, it should guide the medical doctors throughout the calibration and measurement processes, performing the diagnosis, and presenting and storing the data. And finally, regardless of the detection system considered, medical experts have to be trained in the setup and handle of the hardware, in the use of the application and in the interpretation of the results.

As aforementioned, the development of the system of analysis of biopsies is simply a miniaturizing process of the elements (reflectometer and sensor), ideally all compacted within a single hardware element. Being an *ex vivo* method, its use in real samples even inside endoscopy rooms would be straightforward. A validation period comparing diagnosis with anatomical pathology results should be satisfied, evaluating its performance. Finally, before being commercially exploited, the system must be validated and certified by an authorized regional representative (for instance, in Europe it must have a CE certification mark).

On the other hand, having a functional CRC detection system embedded into colonoscopes is still quite far-fetched. However, we believe that this solution can be much more accurate once its issues are solved or minimized, and besides medical experts can find it easier to work with in comparison to the *ex vivo* solution. With respect to the sensor considered within the fulfillment of this thesis, the following features and aspects have to be addressed:

- The flexible open-ended coaxial sensor must be watertight and comply with the required regulation regarding biocompatibility.

- Sensor should bear with a suitable sterilization process (steam, dry heat or chemical methods).

- A model with much better phase stability with bendings should be used, as in this manner the measurement constrains related to movements are reduced and then its handling is facilitated.

- The differences between cancerous and healthy human colon cells have to be studied *in vivo*. Although it is expected that these differences even increase in this condition, it is not absolutely certain and thus they must be assessed.

- Clinical trials in real patients should be performed before its commercialization. Apart from having solved the previous steps, these trials have to be previously approved by the respective ethical committees.

- Not only the sensor but also the whole system and procedure must be validated and certified by an authorized regional representative, as with the other system.

6.2.3 Assessment of other pathologies

Since it was proved that cancerous and healthy tissue do not interact in the same manner with electromagnetic fields, the most studied techniques to exploit it for cancer detection are based on medical imaging. Only for breast tissue, devices that work in direct contact with tissue have been deployed commercially. In the framework of this thesis, we have focused particularly in colorectal cancer because colonoscopy procedures allow a rather easy access to colon tissues. Even so, this technique can target other diseases such as:

- Barrett's oesophagus and oesophagus cancer. As this organ can be accessed as well by means of endoscopy procedures, the *in vivo* measurement prototype could be exported for detecting these diseases in case that dielectric differences between healthy and pathological samples exist.

- Liver steatosis. A certain amount of steatosis (this is, fat cells present in liver tissue) is accepted in transplants, which is generally analyzed with a single biopsy. As already presented in literature, the higher the degree of steatosis, the lower the dielectric properties of liver. This disease could be a target since it can be accessed during transplants and detected with a modification of the proposed systems. Other liver states such as cirrhosis and cancer could be studied as well.

- Skin melanoma. Although it seems trivial due to its easy access, the related challenges are not easy to solve. Among other issues, the natural inhomogeneity of healthy skin and its variability among patients difficult greatly a possible calibration of the system as well as the diagnosis. In addition, skin is a very thin tissue, and the presence of subcutaneous fat tissue below it could alter the diagnosis.

Appendix A

Electromagnetic properties of biological tissues

There is a great number of studies reporting measurements of electromagnetic properties of biological tissues. Most of these studies have been carried out on animal species and in *ex vivo* or *in vitro* conditions. Almost all of them have been performed using the open-ended coaxial technique. Although not having the best accuracy among the available methods, it is the most suitable one for measuring semi-solid materials in wide bandwidths. In the Table A.1, a collection of works performed on animal species is presented. It should be highlighted that we have focused on the most characteristic tissues, and that some contributions may have not been included.

Tissue	**Animal**	**Cond.**	**Frequencies**	**Reference**
Bone	Ovine	*Ex vivo*	1 MHz - 20 GHz	[87]
Bladder	Bovine		500 MHz - 20 GHz	[110]
	Porcine			
Breast tissue	Mice	*In vivo*	500 MHz - 5 GHz	[52]
			500 MHz - 30 GHz	[134]
Cartilage	Ovine	*Ex vivo*	1 MHz - 20 GHz	[87]
Cerebellum				
Colon			20 Hz - 20 GHz	
	Porcine	*In vivo*	433 MHz - 434 MHz	[138]
			500 MHz - 5 GHz	[52]
Cornea	Ovine	*Ex vivo*	10 Hz - 20 GHz	[87]

Dermis and Epidermis	Porcine	*In vitro*	500 MHz - 110 GHz	[139]
Fat tissue	Bovine	*Ex vivo*	10 Hz - 20 GHz	[87]
Grey matter	Canine	*In vivo*	100 MHz - 2 GHz	[104]
		Ex vivo	10 MHz - 10 GHz	[140]
		In vitro	100 MHz - 11 GHz	[113]
			300 MHz- 3 GHz	[141]
	Feline	*In vitro, In vivo*	100 MHz - 8 GHz	[108]
		In vivo	10 MHz - 1 GHz	[112]
	Mice		500 MHz - 5 GHz	[52]
	Ovine	*Ex vivo*	10 Hz - 20 GHz	[87]
	Rabbit		1 GHz - 18 GHz	[142]
	Rat	*Ex vivo*	130 MHz - 10 GHz	[93]
		In vitro	45 MHz - 26.5 GHz	[78]
		In vivo	100 MHz - 11 GHz	[104]
Heart	Canine	*In vitro*		[113]
	Frog	*In vitro, In vivo*	200 MHz - 8 GHz	[101]
	Ovine	*Ex vivo*	10 Hz - 20 GHz	[87]
Kidney	Bovine		20 kHz - 100 MHz	[143]
		In vitro	2 GHz - 4 GHz	[103]
	Canine		100 MHz - 11 GHz	[113]
		In vivo	100 MHz - 4 GHz	[104]
	Feline	*In vitro, In vivo*	100 MHz - 8 GHz	[108]
		In vivo	10 MHz - 1 GHz	[112]
	Ovine	*Ex vivo*	10 Hz - 20 GHz	[87]
	Rat		130 MHz - 10 GHz	[93]
		In vivo	100 MHz - 12 GHz	[108]
Liver	Bovine	*Ex vivo*	20 kHz - 100 MHz	[143]
			500 MHz - 20 GHz	[109]
			500 MHz - 40 GHz	[102]
		In vitro	2 GHz - 4 GHz	[103]
	Canine		100 MHz - 11 GHz	[113]
	Feline	*In vitro, In vivo*	100 MHz - 8 GHz	[108]
		In vivo	10 MHz - 1 GHz	[112]
			100 MHz - 10 GHz	[96]

	Ovine	*Ex vivo*	10 Hz - 20 GHz	[87]
	Porcine		500 MHz - 40 GHz	[102]
	Rat		130 MHz - 10 GHz	[93]
		In vivo	100 MHz - 10 GHz	[96]
			100 MHz - 12 GHz	[108]
			500 MHz - 6 GHz	[114]
			500 MHz - 40 GHz	[105]
Lung	Ovine	*Ex vivo*	10 Hz - 20 GHz	[87]
Muscle	Bovine		500 MHz - 40 GHz	[102]
		In vitro	2 GHz - 4 GHz	[103]
	Canine		100 MHz - 11 GHz	[113]
		In vivo		[104]
	Feline	*In vitro, In vivo*	100 MHz - 8 GHz	[108]
		In vivo	10 MHz - 1 GHz	[112]
			100 MHz - 10 GHz	[96]
	Frog		200 MHz - 8 GHz	[101]
	Mice	*Ex vivo*	50 MHz - 10 GHz	[144]
	Ovine		10 Hz - 20 GHz	[87]
	Porcine		500 MHz - 40 GHz	[102]
	Rat		130 MHz - 10 GHz	[93]
		In vivo	100 MHz - 10 GHz	[96]
			100 MHz - 11 GHz	[104]
			100 MHz - 12 GHz	[108]
Oesophagus	Porcine	*In vivo*	433 MHz - 434 MHz	[52]
Skin	Canine	*In vitro*	100 MHz - 11 GHz	[113]
	Frog		200 MHz - 8 GHz	[101]
	Ovine	*In vivo*	100 MHz - 10 GHz	[145]
	Porcine			
		In vitro	1 GHz - 15 GHz	[146]
	Rat	*Ex vivo*	130 MHz - 10 GHz	[93]
	Sea Lion	*In vivo*	100 MHz - 10 GHz	[145]
Small Intestine	Porcine		433 MHz - 434 MHz	[138]
Spleen	Bovine	*Ex vivo*	20 kHz - 100 MHz	[143]
	Feline	*In vitro, In vivo*	100 MHz - 8 GHz	[108]
		In vivo	10 MHz - 1 GHz	[112]
			100 MHz - 10 GHz	[96]
	Ovine	*Ex vivo*	10 Hz - 20 GHz	[87]
	Rat		130 MHz - 10 GHz	[93]

		In vivo	100 MHz - 10 GHz	[96]
			100 MHz - 12 GHz	[108]
Stomach	Mice		500 MHz - 5 GHz	[52]
	Porcine		433 - 434 MHz	[138]
Tongue	Rat	*Ex vivo*	130 MHz - 10 GHz	[93]
White matter	Canine		10 MHz - 10 GHz	[140]
		In vitro	100 MHz - 11 GHz	[113]
			300 MHz - 3 GHz	[141]
	Feline	*In vivo*	10 MHz - 1 GHz	[112]
	Ovine	*Ex vivo*	10 Hz - 20 GHz	[87]
	Rabbit		1 GHz - 18 GHz	[142]
	Rat	*In vitro*	45 MHz - 26.5 GHz	[78]

Table A.1: Dielectric characterization studies of biological tissues performed on animal specimens available in literature.

One can observe from the former table that there is a large heterogeneity regarding the measured frequencies, the animal species considered and the measurement conditions. Besides, many of them are focused just on a few tissues. The most complete collection available is the so-called Gabriel's database [87]. The measurements of this collection were carried out in a wide frequency bandwidth, from 1 MHz (or below for many tissues) up to 20 GHz, considering more than 40 different tissues. Many of these measurements were performed on animal specimens, mostly sheep, in *ex vivo* conditions. However, a few tissues were characterized *ex vivo* or *in vivo* from human samples, causing that not the entire database has been performed under the same conditions.

A collection of the found dielectric studies performed on human tissues is gathered in the Table A.2. One can easily observe that the quantity of characterized tissues and the number of studies are much lower in humans than in animals. In addition, due mainly to ethical constraints, only a few tissues have been characterized *in vivo* so far.

Tissue	**Condition**	**Frequencies**	**Reference**
Bladder	*Ex vivo*	1 MHz - 20 GHz	[87]
Bone			
Breast tissue		50 MHz - 900 MHz	[51]
		500 MHz - 20 GHz	[147]
Colon		50 MHz - 900 MHz	[51]
		500 MHz - 18 GHz	[106]
Fat tissue		1 MHz - 20 GHz	[87]
Grey matter		800 MHz - 2.45 GHz	[148]

Kidney		50 MHz - 900 MHz	[51]
Liver	*Ex vivo, In vivo*	500 MHz - 20 GHz	[53]
	In vitro	100 MHz - 5 GHz	[149]
Lung	*Ex vivo*	10 Hz - 20 GHz	[87]
		500 MHz - 900 MHz	[51]
	In vitro	100 Hz - 100 MHz	[150]
Muscle	*Ex vivo*	50 MHz - 900 MHz	[51]
Skin	*In vivo*	100 Hz - 20 GHz	[87]
Small intestine	*Ex vivo*	1 MHz - 20 GHz	
Stomach			
Tongue	*In vivo*		

Table A.2: Dielectric characterization studies of biological tissues performed on human samples available in literature.

References

[1] K. R. Foster and S. H. P, "Dielectric properties of tissues and biological materials: a critical review," *Critical reviews in biomedical engineering*, vol. 17, no. 1, pp. 25–104, jan 1989.

[2] R. Pethig, "Dielectric properties of body tissues," *Clin. Phys. Physiol. Meas*, vol. 8, pp. 5–12, 1987.

[3] S. Mandija, "Non-Invasive Characterization of Brain Tissue Electrical Properties with MRI," Ph.D. dissertation, Utrecht University, jan 2017.

[4] D. H. Werner and Z. H. Jiang, *Electromagnetics of body-area networks : antennas, propagation, and RF circuits.* Wiley-IEEE Press, 2016.

[5] M. Vallejo, J. Recas, P. García del Valle, and J. L. Ayala, "Accurate human tissue characterization for energy-efficient wireless on-body communications," *Sensors (Basel)*, vol. 13, no. 6, pp. 7546–69, jun 2013.

[6] K. N. Bocan, M. H. Mickle, and E. Sejdic, "Tissue Variability and Antennas for Power Transfer to Wireless Implantable Medical Devices," *IEEE Journal of Translational Engineering in Health and Medicine*, vol. 5, pp. 1–11, 2017.

[7] S. Oh, Y.-C. Ryu, G. Carluccio, C. T. Sica, and C. M. Collins, "Measurement of SAR-induced temperature increase in a phantom and in vivo with comparison to numerical simulation," *Magnetic resonance in medicine*, vol. 71, no. 5, pp. 1923–31, may 2014.

[8] ICNIRP, "Guidelines for limiting exposure to time-varying electric, magnetic, and electromagnetic fields (up to 300 GHz). International Commission on Non-Ionizing Radiation Protection." *Health physics*, vol. 74, no. 4, pp. 494–522, apr 1998.

[9] IEEE, *IEEE standard for safety levels with respect to human exposure to radio frequency electromagnetic fields, 3kHz to 300 GHz.* Institute of Electrical and Electronics Engineers, 2006.

[10] ——, *IEEE standard for military workplaces– force health protection regarding personnel exposure to electric, magnetic, and electromagnetic fields, 0 Hz to 300 GHz.* Institute of Electrical and Electronics Engineers, 2014.

[11] C. Garcia-Pardo, C. Andreu, A. Fornes-Leal, S. Castello-Palacios, S. Perez-Simbor, M. Barbi, A. Valles-Lluch, and N. Cardona, "Ultrawideband Technology for Medical In-Body Sensor Networks: An Overview of the Human Body as a Propagation Medium, Phantoms, and Approaches for Propagation Analysis," *IEEE Antennas and Propagation Magazine*, vol. 60, no. 3, pp. 19–33, jun 2018.

[12] J. B. Van De Kamer, N. Van Wieringen, A. A. C. De Leeuw, and J. J. W. Lagendijk, "The significance of accurate dielectric tissue data for hyperthermia treatment planning," *International Journal of Hyperthermia*, vol. 17, no. 2, pp. 123–42, jan 2001.

[13] N. Siauve and C. Lormel, "Interstitial microwave hyperthermia treatment investigations," *Journal of Physics: Conference Series*, vol. 395, no. 1, p. 012001, nov 2012.

[14] A. Rahman, M. T. Islam, M. J. Singh, S. Kibria, and M. Akhtaruzzaman, "Electromagnetic Performances Analysis of an Ultra-wideband and Flexible Material Antenna in Microwave Breast Imaging: To Implement A Wearable Medical Bra," *Scientific Reports*, vol. 6, no. 1, p. 38906, dec 2016.

[15] F. Bray, J. Ferlay, I. Soerjomataram, R. L. Siegel, L. A. Torre, and A. Jemal, "Global cancer statistics 2018: GLOBOCAN estimates of incidence and mortality worldwide for 36 cancers in 185 countries," *CA: A Cancer Journal for Clinicians*, vol. 68, no. 6, pp. 394–424, nov 2018.

[16] The Lancet, "GLOBOCAN 2018: counting the toll of cancer," *The Lancet*, vol. 392, no. 10152, p. 985, sep 2018.

[17] D. Schottenfeld and J. F. Fraumeni, *Cancer epidemiology and prevention.* Oxford University Press, 2006.

[18] G. Danaei, S. Vander Hoorn, A. D. Lopez, C. J. Murray, M. Ezzati, and Comparative Risk Assessment collaborating group (Cancers), "Causes of

cancer in the world: comparative risk assessment of nine behavioural and environmental risk factors," *The Lancet*, vol. 366, no. 9499, pp. 1784–93, nov 2005.

[19] H. S. Gandomani, S. M. Yousefi, M. Aghajani, A. Mohammadian-Hafshejani, A. A. Tarazoj, V. Pouyesh, H. Salehiniya, and H. Salehiniya, "Colorectal cancer in the world: incidence, mortality and risk factors," *Biomedical Research and Therapy*, vol. 4, no. 10, pp. 1656–75, oct 2017.

[20] M. L. Slattery, K. M. Boucher, B. J. Caan, J. D. Potter, and K. N. Ma, "Eating patterns and risk of colon cancer." *American journal of epidemiology*, vol. 148, no. 1, pp. 4–16, jul 1998.

[21] P. Terry, E. Giovannucci, K. B. Michels, L. Bergkvist, H. Hansen, L. Holmberg, and A. Wolk, "Fruit, Vegetables, Dietary Fiber, and Risk of Colorectal Cancer," *JNCI Journal of the National Cancer Institute*, vol. 93, no. 7, pp. 525–33, apr 2001.

[22] E. Negri, S. Franceschi, M. Parpinel, and C. La Vecchia, "Fiber intake and risk of colorectal cancer." *Cancer epidemiology, biomarkers & prevention : a publication of the American Association for Cancer Research, cosponsored by the American Society of Preventive Oncology*, vol. 7, no. 8, pp. 667–71, aug 1998.

[23] W. C. Willett, M. J. Stampfer, G. A. Colditz, B. A. Rosner, and F. E. Speizer, "Relation of Meat, Fat, and Fiber Intake to the Risk of Colon Cancer in a Prospective Study among Women," *New England Journal of Medicine*, vol. 323, no. 24, pp. 1664–72, dec 1990.

[24] S. A. Bingham, N. E. Day, R. Luben, P. Ferrari, N. Slimani, T. Norat, F. Clavel-Chapelon, E. Kesse, A. Nieters, H. Boeing, A. Tjønneland, K. Overvad, C. Martinez, M. Dorronsoro, C. A. Gonzalez, T. J. Key, A. Trichopoulou, A. Naska, P. Vineis, R. Tumino, V. Krogh, H. B. Bueno-de Mesquita, P. H. M. Peeters, G. Berglund, G. Hallmans, E. Lund, G. Skeie, R. Kaaks, E. Riboli, and European Prospective Investigation into Cancer and Nutrition, "Dietary fibre in food and protection against colorectal cancer in the European Prospective Investigation into Cancer and Nutrition (EPIC): an observational study." *The Lancet*, vol. 361, no. 9368, pp. 1496–501, may 2003.

[25] S. C. Larsson, E. Giovannucci, L. Bergkvist, and A. Wolk, "Whole grain consumption and risk of colorectal cancer: a population-based cohort of 60.000 women," *British Journal of Cancer*, vol. 92, no. 9, pp. 1803–7, may 2005.

[26] A. Chao, M. J. Thun, C. J. Connell, M. L. McCullough, E. J. Jacobs, W. D. Flanders, C. Rodriguez, R. Sinha, and E. E. Calle, "Meat Consumption and Risk of Colorectal Cancer," *JAMA*, vol. 293, no. 2, pp. 172–82, jan 2005.

[27] T. Norat, S. Bingham, P. Ferrari, N. Slimani, M. Jenab, M. Mazuir, K. Overvad, A. Olsen, A. Tjønneland, F. Clavel, M.-C. Boutron-Ruault, E. Kesse, H. Boeing, M. M. Bergmann, A. Nieters, J. Linseisen, A. Trichopoulou, D. Trichopoulos, Y. Tountas, F. Berrino, D. Palli, S. Panico, R. Tumino, P. Vineis, H. B. Bueno-de Mesquita, P. H. M. Peeters, D. Engeset, E. Lund, G. Skeie, E. Ardanaz, C. González, C. Navarro, J. R. Quirós, M.-J. Sanchez, G. Berglund, I. Mattisson, G. Hallmans, R. Palmqvist, N. E. Day, K.-T. Khaw, T. J. Key, M. San Joaquin, B. Hémon, R. Saracci, R. Kaaks, and E. Riboli, "Meat, Fish, and Colorectal Cancer Risk: The European Prospective Investigation into Cancer and Nutrition," *JNCI: Journal of the National Cancer Institute*, vol. 97, no. 12, pp. 906–16, jun 2005.

[28] E. K. Wei, E. Giovannucci, K. Wu, B. Rosner, C. S. Fuchs, W. C. Willett, and G. A. Colditz, "Comparison of risk factors for colon and rectal cancer," *International Journal of Cancer*, vol. 108, no. 3, pp. 433–42, jan 2004.

[29] M. E. Martinez, E. T. Jacobs, E. L. Ashbeck, R. Sinha, P. Lance, D. S. Alberts, and P. A. Thompson, "Meat intake, preparation methods, mutagens and colorectal adenoma recurrence," *Carcinogenesis*, vol. 28, no. 9, pp. 2019–27, aug 2007.

[30] V. Fedirko, I. Tramacere, V. Bagnardi, M. Rota, L. Scotti, F. Islami, E. Negri, K. Straif, I. Romieu, C. La Vecchia, P. Boffetta, and M. Jenab, "Alcohol drinking and colorectal cancer risk: an overall and dose-response meta-analysis of published studies," *Annals of Oncology*, vol. 22, no. 9, pp. 1958–72, sep 2011.

[31] E. Cho, S. A. Smith-Warner, J. Ritz, P. A. van den Brandt, G. A. Colditz, A. R. Folsom, J. L. Freudenheim, E. Giovannucci, R. A. Goldbohm, S. Graham, L. Holmberg, D.-H. Kim, N. Malila, A. B. Miller, P. Pietinen, T. E. Rohan, T. A. Sellers, F. E. Speizer, W. C. Willett, A. Wolk, and D. J. Hunter, "Alcohol Intake and Colorectal Cancer: A Pooled Analysis of 8 Cohort Studies," *Annals of Internal Medicine*, vol. 140, no. 8, pp. 603–13, apr 2004.

[32] F. B. Hu, J. E. Manson, S. Liu, D. Hunter, G. A. Colditz, K. B. Michels, F. E. Speizer, and E. Giovannucci, "Prospective Study of Adult Onset

Diabetes Mellitus (Type 2) and Risk of Colorectal Cancer in Women," *JNCI Journal of the National Cancer Institute*, vol. 91, no. 6, pp. 542–7, mar 1999.

[33] J. C. Will, D. A. Galuska, F. Vinicor, and E. E. Calle, "Colorectal Cancer: Another Complication of Diabetes Mellitus?" *American Journal of Epidemiology*, vol. 147, no. 9, pp. 816–25, may 1998.

[34] A. Ekbom, C. Helmick, M. Zack, and H.-O. Adami, "Ulcerative Colitis and Colorectal Cancer," *New England Journal of Medicine*, vol. 323, no. 18, pp. 1228–33, nov 1990.

[35] D. T. Rubin, D. Huo, J. A. Kinnucan, M. S. Sedrak, N. E. McCullom, A. P. Bunnag, E. P. Raun−Royer, R. D. Cohen, S. B. Hanauer, J. Hart, and J. R. Turner, "Inflammation Is an Independent Risk Factor for Colonic Neoplasia in Patients With Ulcerative Colitis: A Case—Control Study," *Clinical Gastroenterology and Hepatology*, vol. 11, no. 12, pp. 1601–08.e4, dec 2013.

[36] E. S. Schernhammer, M. F. Leitzmann, D. S. Michaud, F. E. Speizer, E. Giovannucci, G. A. Colditz, and C. S. Fuchs, "Cholecystectomy and the risk for developing colorectal cancer and distal colorectal adenomas," *British Journal of Cancer*, vol. 88, no. 1, pp. 79–83, jan 2003.

[37] T. Shao and Y.-X. Yang, "Cholecystectomy and the Risk of Colorectal Cancer," *The American Journal of Gastroenterology*, vol. 100, no. 8, pp. 1813–20, aug 2005.

[38] R. S. Sandler and D. P. Sandler, "Radiation-induced cancers of the colon and rectum: Assessing the risk," *Gastroenterology*, vol. 84, no. 1, pp. 51–7, 1983.

[39] N. N. Baxter, J. E. Tepper, S. B. Durham, D. A. Rothenberger, and B. A. Virnig, "Increased risk of rectal cancer after prostate radiation: A population-based study," *Gastroenterology*, vol. 128, no. 4, pp. 819–24, apr 2005.

[40] M. Bardou, A. N. Barkun, and M. Martel, "Obesity and colorectal cancer." *Gut*, vol. 62, no. 6, pp. 933–47, jun 2013.

[41] I.-M. Lee, E. J. Shiroma, F. Lobelo, P. Puska, S. N. Blair, P. T. Katzmarzyk, and Lancet Physical Activity Series Working Group, "Effect of physical inactivity on major non-communicable diseases worldwide: an analysis of burden of disease and life expectancy," *The Lancet*, vol. 380, no. 9838, pp. 219–29, jul 2012.

[42] L. H. Colbert, T. J. Hartman, N. Malila, P. J. Limburg, P. Pietinen, J. Virtamo, P. R. Taylor, and D. Albanes, "Physical activity in relation to cancer of the colon and rectum in a cohort of male smokers." *Cancer epidemiology, biomarkers & prevention : a publication of the American Association for Cancer Research, cosponsored by the American Society of Preventive Oncology*, vol. 10, no. 3, pp. 265–8, mar 2001.

[43] H. J. Kim, S. Lee, N.-K. Choi, S. H. Kim, H.-J. Song, Y. K. Cho, and B. J. Park, "Smoking and colorectal cancer risk in the Korean elderly." *Journal of preventive medicine and public health = Yebang Uihakhoe chi*, vol. 39, pp. 123–29, 2006.

[44] E. Giovannucci, E. B. Rimm, M. J. Stampfer, G. A. Colditz, A. Ascherio, J. Kearney, and W. C. Willett, "A prospective study of cigarette smoking and risk of colorectal adenoma and colorectal cancer in U.S. men." *Journal of the National Cancer Institute*, vol. 86, no. 3, pp. 183–91, feb 1994.

[45] E. D. Paskett, K. W. Reeves, T. E. Rohan, M. A. Allison, C. D. Williams, C. R. Messina, E. Whitlock, A. Sato, and J. R. Hunt, "Association Between Cigarette Smoking and Colorectal Cancer in the Women's Health Initiative," *JNCI Journal of the National Cancer Institute*, vol. 99, no. 22, pp. 1729–35, nov 2007.

[46] A. S. Butterworth, J. P. Higgins, and P. Pharoah, "Relative and absolute risk of colorectal cancer for individuals with a family history: A meta-analysis," *European Journal of Cancer*, vol. 42, no. 2, pp. 216–27, jan 2006.

[47] J. M. Wilson and G. Jungner, "Principles and practice of mass screening for disease," *Boletin de la Oficina Sanitaria Panamericana. Pan American Sanitary Bureau*, vol. 65, no. 4, pp. 281–393, 1968.

[48] H. Fricke and S. Morse, "The Electric Capacity of Tumors of the Breast," *Journal of Cancer Research*, vol. 10, pp. 340–76, 1926.

[49] W. T. Joines, R. L. Jirtle, M. D. Rafal, and D. J. Schaefer, "Microwave power absorption differences between normal and malignant tissue." *International journal of radiation oncology, biology, physics*, vol. 6, no. 6, pp. 681–7, jun 1980.

[50] W. T. Joines, "Frequency-dependent absorption of electromagnetic energy in biological tissue." *IEEE transactions on biomedical engineering*, vol. 31, no. 1, pp. 17–20, jan 1984.

[51] W. T. Joines, Y. Zhang, C. Li, and R. L. Jirtle, "The measured electrical properties of normal and malignant human tissues from 50 to 900 MHz," *Medical physics*, vol. 21, no. 4, pp. 547–50, 1994.

[52] D.-S. Yoo, "The dielectric properties of cancerous tissues in a nude mouse xenograft model," *Bioelectromagnetics*, vol. 25, no. 7, pp. 492–7, oct 2004.

[53] A. P. O'Rourke, M. Lazebnik, J. M. Bertram, M. C. Converse, S. C. Hagness, J. G. Webster, and D. M. Mahvi, "Dielectric properties of human normal, malignant and cirrhotic liver tissue: in vivo and ex vivo measurements from 0.5 to 20 GHz using a precision open-ended coaxial probe." *Physics in medicine and biology*, vol. 52, no. 15, pp. 4707–19, 2007.

[54] M. Lazebnik, D. Popovic, L. McCartney, C. B. Watkins, M. J. Lindstrom, J. Harter, S. Sewall, T. Ogilvie, A. Magliocco, T. M. Breslin, W. Temple, D. Mew, J. H. Booske, M. Okoniewski, and S. C. Hagness, "A large-scale study of the ultrawideband microwave dielectric properties of normal, benign and malignant breast tissues obtained from cancer surgeries." *Physics in medicine and biology*, vol. 52, no. 20, pp. 6093–115, oct 2007.

[55] A. Martellosio, M. Pasian, M. Bozzi, L. Perregrini, A. Mazzanti, F. Svelto, P. E. Summers, G. Renne, L. Preda, and M. Bellomi, "Dielectric Properties Characterization From 0.5 to 50 GHz of Breast Cancer Tissues," *IEEE Transactions on Microwave Theory and Techniques*, vol. 65, no. 3, pp. 998–1011, mar 2017.

[56] C. Bellorofonte, C. Vedruccio, P. Tombolini, M. Ruoppolo, and A. Tubaro, "Non-invasive detection of prostate cancer by electromagnetic interaction," *European Urology*, vol. 47, no. 1, pp. 29–37, 2005.

[57] L. Da Pozzo, V. Scattoni, B. Mazzoccoli, P. Rigatti, F. Manferrari, G. Martorana, F. Pietropaolo, E. Belgrano, D. Prezioso, T. Lotti, D. Villari, and G. Nicita, "Tissue-resonance interaction method for the non-invasive diagnosis of prostate cancer: analysis of a multicentre clinical evaluation." *BJU international*, vol. 100, no. 5, pp. 1055–9, nov 2007.

[58] A. Tubaro, C. De Nunzio, A. Trucchi, A. Stoppacciaro, and L. Miano, "The electromagnetic detection of prostatic cancer: evaluation of diagnostic accuracy." *Urology*, vol. 72, no. 2, pp. 340–4, aug 2008.

[59] D. D. I. Viccaro, G. Perugia, C. Cerulli, V. Olivieri, G. Bova, J. Balla, C. Zanza, S. Teodonio, and M. Liberti, "The accuracy of tissue resonance interaction method probe (Trimprob tm) in non-invasive diagno-

sis of prostatic cancer . Analysis of the results of 782 patients," *Urologia*, vol. 76, no. 3, pp. 3–5, 2009.

[60] O. Gokce, O. Sanli, A. Salmaslioglu, A. Tunaci, C. Ozsoy, and F. Ozcan, "Tissue Resonance Interaction Method (TRIMprob) has the potential to be used alongside the recognized tests in the screening protocols for prostate cancer." *International journal of urology : official journal of the Japanese Urological Association*, vol. 16, no. 6, pp. 580–3, jun 2009.

[61] C. De Cicco, L. Mariani, C. Vedruccio, C. Ricci, M. Balma, N. Rotmensz, M. E. Ferrari, E. Autino, G. Trifirò, V. Sacchini, G. Viale, and G. Paganelli, "Clinical application of spectral electromagnetic interaction in breast cancer: diagnostic results of a pilot study." *Tumori*, vol. 92, no. 3, pp. 207–12, jan 2006.

[62] R. Sacco, N. Innaro, F. Pata, a. M. Lucisano, C. Talarico, and S. Aversa, "Preoperative diagnosis of incidental carcinoma in multinodular goitre by means of electromagnetic interactions," *Chirurgia italiana*, vol. 59, no. 2, pp. 247–51, jan 2007.

[63] R. Sacco, G. Sammarco, R. De Vinci, G. Vescio, A. Scarpelli, A. M. Lucisano, F. Pata, E. Mascia, and V. Martines, "Relief of gastric cancer with an electromagnetic interaction system (TRIMprob) in outpatients." *Chirurgia italiana*, vol. 59, no. 6, pp. 823–8, jan 2007.

[64] A. Vannelli, L. Battaglia, E. Poiasina, and E. Leo, "Diagnosis of rectal cancer by Tissue Resonance Interaction Method." *BMC gastroenterology*, vol. 10, no. 1, pp. 45–51, jan 2010.

[65] G. Gervino, E. Autino, E. Kolomoets, G. Leucci, and M. Balma, "Diagnosis of bladder cancer at 465 MHz." *Electromagnetic biology and medicine*, vol. 26, no. 2, pp. 119–34, jan 2007.

[66] C. Vedruccio and C. R. Vedruccio, "Non invasive radiofrequency diagnostics of cancer. The Bioscanner — Trimprob technology and clinical applications," *Journal of Physics: Conference Series*, vol. 329, p. 012038, 2011.

[67] S. Kwon and S. Lee, "Recent Advances in Microwave Imaging for Breast Cancer Detection," *International Journal of Biomedical Imaging*, vol. 2016, pp. 1–26, dec 2016.

[68] DUNE, "MarginProbe." [Online]. Available: https://www.dunemedical.com/lumpectomy-surgery-clean-margins/

[69] J. C. Lin, *Advances in electromagnetic fields in living systems.* Springer, 2005.

[70] A. V. Vorst, A. Rosen, and Y. Kotsuka, *RF/microwave interaction with biological tissues.* John Wiley & Sons, 2006.

[71] M. Wolf, R. Gulich, P. Lunkenheimer, and A. Loidl, "Relaxation dynamics of a protein solution investigated by dielectric spectroscopy," *Biochimica et biophysica acta*, vol. 1824, no. 5, pp. 723–30, may 2012.

[72] B. Filali, F. Boone, J. Rhazi, and G. Ballivy, "Design and Calibration of a Large Open-Ended Coaxial Probe for the Measurement of the Dielectric Properties of Concrete," *IEEE Transactions on Microwave Theory and Techniques*, vol. 56, no. 10, pp. 2322–28, oct 2008.

[73] K. Y. You, H. K. Mun, L. L. You, J. Salleh, and Z. Abbas, "A small and slim coaxial probe for single rice grain moisture sensing." *Sensors (Basel, Switzerland)*, vol. 13, no. 3, pp. 3652–63, mar 2013.

[74] L. Zhang, X. Shi, F. You, P. Liu, and X. Dong, "Improved circuit model of open-ended coaxial probe for measurement of the biological tissue dielectric properties between megahertz and gigahertz," *Physiological Measurement*, vol. 34, no. 10, pp. N83–96, oct 2013.

[75] A. Fornes-Leal, C. Garcia-Pardo, N. Cardona, S. Sergio Castello-Palacios, and A. Valles-Lluch, "Accurate broadband measurement of electromagnetic tissue phantoms using open-ended coaxial systems," in *2017 11th International Symposium on Medical Information and Communication Technology (ISMICT)*, Lisbon, feb 2017, pp. 32–6.

[76] T. Marsland and S. Evans, "Dielectric measurements with an open-ended coaxial probe," *IEE Proceedings H Microwaves, Antennas and Propagation*, vol. 134, no. 4, pp. 341–9, 1987.

[77] A. Nyshadham, C. Sibbald, and S. Stuchly, "Permittivity measurements using open-ended sensors and reference liquid calibration-an uncertainty analysis," *IEEE Transactions on Microwave Theory and Techniques*, vol. 40, no. 2, pp. 305–14, 1992.

[78] J. Z. Bao, S.-T. Lu, and W. Hurt, "Complex dielectric measurements and analysis of brain tissues in the radio and microwave frequencies," *IEEE Transactions on Microwave Theory and Techniques*, vol. 45, no. 10, pp. 1730–41, 1997.

[79] M. A. Stuchly and S. S. Stuchly, "Coaxial Line Reflection Methods for Measuring Dielectric Properties of Biological Substances at Radio and Microwave Frequencies-A Review," *IEEE Transactions on Instrumentation and Measurement*, vol. 29, no. 3, pp. 176–83, 1980.

[80] D. V. Blackham and R. D. Pollard, "An Improved Technique for Perimittivity Measurements Using a Coaxial Probe," *IEEE Transactions on Instrumentation and Measurement*, vol. 46, no. 5, pp. 1093–9, 1997.

[81] D. Misra, M. Chabbra, B. Epstein, M. Microtznik, and K. Foster, "Noninvasive electrical characterization of materials at microwave frequencies using an open-ended coaxial line: test of an improved calibration technique," *IEEE Transactions on Microwave Theory and Techniques*, vol. 38, no. 1, pp. 8–14, 1990.

[82] A. P. Gregory and R. N. Clarke, "Tables of the Complex Permittivity of Dielectric Reference Liquids; NPL Report MAT 23," pp. 1–87, 2009.

[83] C. Gabriel and A. Peyman, "Dielectric measurement: error analysis and assessment of uncertainty," *Physics in Medicine and Biology*, vol. 51, no. 23, pp. 6033–46, dec 2006.

[84] ISO, *Guide to the Expression of Uncertainty in Measurement.* Geneva: International Organization for Standardisation, 1995.

[85] NIST, *Guidelines for Evaluating and Expressing the Uncertainty of NIST Measurement Results*, B. N. Taylor and C. E. Kuyatt, Eds. Washington, DC: United States Department of Commerce, 1994.

[86] R. Buchner, G. T. Hefter, and P. M. May, "Dielectric Relaxation of Aqueous NaCl Solutions," *The Journal of Physical Chemistry A*, vol. 103, no. 1, pp. 1–9, jan 1999.

[87] C. Gabriel, "Compilation of the dielectric properties of body tissues at RF and microwave frequencies," *Report N.AL/OE-TR- 1996-0037*, p. 276, 1996.

[88] A. Shahzad, S. Khan, M. Jones, R. M. Dwyer, and M. O'Halloran, "Investigation of the effect of dehydration on tissue dielectric properties in ex vivo measurements," *Biomedical Physics & Engineering Express*, vol. 3, no. 4, p. 045001, jun 2017.

[89] A. La Gioia, E. Porter, I. Merunka, A. Shahzad, S. Salahuddin, M. Jones, and M. O'Halloran, "Open-Ended Coaxial Probe Technique for Dielectric

Measurement of Biological Tissues: Challenges and Common Practices," *Diagnostics*, vol. 8, no. 2, p. 40, jun 2018.

[90] R. H. Byrd, R. B. Schnabel, and G. A. Shultz, "Approximate solution of the trust region problem by minimization over two-dimensional subspaces," *Mathematical Programming*, vol. 40, no. 1-3, pp. 247–63, jan 1988.

[91] M. A. Branch, T. F. Coleman, and Y. Li, "A Subspace, Interior, and Conjugate Gradient Method for Large-Scale Bound-Constrained Minimization Problems," *SIAM Journal on Scientific Computing*, vol. 21, no. 1, pp. 1–23, jan 1999.

[92] A. M. Abad-García, A. Fornes-Leal, and N. Cardona, "Electromagnetic characterization of in vivo biological tissues of the abdominal and thoracic regions," 2018. [Online]. Available: https://www.mcg.upv.es/studer-results/

[93] A. Peyman, A. A. Rezazadeh, and C. Gabriel, "Changes in the dielectric properties of rat tissue as a function of age at microwave frequencies," *Physics in Medicine and Biology*, vol. 46, no. 6, pp. 1617–29, jun 2001.

[94] D. Andreuccetti, R. Fossi, and C. Petrucci, "Calculation of the Dielectric Properties of Body Tissues," 1997. [Online]. Available: http://niremf.ifac.cnr.it/tissprop/htmlclie/htmlclie.php

[95] C. Andreu, C. Garcia-Pardo, A. Fomes-Leal, M. Cabedo-Fabres, and N. Cardona, "UWB in-body channel performance by using a direct antenna designing procedure," in *2017 11th European Conference on Antennas and Propagation (EUCAP)*. IEEE, mar 2017, pp. 278–82.

[96] M. A. Stuchly, A. Kraszewski, S. S. Stuchly, and A. M. Smith, "Dielectric properties of animal tissues in vivo at radio and microwave frequencies: comparison between species," *Physics in Medicine and Biology*, vol. 27, no. 7, pp. 927–36, jul 1982.

[97] M. M. Suzan, K. Haneda, C. Icheln, A. Khatun, and K.-i. Takizawa, "An ultrawideband conformal loop antenna for ingestible capsule endoscope system," in *2016 10th European Conference on Antennas and Propagation (EuCAP)*. IEEE, apr 2016, pp. 1–5.

[98] Z. Duan, L.-J. Xu, S. Gao, and W. Geyi, "Integrated Design of Wideband Omnidirectional Antenna and Electronic Components for Wireless Capsule Endoscopy Systems," *IEEE Access*, vol. 6, pp. 29 626–36, 2018.

[99] C. Tarin, P. Marti, L. Traver, N. Cardona, J. A. Diaz, and E. Antonino, "UWB Channel Measurements for Hand-Portable Devices: A Comparative Study," in *2007 IEEE 18th International Symposium on Personal, Indoor and Mobile Radio Communications*. IEEE, 2007, pp. 1–5.

[100] D. Nikolayev, M. Zhadobov, L. Le Coq, P. Karban, and R. Sauleau, "Robust Ultraminiature Capsule Antenna for Ingestible and Implantable Applications," *IEEE Transactions on Antennas and Propagation*, vol. 65, no. 11, pp. 6107–19, nov 2017.

[101] J. L. Schwartz and G. A. R. Mealing, "Dielectric properties of frog tissues in vivo and in vitro," *Physics in Medicine and Biology*, vol. 30, no. 2, pp. 117–24, feb 1985.

[102] L. Abdilla, C. Sammut, and L. Z. Mangion, "Dielectric properties of muscle and liver from 500 MHz − 40 GHz," *Electromagnetic Biology and Medicine*, vol. 32, no. 2, pp. 244–52, 2013.

[103] M. M. Brady, S. A. Symons, and S. S. Stuchly, "Dielectric behavior of selected animal tissues in vitro at frequencies from 2 to 4 GHz." *IEEE transactions on biomedical engineering*, vol. 28, no. 3, pp. 305–7, mar 1981.

[104] E. Burdette, F. Cain, and J. Seals, "In Vivo Probe Measurement Technique for Determining Dielectric Properties at VHF through Microwave Frequencies," *IEEE Transactions on Microwave Theory and Techniques*, vol. 28, no. 4, pp. 414–27, apr 1980.

[105] L. Farrugia, P. S. Wismayer, L. Z. Mangion, and C. V. Sammut, "Accurate in vivo dielectric properties of liver from 500 MHz to 40 GHz and their correlation to ex vivo measurements," *Electromagnetic Biology and Medicine*, vol. 35, no. 4, pp. 365–73, oct 2016.

[106] A. Fornes-Leal, C. Garcia-Pardo, M. Frasson, V. Pons Beltrán, and N. Cardona, "Dielectric characterization of healthy and malignant colon tissues in the 0.5 − 18 GHz frequency band," *Physics in Medicine and Biology*, vol. 61, no. 20, pp. 7334–46, oct 2016.

[107] M. Guardiola, S. Buitrago, G. Fernández-Esparrach, J. M. O'Callaghan, J. Romeu, M. Cuatrecasas, H. Córdova, M. Á. González Ballester, and O. Camara, "Dielectric properties of colon polyps, cancer, and normal mucosa: Ex vivo measurements from 0.5 to 20 GHz," *Medical Physics*, vol. 45, no. 8, pp. 3768–82, aug 2018.

[108] A. Kraszewski, M. A. Stuchly, S. S. Stuchly, and A. M. Smith, "In vivo and in vitro dielectric properties of animal tissues at radio frequencies," *Bioelectromagnetics*, vol. 3, no. 4, pp. 421–32, 1982.

[109] M. Lazebnik, M. C. Converse, J. H. Booske, and S. C. Hagness, "Ultrawideband temperature-dependent dielectric properties of animal liver tissue in the microwave frequency range," *Physics in medicine and biology*, vol. 51, no. 7, pp. 1941–55, apr 2006.

[110] E. Porter, S. Salahuddin, A. La Gioia, M. A. Elahi, A. Shahzad, A. Kumar, D. Kilroy, and M. O'Halloran, "Characterization of the Dielectric Properties of the Bladder Over the Microwave Range," *IEEE Journal of Electromagnetics, RF and Microwaves in Medicine and Biology*, vol. 2, no. 3, pp. 208–15, sep 2018.

[111] S. Salahuddin, A. L. Gioia, A. Shahzad, M. A. Elahi, A. Kumar, D. Kilroy, E. Porter, and M. O'Halloran, "An anatomically accurate dielectric profile of the porcine kidney," *Biomedical Physics & Engineering Express*, vol. 4, no. 2, p. 025042, feb 2018.

[112] M. A. Stuchly, T. W. Athey, S. S. Stuchly, G. M. Samaras, and G. Taylor, "Dielectric properties of animal tissues in vivo at frequencies 10 MHz − 1 GHz," *Bioelectromagnetics*, vol. 2, no. 2, pp. 93–103, 1981.

[113] Deming Xu, Liping Liu, and Zhiyan Jiang, "Measurement of the Dielectric Properties of Biological Substances Using an Improved Open-Ended Coaxial Line Resonator Method," *IEEE Transactions on Microwave Theory and Techniques*, vol. 35, no. 12, pp. 1424–8, dec 1987.

[114] T. Yilmaz, M. Kiliç, M. Erdoğan, M. Çayören, D. Tunaoğlu, I. Kurtoğlu, Y. Yaslan, H. Çayören, A. Arkan, S. Teksöz, G. Cancan, N. Kepil, S. Erdamar, M. Özcan, I. Akduman, and T. Kalkan, "Machine learning aided diagnosis of hepatic malignancies through in vivo dielectric measurements with microwaves," *Physics in Medicine and Biology*, vol. 61, no. 13, pp. 5089–102, 2016.

[115] C. Gabriel, "Dielectric properties of biological tissue: Variation with age," *Bioelectromagnetics*, vol. 26, no. S7, pp. S12–18, 2005.

[116] K. W. Kinzler and B. Vogelstein, "Lessons from Hereditary Colorectal Cancer," *Cell*, vol. 87, no. 2, pp. 159–70, oct 1996.

[117] J. Cohen, B. P. Bosworth, A. Chak, B. J. Dunkin, D. S. Early, L. B. Gerson, R. H. Hawes, A. V. Haycock, J. H. Hochberger, J. H. Hwang, J. A.

Martin, P. R. McNally, R. E. Sedlack, and M. C. Vassiliou, "Preservation and Incorporation of Valuable Endoscopic Innovations (PIVI) on the use of endoscopy simulators for training and assessing skill," *Gastrointestinal Endoscopy*, vol. 76, no. 3, pp. 471–5, sep 2012.

[118] J. L. Schepps and K. R. Foster, "The UHF and microwave dielectric properties of normal and tumour tissues: variation in dielectric properties with tissue water content," *Physics in Medicine and Biology*, vol. 25, no. 6, pp. 1149–59, nov 1980.

[119] C. J. Kahi, T. F. Imperiale, B. E. Juliar, and D. K. Rex, "Effect of Screening Colonoscopy on Colorectal Cancer Incidence and Mortality," *Clinical Gastroenterology and Hepatology*, vol. 7, no. 7, pp. 770–5, jul 2009.

[120] A. I. Neugut and B. Lebwohl, "Colonoscopy vs Sigmoidoscopy Screening," *JAMA*, vol. 304, no. 4, pp. 461–2, jul 2010.

[121] H. Brenner, J. Chang-Claude, C. M. Seiler, A. Rickert, and M. Hoffmeister, "Protection From Colorectal Cancer After Colonoscopy," *Annals of Internal Medicine*, vol. 154, no. 1, pp. 22–30, jan 2011.

[122] L. K. Wanders, S. C. van Doorn, P. Fockens, and E. Dekker, "Quality of colonoscopy and advances in detection of colorectal lesions: a current overview," *Expert Review of Gastroenterology & Hepatology*, vol. 9, no. 4, pp. 417–30, apr 2015.

[123] I. A. Issa and M. Noureddine, "Colorectal cancer screening: An updated review of the available options," *World Journal of Gastroenterology*, vol. 23, no. 28, pp. 5086–96, jul 2017.

[124] I. Lansdorp-Vogelaar, M. van Ballegooijen, R. Boer, A. Zauber, and J. D. F. Habbema, "A novel hypothesis on the sensitivity of the fecal occult blood test," *Cancer*, vol. 115, no. 11, pp. 2410–9, jun 2009.

[125] J. E. Allison, I. S. Tekawa, L. J. Ransom, and A. L. Adrain, "A Comparison of Fecal Occult-Blood Tests for Colorectal-Cancer Screening," *New England Journal of Medicine*, vol. 334, no. 3, pp. 155–60, jan 1996.

[126] J. K. Lee, E. G. Liles, S. Bent, T. R. Levin, and D. A. Corley, "Accuracy of Fecal Immunochemical Tests for Colorectal Cancer," *Annals of Internal Medicine*, vol. 160, no. 3, pp. 171–81, feb 2014.

[127] T. F. Imperiale, D. F. Ransohoff, S. H. Itzkowitz, T. R. Levin, P. Lavin, G. P. Lidgard, D. A. Ahlquist, and B. M. Berger, "Multitarget Stool DNA Testing for Colorectal-Cancer Screening," *New England Journal of Medicine*, vol. 370, no. 14, pp. 1287–97, apr 2014.

[128] J. Nian, X. Sun, S. Ming, C. Yan, Y. Ma, Y. Feng, L. Yang, M. Yu, G. Zhang, and X. Wang, "Diagnostic Accuracy of Methylated SEPT9 for Blood-based Colorectal Cancer Detection: A Systematic Review and Meta-Analysis." *Clinical and translational gastroenterology*, vol. 8, no. 1, p. e216, jan 2017.

[129] A. Parodi, G. Vanbiervliet, C. Hassan, X. Hebuterne, A. De Ceglie, R. A. Filiberti, C. Spada, and M. Conio, "Colon capsule endoscopy to screen for colorectal neoplasia in those with family histories of colorectal cancer," *Gastrointestinal Endoscopy*, vol. 87, no. 3, pp. 695–704, mar 2018.

[130] E. Rondonotti, C. Borghi, G. Mandelli, F. Radaelli, S. Paggi, A. Amato, G. Imperiali, N. Terreni, N. Lenoci, V. Terruzzi, A. Baccarin, A. Martegani, and G. Spinzi, "Accuracy of Capsule Colonoscopy and Computed Tomographic Colonography in Individuals With Positive Results From the Fecal Occult Blood Test," *Clinical Gastroenterology and Hepatology*, vol. 12, no. 8, pp. 1303–10, aug 2014.

[131] P. M. Meaney, A. P. Gregory, N. R. Epstein, and K. D. Paulsen, "Microwave open-ended coaxial dielectric probe: interpretation of the sensing volume re-visited." *BMC medical physics*, vol. 14, p. 3, 2014.

[132] D. Popovic, L. McCartney, C. Beasley, M. Lazebnik, M. Okoniewski, S. Hagness, and J. Booske, "Precision open-ended coaxial probes for in vivo and ex vivo dielectric spectroscopy of biological tissues at microwave frequencies," *IEEE Transactions on Microwave Theory and Techniques*, vol. 53, no. 5, pp. 1713–22, may 2005.

[133] A. Richmond and Y. Su, "Mouse xenograft models vs GEM models for human cancer therapeutics." *Disease models & mechanisms*, vol. 1, no. 2-3, pp. 78–82, 2008.

[134] J. Cho, J. Yoon, S. Cho, K. Kwon, S. Lim, D. Kim, E. S. Lee, C. H. Kim, J. W. Choi, C. Cheon, and Y. Kwon, "In-vivo measurements of the dielectric properties of breast carcinoma xenografted on nude mice," *International Journal of Cancer*, vol. 119, no. 3, pp. 593–8, aug 2006.

[135] S. Castello-Palacios, C. Garcia-Pardo, A. Fornes-Leal, N. Cardona, and A. Valles-Lluch, "Tailor-Made Tissue Phantoms Based on Acetonitrile

Solutions for Microwave Applications up to 18 GHz," *IEEE Transactions on Microwave Theory and Techniques*, vol. 64, no. 11, pp. 3987–94, nov 2016.

[136] ——, "Wideband phantoms of different body tissues for heterogeneous models in body area networks," in *2017 39th Annual International Conference of the IEEE Engineering in Medicine and Biology Society (EMBC)*. IEEE, jul 2017, pp. 3032–5.

[137] S. Castello-Palacios, C. Garcia-Pardo, A. Fornes-Leal, N. Cardona, M. Alloza-Pascual, and A. Valles-Lluch, "Initial Results of Semisolid Phantoms Based on Synthetic Hydrogels for the cmWave Band," in *2018 IEEE 29th Annual International Symposium on Personal, Indoor and Mobile Radio Communications (PIMRC)*. IEEE, sep 2018, pp. 1128–9.

[138] E. S. Nadimi, V. Blanes-Vidal, J. L. F. Harslund, M. H. Ramezani, J. Kjeldsen, P. M. Johansen, D. Thiel, and V. Tarokh, "In vivo and in situ measurement and modelling of intra-body effective complex permittivity," *Healthcare technology letters*, vol. 2, no. 6, pp. 135–40, dec 2015.

[139] K. Sasaki, K. Wake, and S. Watanabe, "Measurement of the dielectric properties of the epidermis and dermis at frequencies from 0.5 GHz to 110 GHz," *Physics in Medicine and Biology*, vol. 59, no. 16, pp. 4739–47, aug 2014.

[140] K. R. Foster, J. L. Schepps, R. D. Stoy, and H. P. Schwan, "Dielectric properties of brain tissue between 0.01 and 10 GHz," *Physics in Medicine and Biology*, vol. 24, no. 6, pp. 1177–87, nov 1979.

[141] B. Mohammed, K. Bialkowski, A. Abbosh, P. C. Mills, and A. P. Bradley, "Dielectric properties of dog brain tissue measured in vitro across the $0.3 - 3$ GHz band," *Bioelectromagnetics*, vol. 37, no. 8, pp. 549–56, dec 2016.

[142] M. C. Steel and R. J. Sheppard, "Dielectric properties of mammalian brain tissue between 1 and 18 GHz," *Physics in Medicine and Biology*, vol. 30, no. 7, pp. 621–30, jul 1985.

[143] A. Surowiec, S. S. Stuchly, and A. Swarup, "Radiofrequency dielectric properties of animal tissues as a function of time following death," *Physics in Medicine and Biology*, vol. 30, no. 10, pp. 1131–41, 1985.

[144] J. A. Rogers, R. J. Sheppard, E. H. Grant, N. M. Bleehen, and D. J. Honess, "The dielectric properties of normal and tumour mouse tissue between 50 MHz and 10 GHz," *The British Journal of Radiology*, vol. 56, no. 665, pp. 335–8, may 1983.

[145] K. O. Olawale, R. J. Petrell, D. G. Michelson, and A. W. Trites, "The dielectric properties of the cranial skin of five young captive Steller sea lions (Eumetopias jubatus), and a similar number of young domestic pigs (Sus scrofa) and sheep (Ovis aries) between 0.1 and 10 GHz," *Physiological Measurement*, vol. 26, no. 5, pp. 627–37, oct 2005.

[146] R. A. Kleismit, G. Kozlowski, B. D. Foy, B. E. Hull, and M. Kazimierczuk, "Local complex permittivity measurements of porcine skin tissue in the frequency range from 1 GHz to 15 GHz by evanescent microscopy," *Physics in Medicine and Biology*, vol. 54, no. 3, pp. 699–713, feb 2009.

[147] M. Lazebnik, L. McCartney, D. Popovic, C. B. Watkins, M. J. Lindstrom, J. Harter, S. Sewall, A. Magliocco, J. H. Booske, M. Okoniewski, and S. C. Hagness, "A large-scale study of the ultrawideband microwave dielectric properties of normal breast tissue obtained from reduction surgeries," *Physics in Medicine and Biology*, vol. 52, no. 10, pp. 2637–56, may 2007.

[148] G. Schmid, G. Neubauer, and P. R. Mazal, "Dielectric Properties of Human Brain Tissue Measured Less Than 10 h Postmortem at Frequencies from 800 to 2450 MHz," *Bioelectromagnetics*, vol. 24, no. 6, pp. 423–30, 2003.

[149] A. Peyman, B. Kos, M. Djokić, B. Trotovšek, C. Limbaeck-Stokin, G. Serša, and D. Miklavčič, "Variation in dielectric properties due to pathological changes in human liver," *Bioelectromagnetics*, vol. 36, no. 8, pp. 603–12, dec 2015.

[150] J.-R. Wang, B.-Y. Sun, H.-X. Wang, S. Pang, X. Xu, and Q. Sun, "Experimental study of dielectric properties of human lung tissue in vitro," *Journal of Medical and Biological Engineering*, vol. 34, no. 6, pp. 598–604, 2014.